UNIVERSITY OF CALIFORNIA,
IRVINE

Framework for modeling and assessing anthropogenic influence on built and natural environments in a changing climate

DISSERTATION

submitted in partial satisfaction of the requirements
for the degree of

DOCTOR OF PHILOSOPHY

in Civil and Environmental Engineering

by

Aneseh Alborzi

Dissertation Committee:
Professor Amir AghaKouchak, Chair
Associate Professor Russell Detwiler
Professor Kuo-lin Hsu

2021

DEDICATION

To

my parents and family, and

my love

in recognition of their worth

TABLE OF CONTENTS

LIST OF FIGURES

LIST OF TABLES

ACKNOWLEDGEMENTS

I would like to express the deepest appreciation to my committee chair, Professor Amir AghaKouchak, who has the attitude and the substance of a genius: he continually and convincingly conveyed a spirit of adventure in regard to research and scholarship, and an excitement in regard to teaching. Without his guidance and persistent help this dissertation would not have been possible.

I would like to thank my committee members, Professor Kuo-lin Hsu and Professor Russell Detwiler, whose constructive comments and feedback improved this effort.

In addition, a thank you to Professor Farshid Vahedifard of Mississippi University, who introduced me to geotechnical perspectives, and the collaboration had lasting effect.

VITA

Aneseh Alborzi

2003 B.A. in Civil Engineering, Sharif University of Technology, Tehran, Iran

2006 M.A. in Civil Engineering, Water Resource Management, K.N. Toosi University of Technology, Tehran, Iran

2007-2015 Water planning specialist, Iran

2016-present Ph.D. student in Civil Engineering,

University of California, Irvine

FIELD OF STUDY

Climatic extremes and infrastructure adaption

PUBLICATIONS

Alborzi, A., Mirchi, A., Moftakhari, H., Mallakpour, I., Alian, S., Nazemi, A., ... & Norouzi, H. (2018). Climate-informed environmental inflows to revive a drying lake facing meteorological and anthropogenic droughts. **Environmental Research Letters**, 13(8), 084010.

Alborzi A., Zhao Y., Mirchi A, Moftakhari H, Mallakpour I, Nazemi A, Ashraf S, Izadi R., AghaKouchak A., (2021) The Tale of Three Floods: From Extreme Events and Cascades of Highs to Anthropogenic Floods, Under Review.

Alborzi, A., Mallakpour, I., Vahedifard, F., & AghaKouchak, A. (2021), Integrating Future Climate Information into Engineering Design Concepts, Under Review.

Alborzi, A., Vahedifard, F., & AghaKouchak, A. (2021), Framework for Adaptive Design of Infrastructure under a Changing Climate, in preparation.

AghaKouchak, A., Mirchi, A., Madani, K., Di Baldassarre, G., Nazemi, A., **Alborzi, A.**, ... & Wanders, N. (2021). Anthropogenic Drought: Definition, Challenges and Opportunities. **Reviews of Geophysics**, e2019RG000683.

Vahedifard, F., Jasim, F. H., Tracy, F. T., Abdollahi, M., **Alborzi, A.**, & AghaKouchak, A. (2020). Levee Fragility Behavior under Projected Future Flooding in a Warming Climate. **Journal of Geotechnical and Geoenvironmental Engineering**, 146(12), 04020139.

Ashraf, Samaneh, Amir AghaKouchak, Ali Nazemi, Ali Mirchi, Mojtaba Sadegh, Hamed R. Moftakhari, Elmira Hassanzadeh, **Aneseh Alborzi et** al. (2019) "Compounding effects of human activities and climatic changes on surface water availability in Iran." **Climatic Change**: 1-13.

.

ABSTRACT OF THE DISSERTATION

Framework for modeling and assessing anthropogenic influence on built and natural environments in a changing climate

by

Aneseh Alborzi

Doctor of Philosophy in Civil and Environmental Engineering

University of California, Irvine, 2021

Professor Amir AghaKouckak, Chair

Human-caused changes in water use, emissions, and land cover have increasingly impacted the natural and built environments. As a result, the natural hydrologic cycle has been disrupted, causing changes in the quantity and quality of water, extreme events (i.e., droughts and floods), and the ecosystem. Further, the warming climate has increased variability in the frequency and/or intensity of climatic hazards, elevating the complexity of water resources management and infrastructure systems planning and risk assessment. This study explores the human influence on extreme events and the resulting impacts on the built environment and infrastructure systems. Specifically, this dissertation addressed the following main objectives: (1) Evaluate compounding effects of meteorological drought and unsustainable water resource management contributing to catastrophic environmental degradation; (2) Investigate the notion of anthropogenic flood events where human disruptions have caused or intensified flood risk to unprecedented levels; and (3) Evaluate performance (i.e., factor of safety) of water infrastructure under anthropogenic climate change, and propose adaptive strategies toward climate-ready infrastructure systems. We

investigate major historical drought and flood events in which human activities have led to substantial regional impacts/losses. Then, we introduce frameworks for evaluating infrastructure performance under future climate projections and offer a path forward for climate-ready infrastructure planning and risk assessment. Finally, a conceptual iterative design framework is presented to show how the proposed adaptive design concept can be employed in practice.

Chapter 1 Introduction

Population growth and industrial developments since the late 18th century have caused dramatic changes in the Earth system interactions (MEA, 2005; Steffen et al., 2007). During the urbanization and agricultural expansion, two primary drivers, including land cover change and resource use, have increasingly impacted the natural environments and the governing balances (Sala et al., 2000). As a result, the natural hydrologic cycle has been disrupted causing changes to the quantity, quality, and distribution of water. Further, land use changes have impacted runoff generation and groundwater replenishment (Vörösmarty et al., 2010; Mirchi et al., 2014; Nazemi and Wheater, 2014, 2015; Hassanzadeh et al., 2015; Mehran et al., 2017; Das et al., 2013; Milly et al., 2005; Pachauri et al., 2014; Wang et al., 2017). Change in water use often parallels change in land use, which leads to compounding hydrologic alterations on different spatial and temporal scales (Lee et al., 2011; Jarsjö et al., 2012; Destouni et al., 2013; Mehran et al., 2017). The surface and groundwater overdraft on the one hand and the massive human activities (e.g., deforestation, dam constructions) in river basins, on the other hand, have influenced extreme events (i.e., droughts and floods), natural environments, and ecosystem.

Further, due to the co-evolution of anthropogenic greenhouse gas emissions with land use and land cover changes, global warming has gradually emerged as a major challenge (Christidis

et al., 2011; Das et al., 2011; FEMA, 2016; Neumann et al., 2015a, 2015b; Reidmiller et al., 2018; Harvey, 2018). A warmer climate may increase evaporation and atmospheric moisture holding capacity, intensifying the hydrological cycle (Trenberth et al., 2007; O'Gorman & Muller, 2010; Scheff & Frierson, 2014). Over the past decades, human□induced climate change has caused additional variabilities in the frequency and/or intensity of climatic, natural hazards such as droughts, heatwaves, floods, and hurricanes (e.g., Das et al., 2013; 72 Milly et al., 2005; Pachauri et al., 2015; Voss et al., 2002; Wang et al., 2017). The growing exposure of people and assets to extreme events has raised the impacts of related damages. For instance, several recent drought events in California, Spain, Brazil, China, and southern Africa (Jiang, 2009; Qiu, 2010; K. Xu et al., 2015; Silva et al., 2015; Van Loon et al., 2016a; Van Loon & Van Lanen, 2009; Diffenbaugh et al., 2015; Yuan et al., 2018) have resulted in costly events with the vast societal impacts (Di Baldassarre et al., 2018b; Etienne et al., 2016; Güneralp et al., 2015; Kreibich et al., 2019; Wilhite et al., 2007). On the other tail of extremes, more intense and frequent rainfall and flood events have been observed, leading to human disaster and substantial loss of assets and infrastructure (e.g., structural failure of Oroville Dam's spillway, Vahedifard et al., 2017; Zhang et al., 2007; Westra, 2013, Cheng; 2014, Knutti, 2016, Mallakpour and Villarini, 2017). For example, in the United States, from 1980 until July 2020, inland floods have caused 617 deaths and over $150 billion of CPI-adjusted losses (NCEI, 2020). These observations highlight that the dramatic human influence is an important driver that has worsened the natural hazard's impacts.

The compounding effects of human□induced climate change with water and land use practices have elevated the complexity of resource (e.g., water, soil) management and infrastructure systems planning (Dale, 1997). Change in local water demand and reservoir management impacts water availability, leading to water scarcity and stress. However, hydrologic

and water resources studies have not adequately accounted for the human component in their hydrological and/or land-surface models (Barnett et al., 2006; Nazemi & Wheater, 2015; Mehran et al. 2015; Döll et al. 2012; Loucks 2015; Oki and Kanae 2006; Scanlon et al. 2012; Sivapalan 2015). More recently, a number of scholars have attempted to incorporate the impacts of human activities on local water availability (e.g., Alborzi et al., 2018; Ashraf et al., 2017, 2019; Castelletti et al., 2008; Garcia et al., 2019; Herman et al., 2016; Srinivasan et al., 2018; You & Cai, 2008; Di Baldassarre et al., 2015; Montanari et al., 2013) and integrate infrastructure systems (e.g., irrigation and reservoirs) into hydrologic models (Mehran et al., 2016; Bertoni et al., 2019; Carmona et al., 2017; Castelletti et al., 2008; Draper et al., 2003; Gupta et al., 2020; Müller et al., 2016; Quinn et al., 2020; Rajsekhar & Gorelick, 2017). In an uncertain future with changing extreme patterns, compounding processes that involve feedback between humans and nature would be helpful to adaptive planning of infrastructure and extreme events management.

This study explores the human influence on extreme events and the resulting impacts on the local ecosystem and Infrastructure. Specifically, the focus is on modeling and assessing human activities in the natural and built environment. First, we study major historical drought and flood events, where human activities have led to massive regional losses/imapcts. We explore frameworks for quantifying human influence on the observed changes and societal impacts. Then, acknowledging the growing risk of climatic extremes, we introduce frameworks for evaluating infrastructure performance and risk assessment under future climate projections and offer a path forward for climate-ready infrastructure planning and management. This study strives explicitly to achieve three main objectives:

(OB) 1- Evaluate compounding effects of meteorological drought and unsustainable water resource management contributing to catastrophic environmental degradation.

(OB) 2- Investigate the notion of anthropogenic flood events where human disruptions have caused or intensified flood risk to unprecedented levels.

(OB) 3- Evaluate performance (i.e., factor of safety) of water infrastructure under anthropogenic climate change, and propose adaptive strategies toward climate-ready infrastructure systems.

In Chapter 2 (OB 1), we study the rapid shrinkage of Lake Urmia, one of the world's largest saline lakes located in northwestern Iran, and its anthropogenic drivers. The objective is to set a framework for evaluating human impacts and deriving dynamic, climate-informed environmental inflows for drying lakes considering both meteorological/climatic and anthropogenic conditions. Using rich datasets of hydrologic attributes, water demands and withdrawals, as well as water management infrastructure (i.e., reservoir capacity and operating policies), we provide a quantitative assessment of the basin's water resources including human activities. We explore a marked overshoot of the basin's hydrologic capacity due to growing anthropogenic drought in the face of extreme climatological stressors. We offer a dynamic environmental inflow plan for different climate conditions (dry, wet, and near normal), combined with three representative water withdrawal scenarios. Finally, for different environmental inflow scenarios, we estimate the expected recovery time for re-establishing the ecological level of Lake Urmia.

In Chapter 3 (Ob 2), we investigate a number of flood events with an unprecedented spatial extent that hit different parts of Iran over the two weeks of March 17th to April 1st, 2019, causing a human disaster and substantial loss of assets and infrastructure. We investigate the natural (e.g., rainfall, snow accumulation/melt, soil moisture) and anthropogenic drivers (e.g., deforestation, urbanization, and management practices) of these events using a range of ground-based data and satellite observations. We evaluate the compounding impacts of natural drivers and anthropogenic triggers in escalating flood risks to unprecedented levels. We argue that a new form of floods, i.e.,

anthropogenic floods, is becoming more common during the "*Anthropocene*". This specific type of flood refers to events primarily caused or largely exacerbated by anthropogenic drivers. We demonstrate how the growing risk of anthropogenic floods can be assessed using a wide range of climatic and non-climatic satellite and in-situ data.

Chapters 4 and 5 (Ob 3) study the reliability of water infrastructure (e.g., levees) subjected to the growing risk of future climatic extremes under future anthropogenic emissions. We use past and future projections to assess the exposure of infrastructure systems to investigate how engineering requirements are needed to adjust in a changing climate. The aim is to create frameworks that can help move toward achieving resilient infrastructure systems against natural hazards and climatic extremes. We develop a theoretical engineering risk models for considering the changing hazards and the impacts on infrastructure vulnerability and exposure, accounting for future uncertainties. The proposed framework will be used to evaluate adaptive approaches to infrastructure investment and management that account for strategic flexibility to promote robustness to many potential future challenges.

Chapter 2 Anthropogenic drought

Climate-Informed Environmental Inflows to Revive a Drying Lake Facing Meteorological and Anthropogenic Droughts

Overview

Global fresh water resources are under growing pressure due to over-allocation of surface water (Vörösmarty et al., 2000; Hoekstra et al., 2012) and groundwater resources (Wada et al., 2010; Gleeson et al., 2012; Ashraf et al., 2017). The compounding effects of human-centered water management and global environmental changes in the Anthropocene have altered the natural hydrologic cycle by changing the quantity and quality of water, as well as changing the time scale of the processes that replenish water resources (Vörösmarty et al., 2010; Mirchi et al., 2014; Nazemi and Wheater, 2014, 2015a, b; Hassanzadeh et al., 2015; Mehran et al., 2017). The disruption of regional water regimes around the globe due to increasing water stress is evident in the growing number of inland water bodies that are facing ecological degradation, especially in irrigated agricultural areas (e.g., Coe and Foley, 2001; Micklin, 2007; Ma et al., 2010; UNEP, 2012; Hatchett et al., 2015; Barnum et al., 2017).

Prime examples of drying terminal lakes in endorheic basins include the Aral Sea in Central Asia (Micklin, 1988), Walker Lake and Great Salt Lake in the U.S. (Wurtsbaugh et al., 2017), Lake Chad in Africa (Gao et al., 2011), and Lake Urmia in northwestern Iran (AghaKouchak et al., 2015). These alarming cases of lake level decline as well as other less dramatic incidents have been subjects of climate change scenario and impact assessments around the world (e.g., Coe and Foley, 2001; Schwartz et al., 2004; Ma et al., 2010; Mohammed and Tarboton, 2012; Shadkam et al., 2016). Water level serves as a key indicator of a lake's stability (Ma et al., 2010). Lake level fluctuations depend on intra- and inter-annual hydrologic variability (Mei et al., 2015) and water management practices in the lake basin (Coe and Foley, 2001; Adrian et al., 2007; Ma et al., 2010). Determining whether the lake level change is primarily due to human factors or climate change bears important implications for lake restoration strategies. In theory, the chance of preserving lakes will be higher if human activities are the chief reason for the water level decline because of opportunities for taking real actions to improve water management in the lake basin.

The shrinkage of Lake Urmia, to less than 20% of its average size (i.e., more than 5000 km^2) over the last two decades (see AghaKouchak et al., 2015; Farzin et al., 2012; Pengra, 2012) is a recent exemplar of an emerging challenge related to unsustainable water management in the face of growing demand and climatic extremes. This designated UNESCO ecosystem and one of the largest saline lakes (Sima and Tajrishi, 2013; Karbassi et al., 2010) is located at the bottom of an approximately 52,000-km^2 basin in northwestern Iran (Figure 1), which is home to about five million people close to international borders with Turkey, Iraq, and Azerbaijan (Iran's Ministry of Energy (IME), 2013). With salinity levels ranging from six to approximately eight times higher than seawater, this shallow terminal lake is the largest natural habitat for brine shrimp Artemia

(Artemia Urmiana), which attracts diverse species of migratory birds (Barigozzi et al., 1987; Vahed et al., 2011; Ahmadi et al., 2011). Such massive decline in a lake area has been witnessed before in the Aral Sea Basin, where diverting Amu Darya and Syr Darya rivers during the Soviet era caused the lake to shrink to less than 10% of its original size (Micklin, 1988 and 2007; Gaybullaev et al., 2012). Remarkable parallels between unsustainable water resource management in the Lake Urmia and Aral Sea basins reinforce speculations of "the Aral Sea syndrome" being a key driver of Lake Urmia's collapse (AghaKouchak et al., 2015), causing negative impacts on both wildlife and humans (Madani et al., 2016; Yamaguchi et al., 2012).

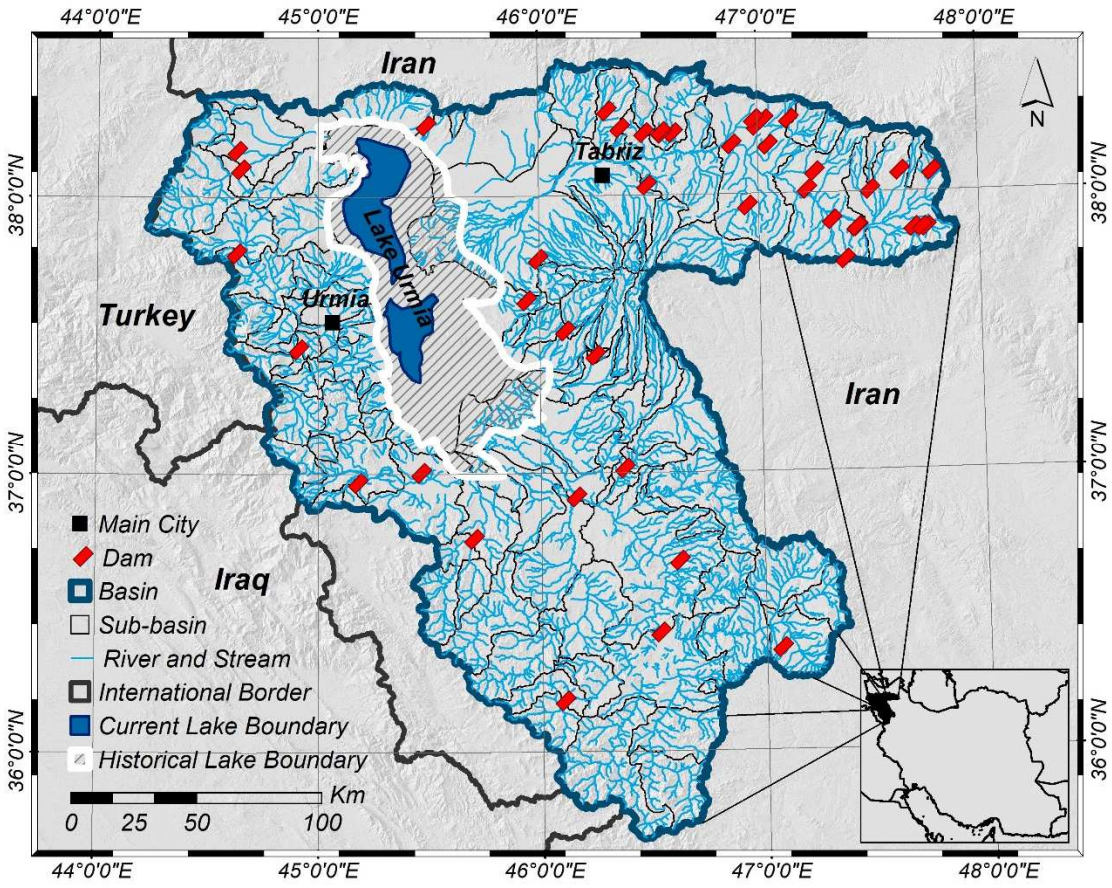

Figure 1 Lake Urmia Basin showing its 117 sub-basins, existing dams and the lake's surface area. The white boundary displays the lake's surface area in 1998 based on Landsat imagery. The dark blue area depicts the current boundary based on 2017 Landsat imagery (only showing area where water can be confidently detected from space).

The contemporary environmental catastrophe in the Lake Urmia Basin is a tragic wake-up call to rethink the water resources management paradigm in water-scarce countries based on hard-learned lessons about the social, economic, and environmental dimensions of sustainability (Madani, 2014). Since the onset of the lake's shoreline recession around the turn of the 21st century, many researchers have investigated various aspects of the problem (Gholampour et al., 2015; Ghaheri et al., 1999; Ahmadzadeh Kokya et al., 2011; Barigozzi et al., 1987; Delju et al., 2013; Nikbakht et al., 2013; Farokhnia and Morid, 2014). The desiccation has been primarily attributed to climate change-induced meteorological droughts (e.g., Fathian et al., 2015; Vaheddoost & Aksoy, 2017; Arkian et al., 2018), as well as anthropogenic drought due to supply-oriented water management (e.g., Hassanzadeh et al., 2012; AghaKouchak et al., 2015; Shadkam et al., 2016; Zarghami et al., 2017; Ghale et al., 2018). These studies have provided a high-level understanding of the problem, highlighting the need for and complexities of synergistic efforts to revive a drying lake that is effectively struggling with "water bankruptcy" (Madani et al, 2016). As shown in Figure 2, the drastic water level decrease after 1998 corresponds to a substantial increase (~25%) in surface water withdrawals to meet upstream potable and agricultural demands, which coincided with 48% decrease in runoff during the prolonged drought of 1998-2002. The largest water withdrawal of 4.75 bcm/yr, of which 2.7 bcm/yr was supplied from surface water was triggered by rapid agricultural expansion (i.e., 14% increase in irrigation area; IME, 2014). The figure also illustrates

the basin's recent wet (blue) and dry (red) periods as indicated by the standardized precipitation index (SPI; McKee et al., 1993) and the variability of naturalized runoff.

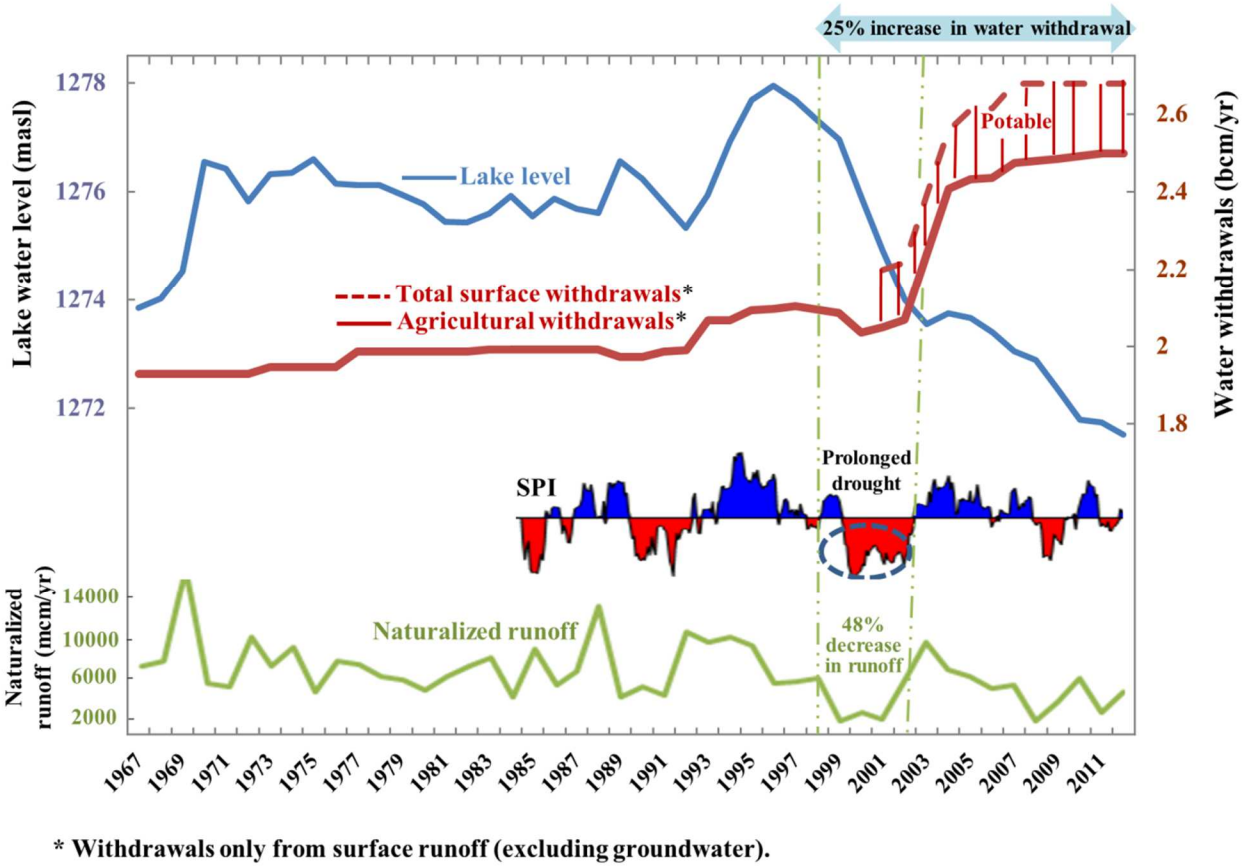

Figure 2. Key attributes of the lake-basin system prior to restoration program in 2013, including observed lake level, standardized precipitation index (SPI), basin-scale naturalized runoff, and surface water withdrawal. The basin's recent wet (blue) and dry (red) periods are illustrated in SPI and naturalized runoff curves. Post-1998 drop in lake level corresponds to a substantial increase (~25%) in surface water withdrawals during the prolonged drought of 1998-2002.

This study attempts to inform the ongoing debate about the causes of Lake Urmia's shrinkage and the planned restoration efforts. It provides a quantitative assessment of the basin's water resources and environmental water requirement as influenced by wet and dry periods, and anthropogenic

water withdrawals. Understanding the large-scale interplay of green water losses (i.e., consumptive water uses in the agricultural sector) and blue water availability (i.e., surface water and groundwater) (Allan, 1998; Hoekstra and Hung, 2002; Falkenmark and Rockström, 2004) superimposed by climate stressors in the basin is essential for effective restoration of Lake Urmia and preempting similar incidences in other areas. Re-establishing Lake Urmia's ecological integrity provides a testbed to evaluate different lake restoration policies and action plans to curb and reverse the unfolding crisis. We examine the compounding effects of climate anomalies and anthropocentric water withdrawals in this highly regulated basin to restore the lake's designated ecological water level of 1274 meters above sea level (masl) used as a monthly and annual threshold based on water quality conditions (240 g/l of NaCl) required to preserve brine shrimp Artemia (Abbaspour and Nazaridoust, 2007). We develop an understanding of lake level changes using comprehensive datasets of water resources management infrastructure (i.e., reservoir capacity and operating policies), observed streamflow data, and agricultural and urban water demand data from 117 sub-basins. The chapter illustrates the need for developing a dynamic, climate informed environmental inflow plan to restore the lake's ecological level. Furthermore, we investigate the lake's expected recovery time under dynamic basin-scale water management scenarios compounded with a wide range of historical climatological conditions.

Methodology and Data

We divided the Lake Urmia Basin into 117 sub-basins (see Figure 1), ranging from 16 km^2 to 3000 km^2 (average sub-basin size: 405 km^2). The sub-basins were delineated based on the presence of streamflow gauges and/or dams as an outlet (i.e., Pour Point). For each sub-basin, we used observed streamflow data to represent the combined contribution of surface runoff and baseflow.

Instead of calculating irrigation water use through estimated soil moisture (i.e. from a hydrological or a land-surface model) implemented in previous basin-scale analyses of this lake (e.g., Shadkam et al., 2016), we used a sub-basin scale dataset of monthly agricultural water demands developed by local water authorities based on irrigated area and crop water requirement (IME, 2014). Thus, we accounted for green water losses over the basin and consequent reduction of the blue water flow to the lake. Likewise, the municipal and industrial demands at the sub-basin scale were obtained based on available monthly observational data (IME, 2013).

MODSIM-DSS, a generalized network flow river basin model (Fredericks et al., 1998; Labadie and Larson, 2007) applied for this study, distributes the available water based on natural inflows, water demands, reservoir capacities and operating policies, and calculates the lake level based on excess water flow to the lake. This modeling tool has been widely used for basin-scale water resources planning (Graham et al., 1986; Sprague and Carlson, 1982; Ahn et al., 2016; Berhe et al., 2013; Ashraf Vaghefi et al., 2017), and it is able to represent the supply/demand priorities. We coupled the sub-basin scale water resource system model with a monthly lake water balance model to better represent lake-basin interactions. Table 1 summarizes key input datasets and sources.

The developed MODSIM-DSS model includes 17 large on-stream and off-stream operational reservoirs (i.e., capacity>5 mcm). These reservoirs collectively store up to 1,560 mcm of water, providing 97% of the total surface storage capacity in the basin (Figure 3). Physical characteristics and operating policies embedded in model inputs include: i) volume-area-elevation curves, ii) net evaporation rate, iii) maximum, minimum and initial reservoir capacities, and iv) reservoir water allocation priorities. Where cascaded reservoirs are present, the model is capable of simulating basin-scale coordinated operation of the reservoirs, i.e., upstream-downstream coordination to meet downstream demands. Without these reservoirs, upstream water could reach the lake quickly,

rendering an inaccurate representation of water availability in different parts of the basin. We used river discharge measurements and observed lake levels to validate the simulated basin-lake interactions. Simulated lake levels and lake inflows closely track the observational data (see Figures S1 through S3 in Appendix A), indicating reasonable model performance, also suggested by model efficiency coefficients (e.g., *i)* monthly lake inflow correlation coefficient (0.96), bias (15.5%), and Nash–Sutcliffe efficiency coefficient (0.9), and *ii)* monthly lake level correlation coefficient (0.96), bias (0.03%), and Nash–Sutcliffe efficiency coefficient (0.79)). Depending on the time of measurement, lake level elevation varies from 1270 m to 1278 masl with average elevation being 1275 masl (average depth: 5.4 m).

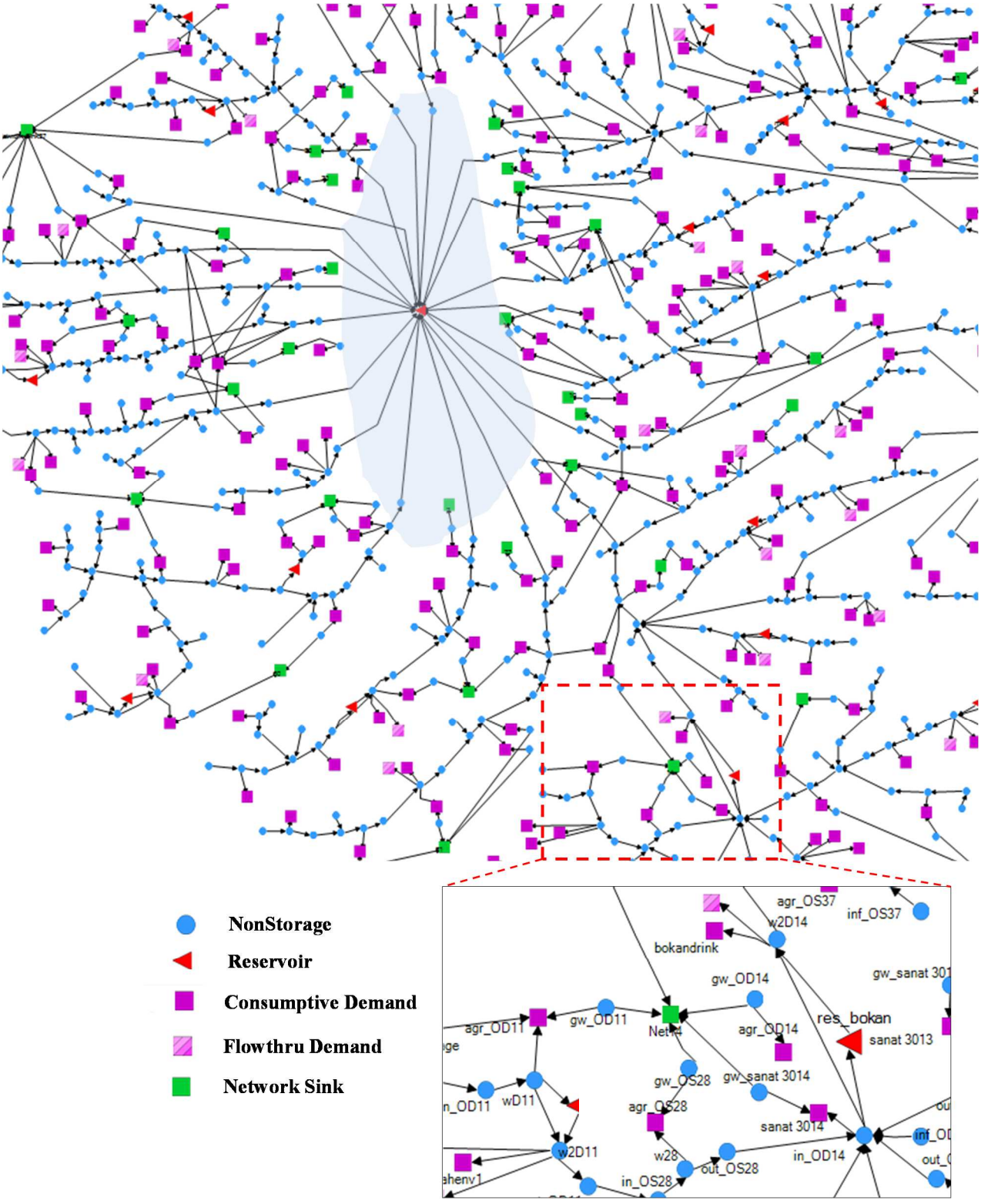

Figure 3. Detailed simulation of the water resources system in the Lake Urmia Basin using MODSIM-DSS.

For the lake scenario analyses (discussed below), a normal year is assumed to receive 350 mm of rainfall (IME, 2013; ULRP, 2016). Furthermore, we used monthly evaporation climatology with annual evaporation of 1100 mm/yr (ULRP, 2016) for the simulation period. This simplification was necessary due to unavailability of monthly evaporation time series for the entire simulation period. To validate this assumption, we compared the performance of the MODSIM-DSS model using both monthly evaporation climatology and available monthly evaporation time series for the period of 1982-2002 for which we had access to monthly lake evaporation. The comparison illustrates that lake levels are consistent with observations using monthly evaporation climatology (Figure S4 in Appendix A). Water demand is partially met using groundwater up to an observed rate of 2000 mcm/yr (IME, 2014). Given the lack of long-term records, we used different constant annual rates, but considering the monthly distributions for each sub-basin based on observations (IME, 2014). Under different water withdrawal scenarios, the annual groundwater withdrawals vary between 1650 mcm/yr to 2000 mcm/yr to supplement surface water supply. We acknowledge that lack of groundwater withdrawal time series introduces uncertainties in the simulations.

Table 1 Datasets used for simulating the basin-lake interactions (Source: Various publications of IME)

	Spatial scale	**Temporal scale**
Lake level-volume-area curve	--	--
Over-lake evaporation and precipitation	Meteorological stations	Monthly Average (1967–2012)
Surface water supply	Streamlines	Monthly (1967–2007)
Surface water withdrawals and irrigated area	Sub-basin	Monthly (2012)
Groundwater withdrawals	Sub-basin	Monthly Mean (2012)

We simulated the interactions between the upstream water resource system and Lake Urmia under scenarios that cover a wide range of climate conditions and water withdrawals combined (Figure 4). The model uses naturalized runoff data to allocate water to different demand nodes. We estimated the naturalized runoff for each sub-basin by adding long-term upstream surface water withdrawals (including return flow) to streamflow gauge at the sub-basin outlet. The climatological scenarios are based on historic climate observations including baseline and near normal climatology and an observed historic drought (i.e., 48% decrease in runoff). The baseline period (1994-1998) is a relatively wet period that precedes the drastic decrease in the lake area. The most extreme drought condition corresponds to 1998-2002 (hereafter, referred to as drought of record scenario). We consider 2003-2007 a near normal period after the 1998-2002 drought because natural runoff during this period is close to long-term mean (1967-2012, 6500 mcm/yr). Water demand scenarios include historical baseline, maximum demand, and target demand reduction. Baseline demand refers to pre-drastic change in lake levels and water withdrawals (i.e., pre-1998). Maximum demand is associated with rapid increase in the overall water withdrawals (i.e., 2003-2012) and it is the most extreme case investigated in our analysis. Target demand is based on the recommendation of the Urmia Lake Restoration Program (ULRP, 2016) that calls for an aggressive 40% decrease in 2013 agricultural water use over a 5-year period (ULRP, 2016). The combination of these scenarios helps evaluate the compounding effects of climatic and anthropogenic conditions on the lake's water level.

For all nine coupled scenarios (i.e., permutations of three inflow scenarios and three demand scenarios) depicted in Figure 4, we investigated both basin-scale water stress and associated changes in the lake level. We used a modified version of the water resources vulnerability index (Raskin et al., 1997), in which Environmental Flow Allocations (EFA) are included in Water Stress

Index (WSI) calculations alongside Human Water Withdrawals (HWW; see Smakhtin et al., 2005; Averyt et al., 2013; Pastor et al., 2014). The dimensionless WSI characterizes the stress imposed on the Total Water Resources (TWR) defined as the summation of both available surface water and groundwater resources (Raskin *et al.* 1997; Vörösmarty *et al.,* 2005).

$$WSI = \frac{HWW + EFA}{TWR} \quad (1)$$

The modified water resources vulnerability index accounts for environmental withdrawals in the water stress index formulation. A WSI of 0.6 represents a moderately exploited basin and WSI values above this threshold indicate that the basin is heavily exploited (Smakhtin *et al*., 2005). Here, we consider the environmental inflow requirement of 3100 mcm/yr as Lake Urmia's annual ecological demand in the historical scenarios (Abbaspour and Nazaridoust, 2007). The lake's required ecological flows were not delivered reliably prior to the implementation of the restoration plan in 2013 due to lower priority of environmental flow compared to human water use. Furthermore, we evaluate the sensitivity of the minimum inflow requirement to lake level dynamics as a critical boundary condition for effective re-establishment of the target ecological level of the lake.

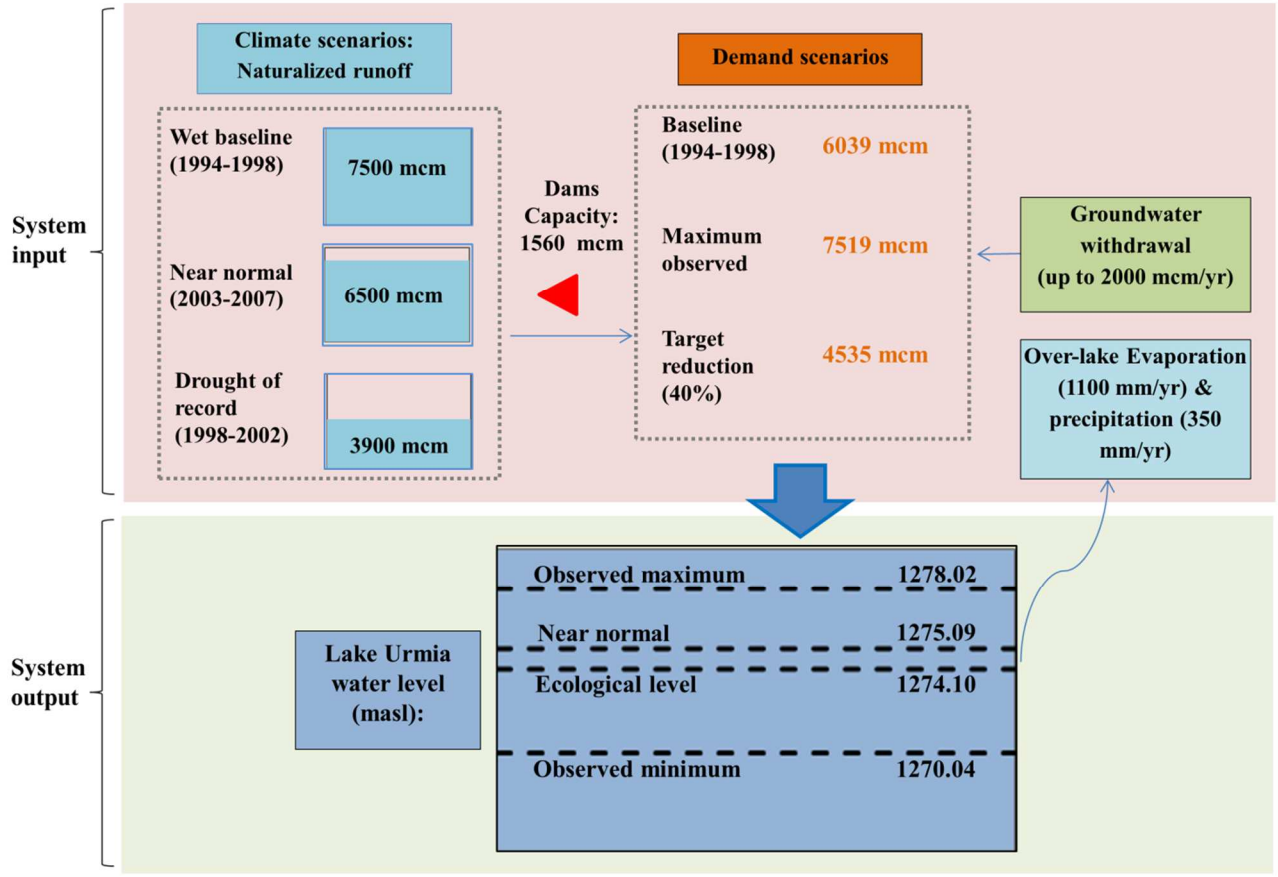

Figure 4. MODSIM-DSS model inputs and outputs along with climate and demand scenarios.

Results and Discussion

Assessment of climate-demand scenarios

Figure 5 summarizes the WSI over the basin along with the percentage of change in the lake's level relative to baseline under the combined climate-demand scenarios. The results show high water stress under all nine scenarios. The basin-wide WSI under an intentionally optimistic scenario of wet period combined with Urmia Lake Restoration Program (ULRP) target demand stands at an alarming level of 60% (i.e., moderately exploited basin). The WSI increases to about 80% under maximum observed demand during wet period, indicating heightened vulnerability in a heavily exploited basin. A similar increasing trend is detected during the near normal period

when the WSI exceeds 80%. In an extremely dry period, in which the annual runoff reduces by 48% (compared to the baseline wet period), the lake is gravely vulnerable to increases in anthropogenic water demands, elevating the WSI to a distressing level of 90%. Percentages of annual change in lake depth (relative to baseline) over the five-year simulation periods (1994-1998, 1998-2002 and 2003-2007) show an increasingly divergent, declining trend of lake-basin interactions under near normal and dry period scenarios, compounded with larger water demand scenarios. The increasing range in boxplots corresponding to change in lake level (Figure 5) illustrates higher vulnerability of the lake to human water withdrawals in dry condition.

In a wet climate and under the maximum demand scenario, the lake level drops by 10%, which highlights the significance of anthropogenic demand alone on the lake water depth. However due to ample surface runoff during a wet period, the lake level remains above the prescribed ecological threshold. Unlike the wet period, the lake is vulnerable to anthropogenic demand during a near normal condition and the lake-basin interactions under the ULRP target demand will be at a fragile hydrologic balance. This means that any rise in demand above the targeted values leads to lake level dropping below the ecological threshold. Notably, even a 5% increase in water demand during the near normal condition pushes the lake level below the ecological level. Expectedly, the largest decline in the lake level (i.e., 1.5m drop below the ecological threshold) occurs during the dry period with maximum observed demand, which is the most extreme case in our analysis. This result confirms the "double devil effect" of 25% increase in water withdrawal in the Lake Urmia Basin during the drought of 1998-2002 that pushed the lake water budget severely out of balance and caused a lasting, drastic drop in the lake level (Figure 5).

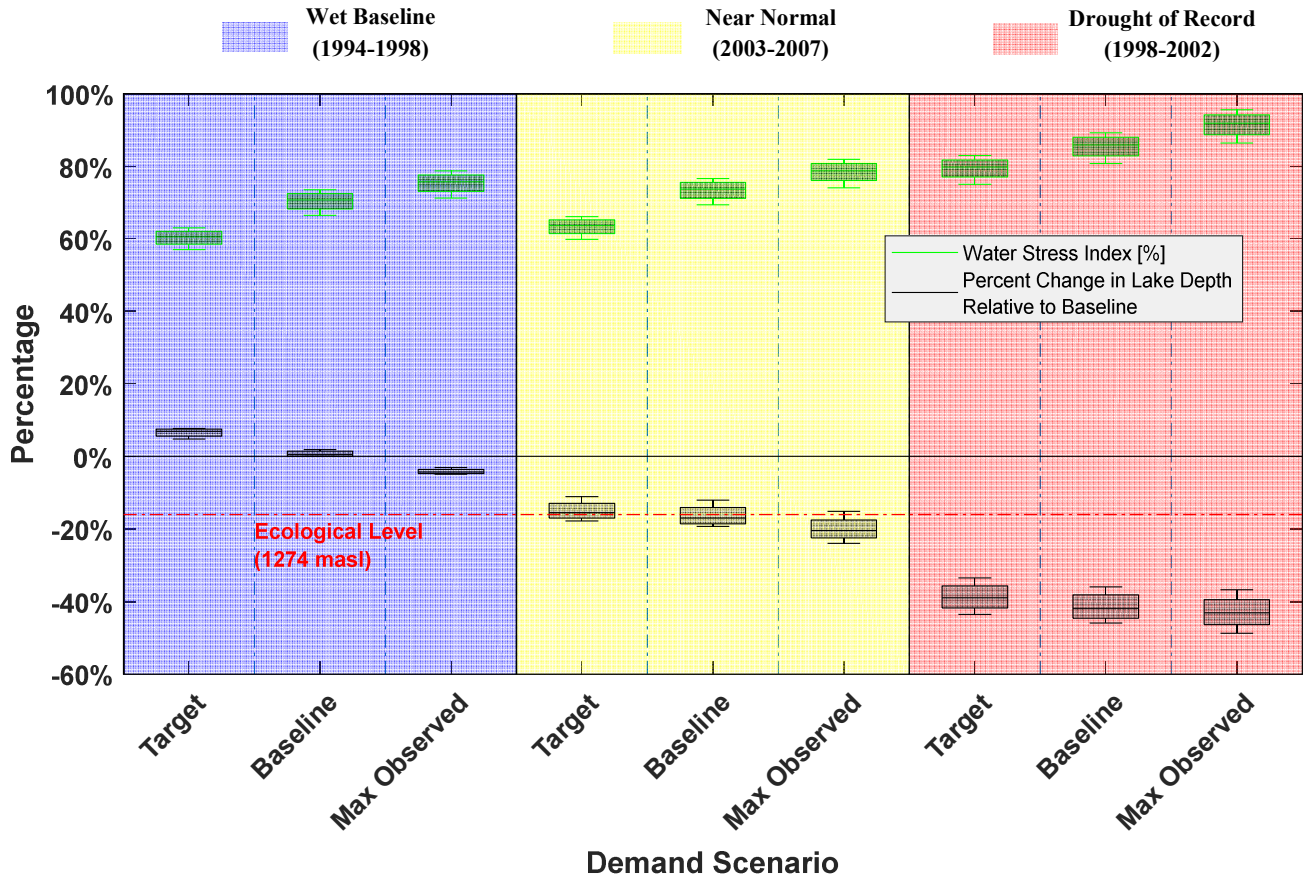

Figure 5. Water Stress Index (WSI) in percentage over the lake basin (green boxplot) and the percentage of change in the lake level relative to the baseline (gray boxplot) under different combinations of climate-demand scenarios. Shaded regions represent wet baseline (purple), near normal (yellow), and dry (pink) periods. Dashed vertical lines demarcate three demand scenarios (i.e., target reduction (40%), baseline, and maximum historical) in each period.

Lake level departure from the ecological threshold

Figure 6 illustrates the sensitivity of lake level to different combinations of total available water resources (including both surface water and groundwater) and total water withdrawal over the basin. The contours were derived from lake level as a model output under different simulation scenarios, which depends on water withdrawals (X axis) and available water resources (Y axis). It is important here to distinguish between basin-scale total water withdrawal and water demand; total water withdrawal depends on the water availability in the basin, and therefore, it may be smaller than the total water demand. With a low supply reliability of 55% to 80% (IME, 2013),

the Lake Urmia Basin faces water deficit, which necessitates water use restrictions. Sectoral water demands are met according to ordinal allocation priorities of domestic, industrial, agricultural, and finally environmental needs. Total water availability (5500 mcm) and water withdrawal (3500 mcm) over the basin during the drought of 1998-2002 caused the lake level to fall to around the 1273.5 contour line (Figure 6a), which is consistent with the observed lake level in the aftermath of this prolonged drought.

We examined the sensitivity of the lake's environmental inflow requirement to initial lake level as a boundary condition in order to quantify the implications for maintaining the lake's ecological level. Figure 6b illustrates the results of lake level contours under coupled climate-withdrawal scenarios for initial lake levels of 1275 masl, 1274 masl, and 1273 masl, which represent water levels above, at, and below the ecological level, respectively. The lake's ability to absorb water stresses while remaining above the critical threshold (i.e., safe ecological zone) declines significantly when the initial lake level decreases as indicated by dramatic decline of the estimated lake level. In the case of low initial water volume, a moderate withdrawal in a near normal climate condition may drive the lake level below the critical ecological threshold. This effect is seen in the post-drought scenario when low runoff for three consecutive years resulted in lake level decline (1373.5 masl) below the critical level. Although the region had near-normal precipitation and runoff immediately after the drought of record (i.e., during the 2003-2012 period), the lake levels continued to fall due to growing water withdrawal and failure to increase the lake's environmental inflow. These results demonstrate the need to prescribe dynamic, climate-informed environmental inflow requirements to sustain the lake as opposed to the existing, static ecological water demand of 3100 mcm/yr.

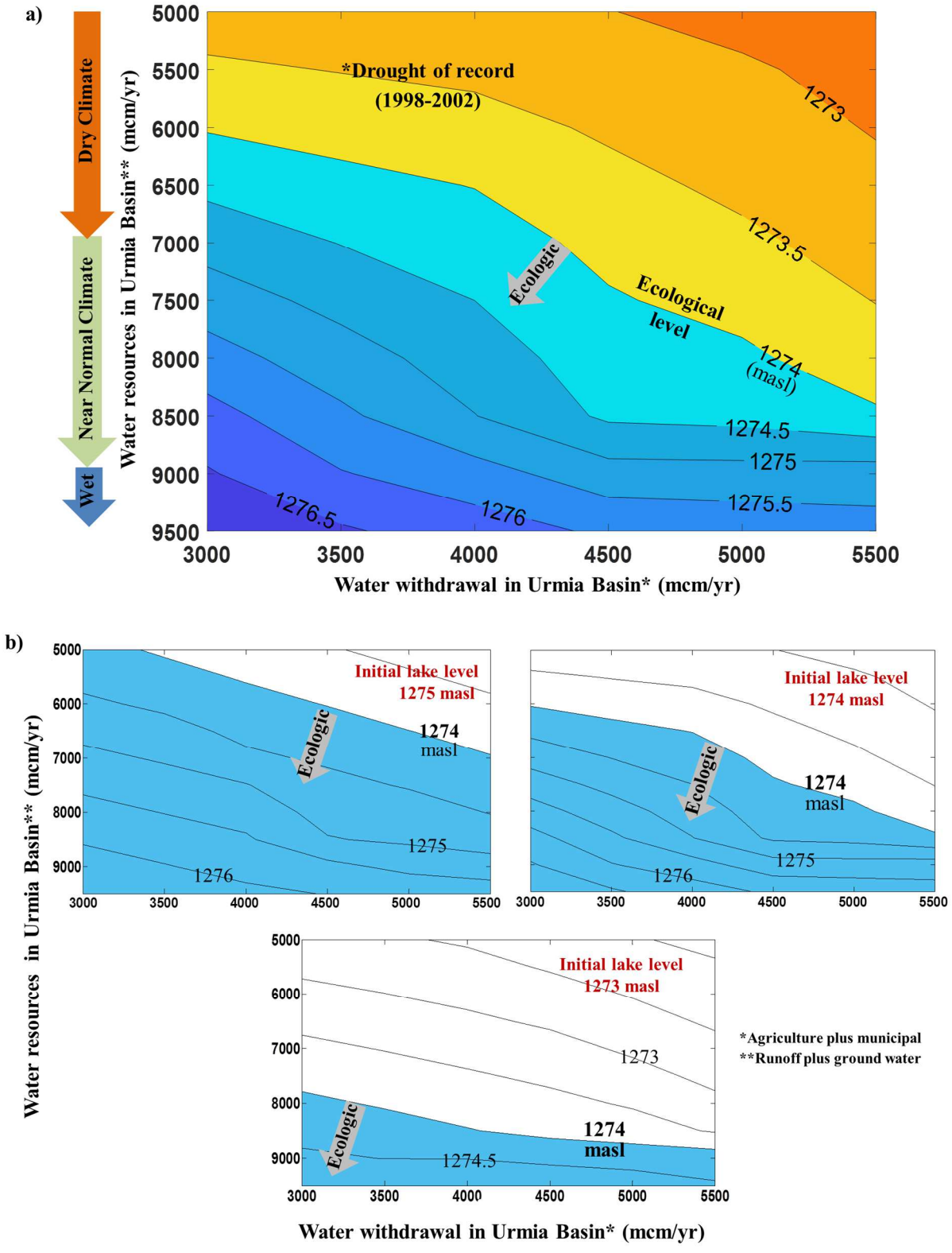

Figure 6. Average lake level contours under different combinations of water availability and water withdrawals with the initial lake level fixed at 1274 masl (a), and when the initial lake level is changed as a variable boundary condition (b).

Lake Urmia's tipping phase and recovery trajectory

Lake Urmia reached a tipping point in the early 2000's when the lake basin's hydrologic carrying capacity was significantly exceeded due to compounding pressures from climatological factors and unsustainable water management practices. Improved understanding of the compounding stressors will be critical to devise an effective restoration process for implementation within a realistic timeframe. The remarkable contrast between lake level simulations under natural (i.e., excluding anthropogenic withdrawals) and existing conditions reveals the critical role of anthropocentric water management in creating this environmental catastrophe. The lake's severely disrupted water balance failed to rebound after the drought of record because the cumulative effect of the routine practice of increasing water diversions to keep up with growing upstream water demand acted as "the last straw that broke the camel's back." Our simulations show that by 1998, total water withdrawals in the basin had already overshot the basin's hydrologic capacity to sustain the lake, although in reality, water withdrawals continued to increase beyond 1998 levels. Even water withdrawals 40% lower than 2012 withdrawals (i.e., target withdrawal reduction for restoration) would not have been sufficient to prevent a significant decline in the lake level below the ecological level immediately after the drought of record, although the reduction would have markedly ameliorated the situation. Simulation results show that maintaining the lake's ecological level would have been attainable by keeping water withdrawals 55% lower than the 2012 levels.

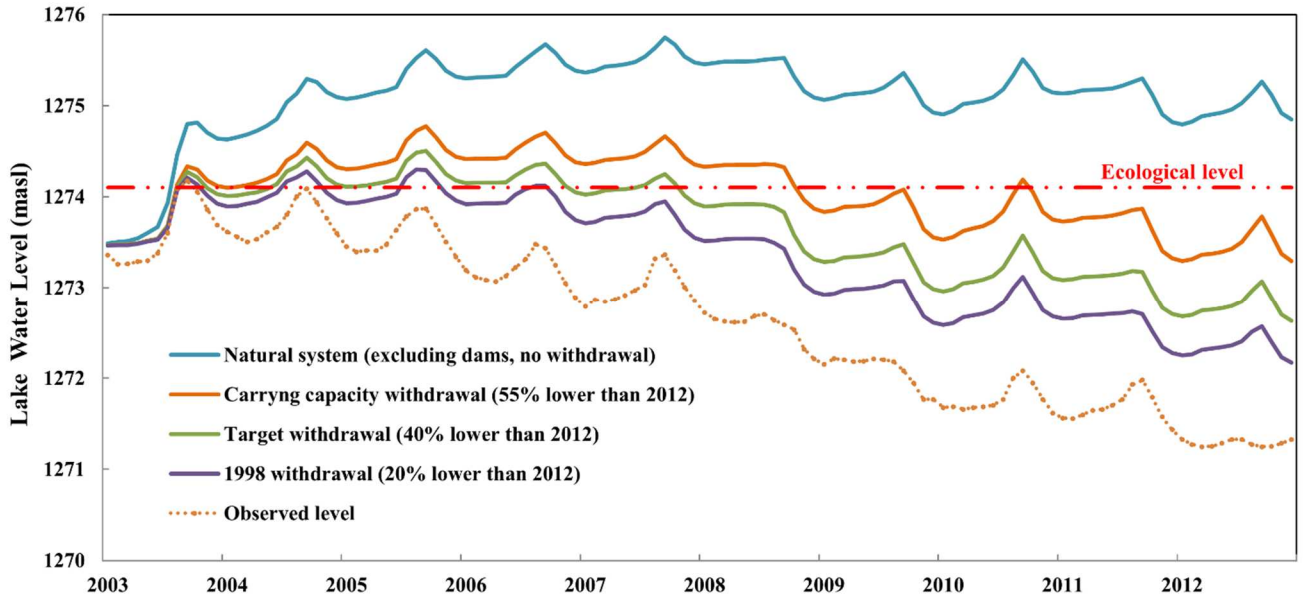

Figure 7. Lake Urmia level under different water withdrawal scenarios. The natural system simulation (i.e., no anthropogenic withdrawals) and different withdrawal scenarios illustrate the overshoot of the basin's hydrologic carrying capacity to sustain the lake due to anthropocentric water management after an extreme drought.

The key structural and non-structural restoration measures set forth by the ULRP include re-connecting the tributaries and the lake, major water transfers from trans-boundary river basins (e.g., Zab and Silveh Dam), limiting additional water withdrawal in the basin, and paying farmers to fallow the surrounding agricultural lands, among others (ULRP, 2016). Water conservation practices in various demand sectors across the lake basin will be crucial for moving in the direction of recovery and should be prioritized. This is particularly important based on the lessons learned from implementing various inter-basin water transfer projects to address water shortage problems in the central plateau of Iran, where the problems have persisted despite artificial increase of surface water supply (Gohari et al., 2013; Gohari et al., 2017). Adoption of low water consuming crops (e.g. grape) in the basin along with increasing irrigation efficiency with the ultimate goal of reducing net water consumption can facilitate the attainment of an ambitious 40% decrease in withdrawals as prescribed by the ULRP (ULRP, 2016).

Our analysis suggests that the Urmia Lake Restoration Program (ULRP) timeline is overambitious (Figure 8). Depending on climatic conditions and assuming effective implementation of the proposed 40% reduction in the current water withdrawal, the required environmental inflows range from 2900 mcm/yr (during dry conditions) to 5400 mcm/yr (during wet conditions) with the average being 4100 mcm/yr. Under a more realistic 20% water withdrawal reduction these values are estimated to range from 3100 mcm/yr (during dry conditions) to 4900 mcm/yr (during wet conditions) with the average being 4000 mcm/yr. Despite restoration efforts after 2013, the lake level in 2017 was more than 3m below the ecological threshold after reaching a post-collapse maximum of 1271.3 masl that has been attributed to implementation of a stabilization phase from 2014 to 2016, and large precipitation events in a relatively normal hydroclimatic period. Enforcement of the 40% decrease in agricultural water withdrawals through purchasing water rights within a five-year period starting in 2015 is a key measure of the ULRP during the rehabilitation phase (i.e., 2017-2022). Using the observed lake level in 2017 as the initial condition, we investigated the sensitivity of the lake's ecological level recovery timeline to reducing the agricultural water withdrawals by projecting lake level into the future under different climate scenarios. Figure 8 shows that under scenarios of increased aridity, when meeting the environmental inflow requirement of the lake will be difficult, restoring the ecological level can take up to 16 years, even if the proposed 40% reduction in agricultural water withdrawal is realized. Failing to reduce agricultural water withdrawals and/or providing the environmental inflows will result in delaying the attainment of the ecological level.

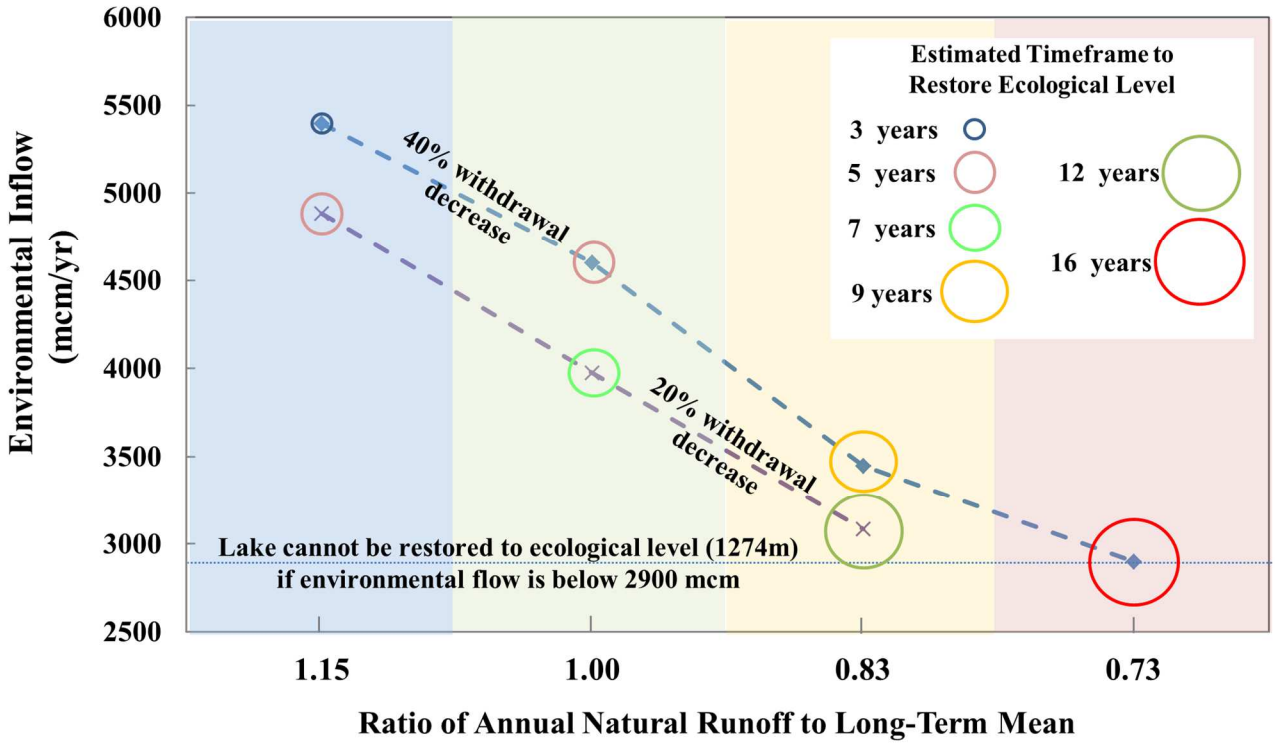

Figure 8. Environmental inflow along with estimated timeframe to restore to ecological level (1274 masl), considering 20% and 40% decrease in water withdrawals over the basin, given the initial lake level of 1270.7 masl. Long-term mean (i.e., 1967-2012) naturalized runoff in the Lake Urmia Basin is estimated at 6500 mcm/yr).

The lake is currently in grave need of receiving adequate environmental inflows. The natural flow regime (Poff et al., 1997) provides a theoretical framework for implementing ecosystem-based water management in the Lake Urmia sub-basins to mitigate adverse socio-ecological impacts. To this end the ULRP includes radical proposals to revive the lake, e.g., operating the reservoirs exclusively for lake restoration purposes, as well as improving the monitoring and regulation of surface water and groundwater withdrawals (ULRP, 2016). However, transitioning to an ecosystem-based water management paradigm by meeting dynamic environmental inflows in the Lake Urmia Basin is evidently difficult because of the presence of multi-sectoral tradeoffs (e.g., financial losses to stakeholders and population redistribution) that put the agricultural economy and socio-ecological sustainability at odds. On the one hand, the water resources that are exploited beyond the basin's natural supply capacity are supporting agrarian and urban livelihoods with significant green and blue water footprints (Hoekstra and Chapagain, 2006; Mekonnen and Hoekstra, 2011).

On the other hand, the loss of tourism (Maleki et al., 2018) and potential public health effects due to salt blowouts from the exposed lake bed (Griffin and Kellogg, 2004) are side-effects that have considerable socioeconomic implications. The high water stress even during wet periods underscores the prevalence of a chronic anthropogenic drought. To cope with this situation, investigating an "environmental hedging" approach guided by hydrologic and biologic forecasting (Adams et al., 2017) may offer a practical strategy to facilitate progress towards ecological recovery of the lake while meeting human demands within the constraints of basin scale water availability and ecological functions of Lake Urmia.

Conclusions

The Lake Urmia Basin in northwestern Iran is an exemplar of how unsustainable water management to meet growing water demand can create massive socio-ecological challenges. We developed a detailed water resources systems model of the basin to investigate the causes of Lake Urmia's shrinkage based on a quantitative assessment of the water balance under wet and dry periods and water withdrawal scenarios. Furthermore, we evaluated potential effectiveness of the planned restoration measures. Our simulations include comprehensive datasets of water resources management infrastructure (i.e., reservoir capacity and operating policies), observed streamflow data, and agricultural and urban water demand data from 117 sub-basins. Results demonstrate that a growing anthropogenic drought combined with meteorological drought drove the lake toward a state of hydrological overshoot and collapse. The rapid water level decline after the drought of record (1998-2002) when annual runoff decreased by 48% is synchronous with an approximately 25% increase in surface water withdrawals, especially in the agricultural sector, which continued long after signs of the lake's tipping phase appeared. The lake level remained significantly below the designated ecological threshold (1274 m above sea level) even in a relatively normal period

immediately after the drought. In the absence of the unsustainable water resources development and growing anthropogenic water stress, the lake would have resisted the climatologic shock without collapsing.

Re-establishing Lake Urmia's ecological integrity requires aggressive restoration policies and action plans aimed at maintaining environmental inflows in the face of compounding climate anomalies and water withdrawals. A dynamic and climate-informed environmental inflow plan is critical for reviving the lake. Taking into account both climatic conditions and assuming the already proposed 40% reduction in the current water withdrawals, we estimate that the lake's environmental inflow requirements range from 2900 mcm/yr (during dry conditions) to 5400 mcm/yr (during wet conditions) with the average being 4100 mcm/yr. These estimates for a more realistic 20% water withdrawal reduction would be 3100 mcm/yr (during dry conditions) to 4900 mcm/yr (during wet conditions) with the average being 4000 mcm/yr. Depending on the climatic condition, water withdrawal reduction plan, and environmental releases, Lake Urmia's recovery time can range from 3 to 16 years.

Chapter 3 Anthropogenic flood

The Tale of Three Floods: From Extreme Events and Cascades of Highs to Anthropogenic Floods

Overview

Flood damages are increasing globally as growing anthropogenic activities in floodplains and changing rainfall extremes raise the exposure of people and assets to flooding (Jongman, 2018; Paprotny et al., 2018; Ragno et al., 2018; Solomon et al., 2007; Winsemius et al., 2015; Youssef et al., 2011). The observed upward trend in flood damages is more pronounced in developing countries (Jongman et al., 2012; Seyedin et al., 2017) such as Iran where increased flood risk is closely associated with rapid development (Heidari, 2009; Norouzi and Taslimi, 2012; Razavi et al., 2020). Iran experienced floods of unprecedented spatial extent over a two-week period (March 17-April 1, 2019) when high precipitation occurred after a multi-year dry period in a vast area of the country (Dezfuli, 2020; Jaafari, 2019; Sharifi et al., 2012; Tabari et al., 2013), impacting 10 million people and causing 76 casualties and damages to 3800 cities and villages (France-Presse, 2019; Shahabi et al., 2020; Shokri et al., 2020; Yadollahie, 2019).

Similar to many other parts of the world, particularly in Africa and Asia (Chang et al., 2009; Jongman, 2018; Jongman et al., 2012; Smith, 2001; Youssef et al., 2011), flood damages in Iran have increased by about 250 percent during the past decades (Khosravi et al., 2016; Norouzi and Taslimi, 2012; Shabanikiya et al., 2014; Yari et al., 2019). The rising flood impacts are primarily attributed to anthropogenic activities such as increased exposure, urbanization, deforestation, and land use change (Alfieri et al., 2015; Alfredsen, 2017; Bronstert, 2003; Garner et al., 2015; Kjeldsen, 2010; Tehrany et al., 2015; Wheater and Evans, 2009), although increases in extreme rainfall events have also been reported globally (Change, 2012; Dettinger et al., 2016; Mallakpour et al., 2018; Pierce et al., 2013; Ragno et al., 2019; Read and Vogel, 2015; Swain et al., 2018; Vahedifard et al., 2017). In northern, western, and southern parts of Iran where the recent floods occurred, contributing river basins have undergone considerable urbanization, construction of dams and levees, land cover change (e.g., agricultural expansion), and deforestation, altering the basins' natural drainage capacity and river channels significantly (Heidari, 2009; Razavi et al., 2020).

Herein, we examine the potential causes of three different floods, including one single extreme event, one cascade of high events, and a non-extreme rainfall event, all leading to significant damages. Since flood formation depends on the dynamics of precipitation, soil moisture, and snow accumulation/melt, we initially discuss the causes of these events based on statistical analyses of ground-based rainfall data and satellite-retrieved data of snow cover (from Moderate Resolution Imaging Spectroradiometer, MODIS) and soil moisture (from Soil Moisture Active Passive, SMAP mission) – see the Data and Methods Section. To explore the change in the return period of the extreme rainfalls, we employ Process-informed Nonstationary Extreme Value Analysis

(ProNEVA (Ragno et al., 2019) – see the Data and Methods Section) that allows incorporating changing extremes in frequency analysis. Further, we investigate potential climatic indicators including shifts in precipitation timing and a transition to rain-over-snow to investigate their possible impacts on the severity of the resulting flood. To understand how these events turned into a disaster, we highlight some of the anthropogenic factors that exacerbated the flood impacts. We estimate the increasing deforestation rate in the Golestam Province based on MODIS land cover dataset, and quantify urbanization in the city of Shiraz, through a comparative rural-urban settlement classification model (GHS-SMOD), which integrates the degree of urbanization (DEGURBA) into the Global Human Settlement Layer (GHSL). The study demonstrates a critical need to revisit floodplain planning and development policies, as well as flood protection infrastructure maintenance under an uncertain future climate.

Results

Golestan Flooding

The first major flood event was caused by a series of frontal precipitation events (March 17-22, 2019) that affected northern parts of Iran("Floods Ravage Iran and Iraq," 2019). Some parts of Golestan Province received as much as 50% of the local mean annual rainfall in three days, e.g., 338 mm at TooskaChal Station; the largest daily (and even 3-day) rainfall accumulation on record in over 70 years of observations (Beitollahi et al., 2019b). Considering the Gorgan Gage Station data, while the 6-hourly annual rainfall maximum in 2019 was not an extreme event (approximately a 5-yr rainfall event), the daily annual rainfall maximum was significantly larger than the second most extreme observation (Figure 9). Using ProNEVA (Ragno et al., 2019), the

March 2019 extreme daily rainfall had a return period of 223 years (See Methods Section for details). If we exclude the March 2019 event from the rainfall frequency analysis, the event would have a return period of > 400 years. The March 2019 event increased the 100-year daily extreme rainfall from 117 mm/day to 127 mm/day (~ 8% increase in what was considered a 100-year event prior to March 2019). This highlights the significance of one single exceptional observation on the return period of extremes, which will have implications for flood protection infrastructure risk assessment (results from other gage stations with shorter records are presented in Appendix B, Figure S2).

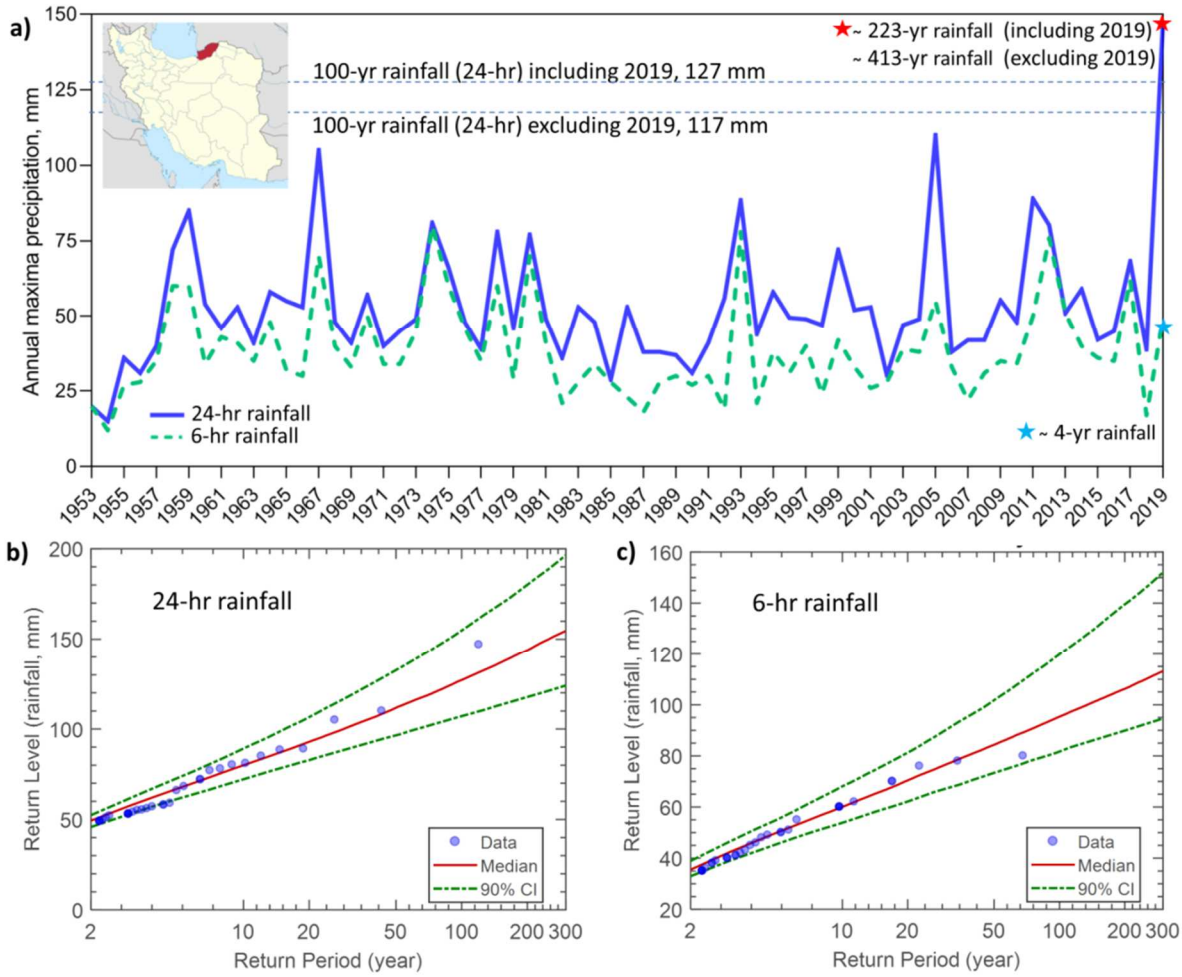

Figure 9 (a) Annual maxima precipitation (24-hourly and 6-hourly) at Gorgan Station; (b) 24- hourly and (c) 6- hourly return levels for different return periods. The median (solid red), 5th and 95th percentiles (dashed green) were derived based on the methodology described in Ragno et al. (2019).

On closer assessment, while the region's annual rainfall exhibits a downward trend, the annual rainfall maxima have an upward trend (significant at 0.02, Figure 10a). This indicates the occurrence of fewer wet years with intensified extreme events in the past decades, possibly due to intensification of the hydrologic cycle (Das et al., 2013; Milly et al., 2005; Pachauri et al., 2014; Wang et al., 2017). This observation is consistent with evidence from other parts of the world, indicating that rainfall extremes have intensified most likely in response to atmospheric warming

(Feng et al., 2016; Fischer and Knutti, 2016; Kunkel et al., 2013; Marvel and Bonfils, 2013; Min et al., 2011; Zhang et al., 2007).

A warming climate is also expected to have an impact on the timing of extreme precipitation (Blöschl et al., 2017; Change, 2012; Ficchì and Stephens, 2019; Merz and Blöschl, 2003; Parajka et al., 2010; Sarauskiene et al., 2015). Based on the long-term records at Gorgan Station, the annual maxima precipitation typically occurs between October to December (Figure 10b). However, the 2019 extreme precipitation event happened in late March, when on average only 7 % of the extremes occurred in the past. Rain-over-snow in the case of spring extreme rainfall events can exacerbate flooding potential through significant snowmelt. However, in this particular case, the rain-over-snow phenomenon is unlikely to have had a major magnifying effect on flooding since the snow cover of the region increased significantly during the event (Figure 10c). Thus, the delayed extreme precipitation in March 2019 reflects a late winter storm, the likes of which have been reported in other parts of the world such as the North Sea and the Mediterranean coast (Blöschl et al., 2017). In terms of extreme streamflow timing, the March 2019 flood in Golestan differs from GorganRood's damaging flash floods, which typically happen during summer (e.g., August 2001 causing 300 fatalities, August 2002, and August 2005 (Ardalan et al., 2009)).

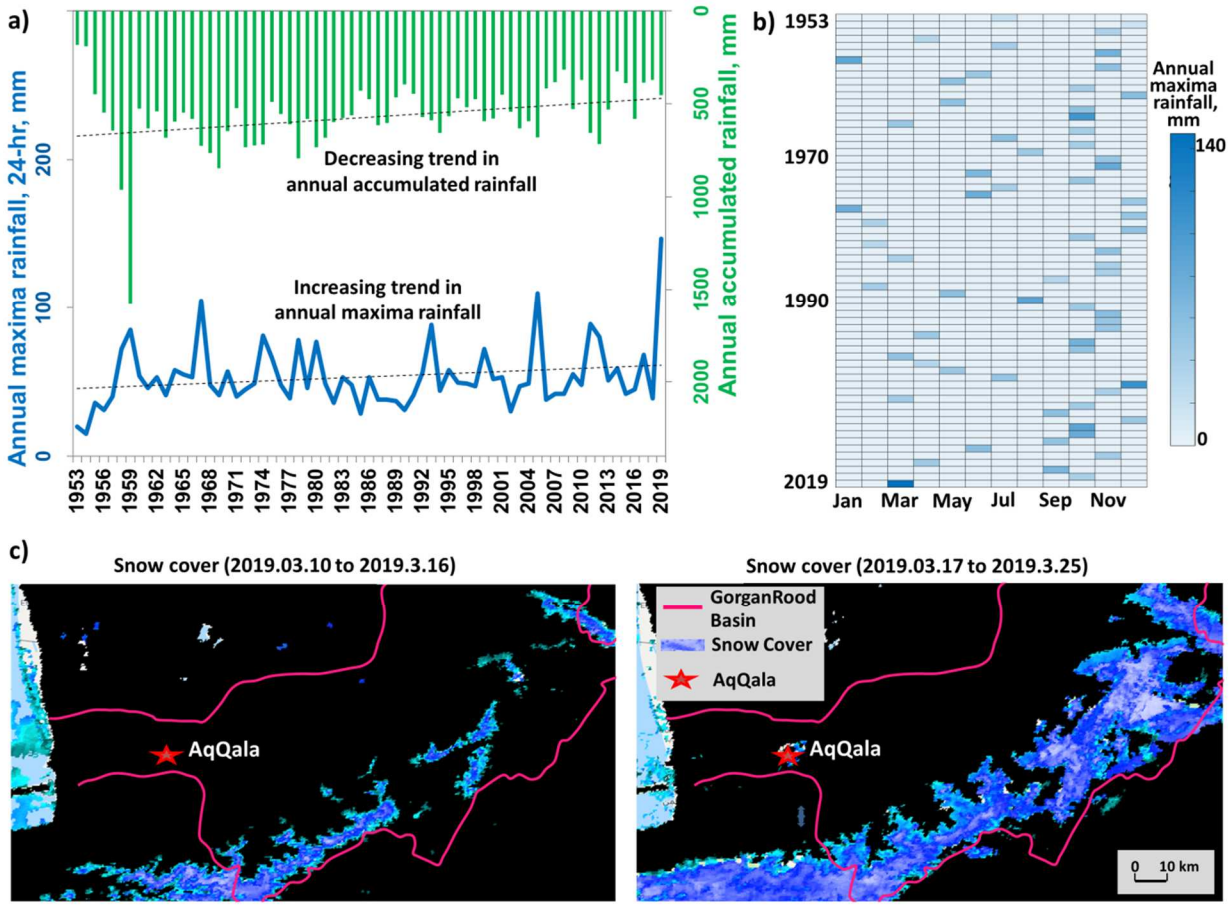

Figure 10 (a) Annual cumulative precipitation and daily annual rainfall maxima over time at Gorgan Station;(b) the months in which the daily annual rainfall maxima occurred; c) snow cover before (left) and after (right) the March 2019 heavy precipitation in Golestan Province.

Although the 2019 rainfall event was indeed an extreme (return period more than 200 years), we contend that the flooding in Golestan was exacerbated by anthropogenic activities, primarily deforestation and poor disaster management. Deforestation has intensified over the past decades in the northern parts of Iran, including Golestan, due to urbanization and agricultural expansion (Jaafari et al., 2014; Khosravi et al., 2016; Kiani et al., 2004). Using Moderate Resolution Imaging Spectroradiometer (MODIS) 500-meter satellite-based land cover data (Parker et al., 2003), we estimate Golestam Province's deforestation between 2006 and 2016 to be about 11%, which is approximately 300 km^2 (Figure 11). The effects of deforestation on intensification of floods have

been documented in numerous publications (Bronstert, 2003; Mahtab and Karim, 1992; Marengo and Espinoza, 2016; Sternberg, 1987; Tan-Soo et al., 2016).

Some short-term management decisions may have also contributed to the severity of the Golestan flooding. The reservoirs in the region (e.g., Golestan Dam) were nearly full even two weeks prior to the flood event. Given the previous droughts, reservoir operation in the region primarily focused on storage conservation rather than making releases to increase flood storage capacity. In fact, at least three regulating dams in the GorganRood Basin (i.e., Voshmgir, Golestan, and Bostan) were operating higher than the flood control zone (up to 154% of the sum of dead, active, and flood storages) during the 2019 flood (Beitollahi et al., 2019b). We postulate that this may have intensified the effect of flooding downstream of the dams when large releases were finally made to accommodate the incoming flood. We note that the March 2019 flood in Golestan was quite vast in spatial scope (see Figure S1 in Appendix B). The water pools remained in the downstream inundated areas for weeks after the event. The Sentinel satellite images (Figure S1) show flood inundation 5 days after the event in AqQala; the most affected city. Incorporating rainfall and flood forecasts in reservoir management, could have partially reduced the inundation and associated impacts.

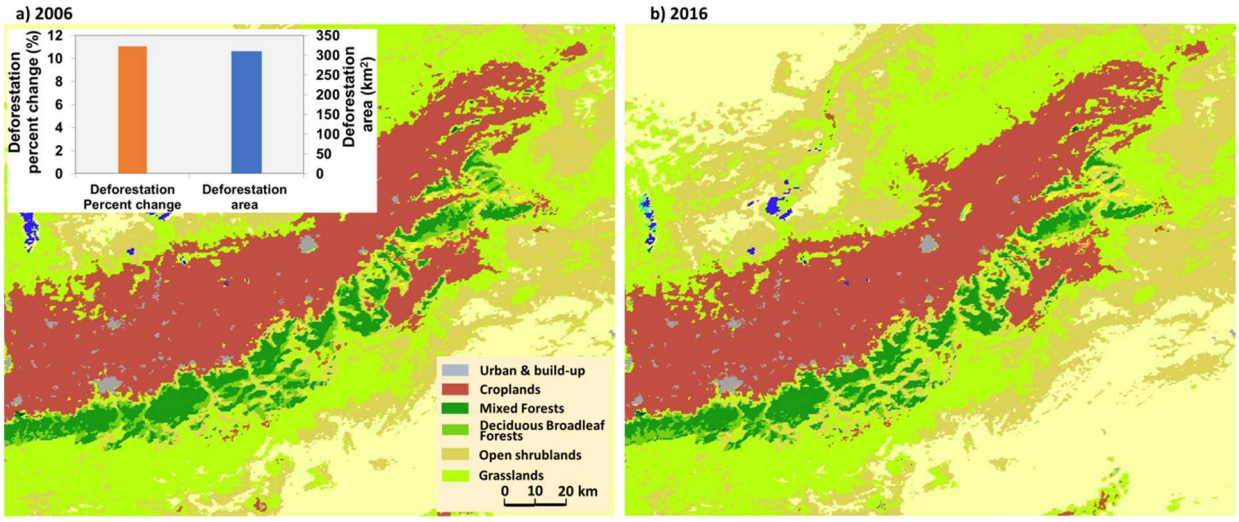

Figure 11. Land cover types in Golestan Province showing significant deforestation over a 10-year period. The dark and light green regions display the mixed and deciduous broadleaf forests' surface area (canopy >2m) in 2006 (a) and 2016 (b) based on NASA's MODIS data. The bar chart depicts deforestation percent change (orange bar) and deforestation area in km^2 (blue bar) in 2016 relative to 2006.

Shiraz Flooding

A devastating flash flood (50 cubic meters per second (cms)) hit the fifth most populated city of Iran on March 25, 2019, leading to the highest flood-driven fatal loss in the city of Shiraz in the past decades (2019). Although the bare and steep mountain hills (slopes up to 60%) of the small-scale Darvazeh Quran basin (24 km^2) potentially triggered flash flooding during the short-duration intense rainfall, several man-made changes greatly altered the hydraulic behavior of this catchment (AbZangi) and the corresponding main water basin of Khoshk River (Beitollahi et al., 2019a; Zare and Talebbeydokhti, 2018). The Khoshk River in Shiraz experienced several major floods during Fall 1986, Winter 1993, and Spring 2002; however, no severe flood had been previously recorded in the small Darvazeh Quran Catchment with an ephemeral channel. Based on ProNEVA and the Generalized Extreme-Value (GEV) distribution, both daily and 6-hourly annual rainfall maxima in 2019 were not extreme events (approximately less than a 5-yr rainfall event, Figure 12). This

reinforces the hypothesis that human-induced changes in the basin caused a record flood event in Shiraz (with a long-term mean precipitation of 344.2 mm) despite the non-extreme nature of the March 2019 rainfall. To quantify the process of urbanization in the Darvazeh Quran Catchment, we further employed a comparative rural-urban settlement classification model (GHS-SMOD, Figure 13) (Englhardt et al., 2019; Melchiorri et al., 2018). The urban-rural area associated with the Darvazeh Quran Catchment increased about 8 km^2 in the time span of 1975 to 2015, which accounts for almost one third of the entire basin creating favorable conditions for a flashy hydrograph, characteristic of severely urbanized catchments.

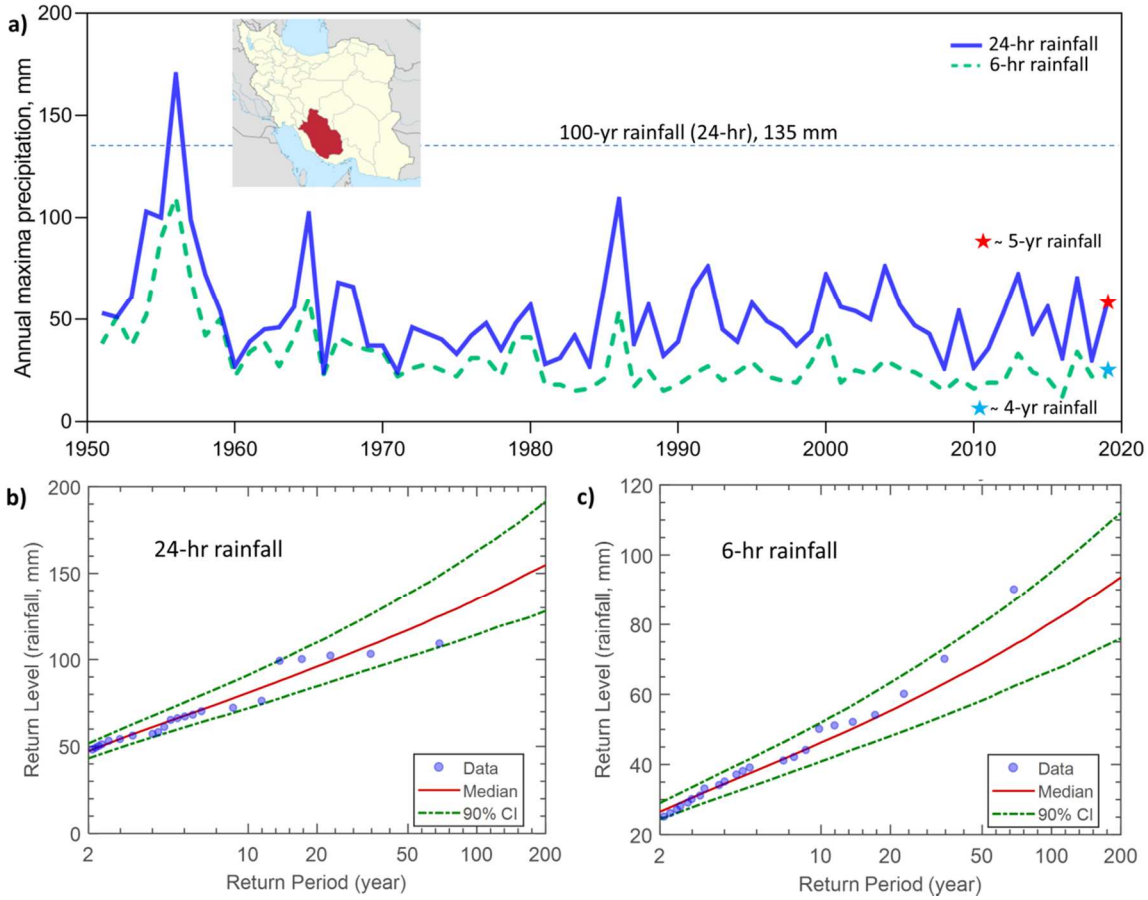

Figure 12. (a) Annual maxima precipitation (24-hourly and 6-hourly) at Shiraz Station. (b) 24- hourly and (c) 6- hourly return levels for different return periods. The median (solid red), 5th and 95th percentiles (dashed green) were derived from ProNEVA (Ragno et al., 2019).

The most significant change in the basin, however, occurred in the 1980s, when the ephemeral river canyon was filled and replaced with a 1.5 m diameter concrete pipeline to construct a road project (Beitollahi et al., 2019a). Draining the stormwater is critical because of the basin's collecting pool is located about 300 m upstream of the Darvazeh Quran Monument (Beitollahi et al., 2019a) – one of the main entrances of the city and a tourist attraction on a major transportation route. The 2019 flood discharge surpassed the 12-cms maximum capacity of the pipeline and created a catastrophe. Flood losses due to substituting natural river canyons with much smaller artificial conduits had happened previously in the 2002's Shiraz flood over the main basin of Khoshk River (Zare and Talebbeydokhti, 2018). The 2019 incident provides a clear evidence for the need to re-evaluate flood hazard in development projects in these flood-prone areas, and possibly modify the flood protection infrastructure in Shiraz and similar areas, especially in environments where the natural landscape has been drastically altered.

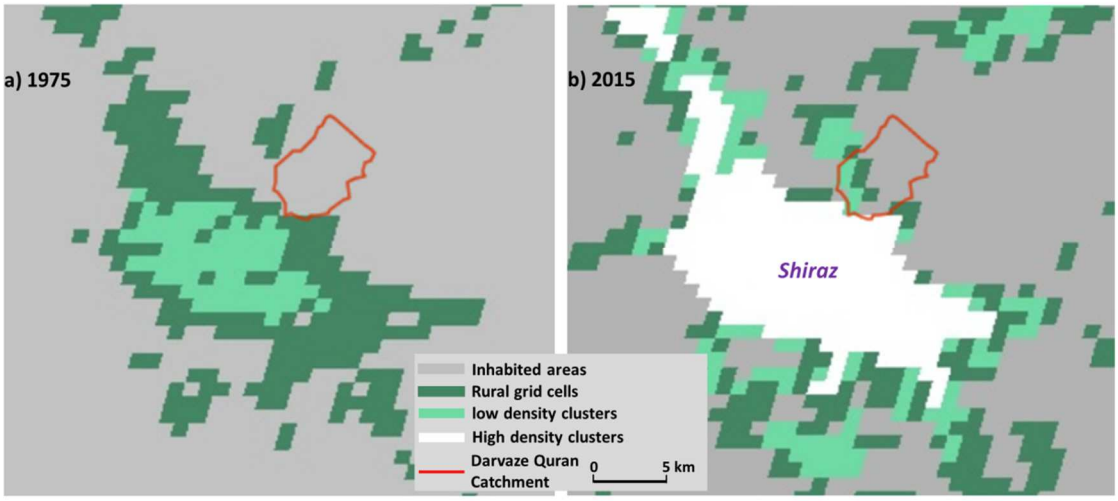

Figure 13. Degree of urbanization in the city of Shiraz for reference epochs: (a) 1975 and (b) 2015 based on comparative rural-urban Settlement classification MODel (GHS-SMOD). Red solid line shows the Darvazeh Quran Catchment where the March 2019 flood occurred before the basin outlet.

Lorestan Flooding

In the western-southern region of Iran, a frontal precipitation system caused extreme flood events on April 1, 2019 in two important river basins (Karkheh and Karoon Basins). The severe flooding occurred soon after a prior heavy rainfall event in the same region on March 25 (the same event that caused significant damages in Shiraz discussed in the previous section). The most significant impacts were observed in KhorramAbad, PolDokhtar, and Mamulan located in the Lorestan Province upstream of the strategic Karkheh Dam.

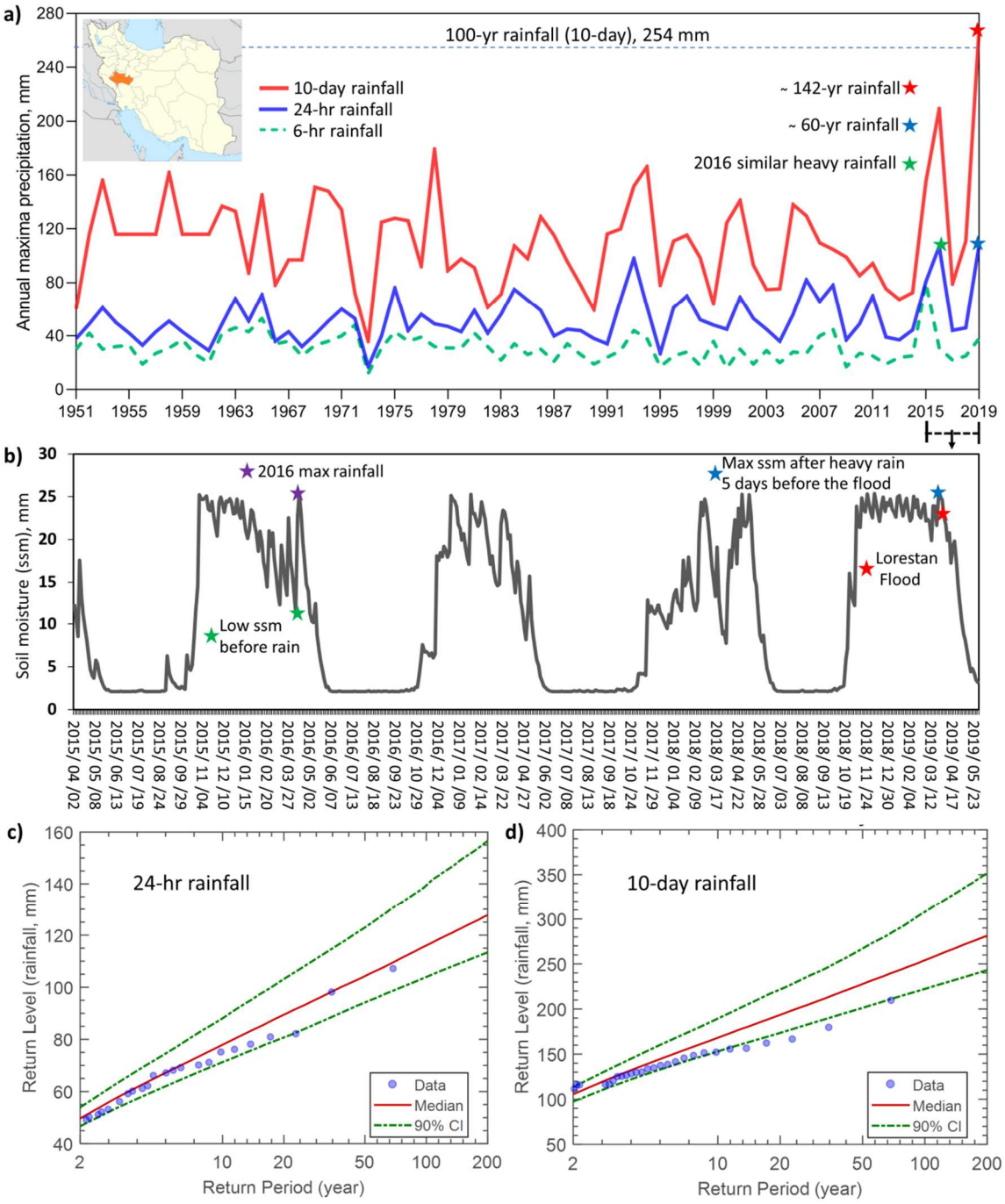

Figure 14. (a) Annual maxima precipitation (10-day, 24-hourly, and 6-hourly) at KhorramAbad Station; (b) Surface soil moisture (mm) during 2016 and 2019 heavy precipitation events from the NASA-USDA SMAP Global soil moisture dataset at 0.25°x0.25° spatial resolution; (c & d) 24-hourly (left) and 10-day (right) return levels for different return periods. The median (solid red), 5th and 95th percentiles (dashed green) were derived from Ragno et al. (2019).

To identify the main natural drivers of the flood, we explored long-term hourly to 10-daily extreme precipitation and the influence of 2019 precipitation events on snow cover and soil moisture change in the region. The 6-hourly annual rainfall maximum in 2019 at the KhorramAbad Station (Figure 14) was not an extreme event (approximately a 5-yr rainfall event) based on the extreme value theory (see the Methods Section). The daily annual rainfall maximum (approximately a 60-yr event), however, was the largest on the historical record (1951-2019). It is worth noting that similar rainfall magnitudes were previously recorded at the KhorramAbad Station. For example, the daily annual rainfall maximum back in 2016 was almost the same as that of 2019. However, the 10-daily annual rainfall maximum in 2019 appears to be a 142-year event – significantly larger than the second most extreme 10-day observation (April of 2016). Nearly saturated antecedent soil moisture condition due to the extreme rainfall (e.g., 108 mm in PolDokhtar City) five days prior to the April 1st flooding is deemed to have resulted in a much larger runoff volume in the latter flood event. NASA Soil Moisture Active and Passive (SMAP (Brown et al., 2013; Entekhabi et al., 2010; Massari et al., 2018)) soil moisture observations (Figure 14b) confirm elevated levels of soil moisture prior to the April 1 flood in Lorestan. Figure 14 highlights the cascading effect of two back-to-back rainfall events with an approximate return period of 60-yr (5 days apart) leading to the region's most significant flood on record (Figure S2).

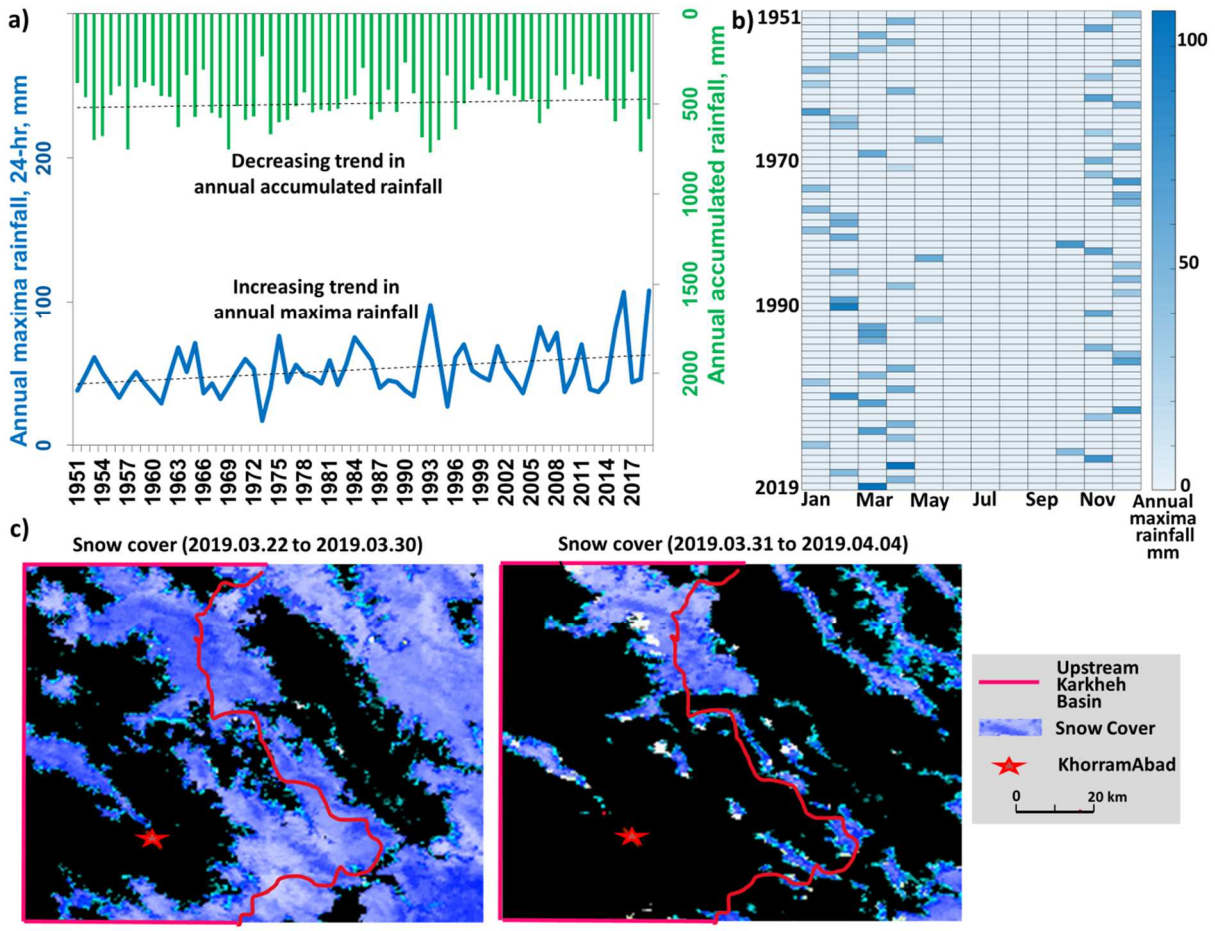

Figure 15. (a) Annual cumulative precipitation and daily annual rainfall maxima over time at KhorramAbad Station; (b) The months in which the daily annual rainfall maxima occurred. (c) Snow cover before (left) and after (right) the late March 2019 heavy precipitation in Lorestan (2019/03/22-2019/03/30 and 2019/03/31-2019/04/05).

The upward trend detected in the annual rainfall maxima at the KhorramAbad Station (significant at 0.04, Figure 15a) indicates intensification of extreme precipitation events in the past decades. With respect to the timing of the annual rainfall maxima, the late March 2019 extreme precipitation event happened within the period (February to April) annual maxima typically occurs (Figure 15b). We further explore the snow cover change obtained from the NASA's MOD10A1 V6 daily global snow cover dataset at 500-m spatial resolution (Figure 7c) because rapid loss of snow (e.g., due to rain-over-snow or rapid warming) can be a major flood driver in snow dominated regions like

Lorestan. Substantial decrease in the snow cover before and after the flood suggests that rain-over-snow likely led to rapid snowmelt, which intensified the flood (PolDokhtar: 5000 cms (MohebZade Fattahi, 2019)) (Figure 15c). This may reflect the rise in earlier spring snowmelt floods that have been observed in other regions such as northeastern Europe (Blöschl et al., 2017), central US (Smith and Schwartz, 2019), and California (Pierce et al., 2018; Vahedifard et al., 2017) due to either an earlier snowfall-to-rain transition or higher spring temperatures.

Discussion

Iran's spatially-unprecedented floods of 2019 demonstrate the critical importance of periodic updating of flood hazard assessments (e.g., changes in 100-yr rainfall/flood return levels) and flood mapping based on improved understanding of the biophysical determinants of runoff generation coupled with analysis of human impacts on the floodplain. Flood frequency analyses will benefit from including new extreme rainfall and flow data as they become available to support flood-resilient infrastructure development and management. Following a multi-year dry period, a series of severe flood events in the course of two weeks (late March and early April 2019) devastated several urban and rural areas across Iran, in some cases strictly due to poor floodplain development.

Although intense storms and prolonged dry spells are not unusual because of the semi-arid nature of the region (Melville, 1984), changing climatic conditions may have contributed to the observed extremes (Jaafari, 2019). Furthermore, the human footprint is a major factor in the recent floods (e.g., deforestation, urbanization). Our analysis of hydro-climatological factors (e.g., precipitation,

snow cover, and soil moisture) and anthropogenic drivers (e.g., land cover change) shows that statistically different precipitation events (from a 5-yr to a 223-yr event) resulted in the most extreme impacts (with respect to damage and loss of life) associated with the least extreme event in a place where man-made changes played the most significant role (Table 2). We broadly define such events as *Anthropogenic Floods* to underscore the role of humans in addition to climatic and meteorological drivers.

Other than the exceptional magnitude of the 2019 Golestan rainfall (223-year event), this flood differs from the previous damaging floods in terms of the spatial extent and timing of the flood. The recent event covered almost the entire GorganRood Basin (~11380 km^2), exhibiting a delayed precipitation timing compared to the recorded historical midsummer flash floods. Because of the delayed rainfall timing from fall to late March, the extreme rainfall happened when the reservoirs in the region (e.g., the Golestan Dam) were nearly full prior to the flood event (Jalili and Fekri, 2020). In the luxury of hindsight and based on the recorded historical flood discharges in Golestan (e.g., 3017 cms in 2001 (Sharifi et al., 2012)), we postulate that the 2019 flood peak of 830 cms (Beitollahi et al., 2019b) would have been partially manageable if the reservoir operation policy had been shifted in a timely manner to handle an extreme rainfall event after a prolonged dry spell. The flood damages could have been reduced with forecast-informed reservoir management. The extent of human footprint in influencing the flood severity is also remarkable. Flood water pools in the area did not drain even weeks after the disaster, causing a long-lasting, wide-spread inundation downstream of the reservoir. Using land cover satellite observations, we estimated 11% deforestation in the flood-affected areas from 2006 to 2016, indicating that anthropogenic deforestation and construction along rivers intensified the flood impacts in the Golestan Province.

Table 2 Anthropogenic and hydro-climatic drivers contributing to the devastating floods of 2019 in Iran.

Location	Date	Return period of precipitation* (years)	Anthropogenic drivers	Hydro-climatic drivers
Golestan	March 17 to 22	223	- Deforestation (about 11%) between 2006 and 2016. - Nearly full reservoirs prior to the 2019 flood for storage conservation after the previous droughts. - Poor disaster management by diverting the river overflow to a place that caused vast inundation downstream.	- Extreme precipitation event. - Late winter storm as compared to previous summer flash floods.
Shiraz	March 25	5	- Replacing river canyon with a 1.5 m diameter concrete pipeline to construct a road project.	- The bare and steep mountain hills (slopes up to 60%).
Lorestan	April 1	60 years for daily 142 years for 10-daily	- Flood zone urbanization.	- Cascade of high precipitation events. - Rain-over-snow causing earlier spring snowmelt.

* Return period of daily annual rainfall maximum derived from ProNEVA (Ragno et al., 2019).

In March 2019, a non-extreme rainfall event over a short period of time became the deadliest flood of Shiraz, creating chaos at one of the main entrances of the city (Darvazeh Quran). Utilizing ProNEVA for frequency analysis, we show that the 2019 flood was caused by approximately a 5-yr rainfall event. Flash floods are to be expected in this small watershed because of the lack of vegetation cover and relatively high slope. However, drastic alternations to the river canyon caused a considerable decline in the natural flood conveyance capacity of the basin outlet. The catastrophic flood damage and fatalities were caused by the failure of a severely undersized pipeline (12-cms maximum capacity), which could not pass the 2019 flood peak discharge (50 cms). Replacing the natural open channel in the 1980s for road-widening purposes is an unequivocal evidence of human encroachment of the natural floodplain. Consequently, the risk of

flooding rose because of anthropogenic factors where a non-extreme rainfall caused an extreme flood.

The largest observed discharges on record in Lorestan Province, were experienced at various river reaches during the 2019 flood upstream of the Karkheh Basin. Our investigation of the interplay of precipitation, snow cover and soil moisture illustrates that the cascading effect of immediate drivers intensified the resulting flood. The 10-daily annual rainfall maximum in 2019 was significantly higher than the second most extreme observation (return period of 142-year). Five days prior to the destructive flood event in Lorestan, the region received an intense precipitation on March 25, which reduced infiltration by saturating the soils (from NASA SMAP), ultimately leading to a cataclysmic flood. The substantial decrease in snow cover in the region after the flood indicates rapid snowmelt triggered by rain-over-snow likely intensified the flood. The two back-to-back rainfall events with an approximate return period of 60-yr exposed the vulnerability of human settlements to flooding under cascading hydro-climatologic effects. Further, the flooding was worsened by significant man-made changes along the rivers in urban areas, creating constrictions (e.g., dykes and buildings) that reduce flood conveyance capacity of the natural channel cross-sections. The combination of these adverse impacts should be taken into account to improve understanding and characterization of flood risks to inform infrastructure development and maintenance, and disaster management.

Our analysis reveals several takeaways pertinent to the interlinked hydro-climatic drivers and anthropogenic catalyzers of flooding. The upward trend detected in the annual rainfall maxima dataset suggests that extreme precipitation events have intensified in Lorestan and Golestan Provinces. In Lorestan, the cascading effect of two intense rainfalls (5 days apart) and early rain-

over-snow resulted in a massive flood. Shifts in rainfall timing resulted in an unseasonably large rainfall that was not expected. These incidents urge revisiting development planning policies for flood management based on the changing characteristics of extremes and associated vulnerability implications. The risk of flooding for loss of life and assets has been remarkably raised by man-made changes to river basins to the point that some urban areas are particularly vulnerable to anthropogenic floods (e.g., Darvazeh Quran Catchment in Shiraz, Fars Province, Iran). We illustrated how spring 2019 flood impacts in Iran were exacerbated by various human-induced changes, including construction along rivers, deforestation, aggradation, natural channel constriction, and poorly sized water conveyance structures. It is necessary to rethink urban planning and floodplain management in light of increased flood risks due to changing extreme events and cascading hydro-climatological effects compounded with growing exposure and severity of flood incidents in urbanizing areas.

Data and Method

The three study areas include Golestan Province, city of Shiraz, and Lorestan Province. We assessed ground-based data on precipitation and satellite observations on snow cover, soil moisture level, land cover type, and degree of urbanization. The 3-hourly precipitation datasets were obtained from synoptic stations of Iran Meteorological Organization with nearly 70 years of records, allowing us to evaluate the climatologic patterns of the extremes. The post-processed satellite imageries are derived from the Google Earth Engine (GEE) platform, which provides global-scale and web-based remote sensing products (Gorelick et al., 2017). A brief description of the satellite imagery used in this study along with the Nonstationarity Extreme Value Analysis employed for precipitation frequency analysis are shown below.

Satellite observations

Land cover data: Extensive land use changes have transformed the natural landscapes to other land use/cover types (e.g., agricultural, urbanization (Kasperson et al., 1995)). The MODIS collection 6 land cover type product (MCD12Q1 V6) classifies land use type at a 500-m spatial resolution (Friedl et al., 2010). To assess land cover change (deforestation) in Golestan Province, we used the IGBP (International Geosphere–Biosphere Programme) land cover classification scheme which has 17 cover classes. On the Google Earth Engine (GEE) platform, MODIS MCD12Q1 V6 product provides land use/cover data from 2001 to 2016 at annual time steps (Belward et al., 1999; Loveland and Belward, 1997).

Comparative rural-urban settlement: To estimate the degree of urbanized/industrialized landscapes in Shiraz, we employed the JRC's Global Human Settlement Layer (GHSL), which is available in GEE (Corbane et al., 2020). This rural-urban settlement classification MODel integrates the degree of urbanization (DEGURBA) concept into the GHSL. Using a clustering algorithm, each grid has been generated for reference epochs of 1975, 1990, 2000, 2015 at a resolution of 1 km². The three main classes include 'high density clusters (HDC)', 'low density clusters (LDC)', and 'rural grid cells (RUR)'.

Soil moisture: We used surface soil moisture data from the NASA-USDA SMAP Global soil moisture dataset at 0.25°x0.25° spatial resolution (Bolten et al., 2009; O'Neill et al., 2016). This global soil moisture dataset provides the surface and subsurface soil moisture (mm), soil moisture profile (%), and surface and subsurface soil moisture anomalies. Available on GEE, this product

integrates satellite-derived Soil Moisture Active Passive (SMAP) Level 3 soil moisture observations into the modified two-layer Palmer model using a 1-D Ensemble Kalman Filter (EnKF) data assimilation approach.

Snow cover: To estimate the change in snow cover in Lorestan, we used the MOD10A1 V6 Snow Cover Daily Global 500m product (Hall et al., 2006). The dataset contains snow cover data which is based on a snow mapping algorithm that employs a Normalized Difference Snow Index (NDSI). The available snow information includes snow cover, snow albedo, fractional snow cover, and quality assessment (QA) data.

Nonstationarity Extreme Value Analysis using ProNEVA

We first utilized the annual block maximum sampling technique to extract the maximum 6-hourly, daily, and 10-day rainfall for each year in a number of rain gage stations. Then, we fit the GEV distribution to estimate the rainfall frequency distribution using Process-informed Nonstationary Extreme Value Analysis (ProNEVA (Cheng et al., 2014; Ragno et al., 2019)). ProNEVA employs a generalized framework for considering nonstationarity assumption in the analysis of climatic extremes, including potential changes in the frequency and variability of extreme events. This framework allows nonstationary analyses employing user-defined covariates, which could be temporal or process-based (i.e., a physical driver such as urbanization or CO_2 emission). ProNEVA offers parameter estimation, uncertainty quantification, and a comprehensive assessment of the goodness of fit. In the study, based on statistical significance trend test, either stationary or nonstationary GEV distributions were fit to each block maxima series.

Generalized Extreme Value (GEV)

The GEV distribution is widely used to model time series of block maxima, such as deriving precipitation Intensity-Duration-Frequency (IDF) curves (The National Oceanic and Atmospheric Administration (NOAA)). The GEV cumulative distribution function is (Coles et al., 2001):

$$\Psi_{GEV}(x) = exp\{-\left(1 + \xi \cdot \left(\frac{x-\mu}{\sigma}\right)\right)^{-\frac{1}{\xi}} \quad (1)$$

The GEV distribution has the location parameter (μ), the scale parameter (σ), and the shape parameter (ξ) to specify the center of the distribution, the deviation around the center, and the tail behavior of the GEV distribution, respectively (Renard et al., 2013).

Under a nonstationary assumption, however, the parameters of the underlying distribution function are time-dependent, and the properties of the distribution would therefore vary with time. This means, we let the parameters of the distribution be a function of a general covariate x_c, i.e., μ (x_c), σ (x_c), ξ (x_c) (Coles et al., 2001). Hence, the nonstationary form of eq. 1 is:

$$\Psi_{GEV}(x|x_c) = exp\{-\left(1 + \xi(x_c) \cdot \left(\frac{x-\mu(x_c)}{\sigma(x_c)}\right)\right)^{-\frac{1}{\xi(x_c)}} \quad (2)$$

σ (x_c) functions in the log scale for the positivity of the scale parameter (Coles et al., 2001; Katz, 2013). As a result, the exponential function is not available for σ (x_c). For the shape parameter ξ (x_c), a linear function is considered (Coles et al., 2001).

Parameter estimation: Bayesian analysis and Markov chain Monte Carlo sampling

A Bayesian approach is integrated into the nonstationary GEV for uncertainty assessment (Stephenson and Tawn, 2004). This approach combines the knowledge brought by a prior distribution and the observation vector of annual maxima into the posterior distribution of parameters (Cheng et al., 2014; Luke et al., 2017; Sadegh et al., 2018, 2017; Thiemann et al., 2001). Assuming independence between observations, the Bayes theorem for estimation of GEV parameters under the nonstationary assumption can be expressed as:

$$\mathrm{p}\left(\theta\middle|\tilde{\mathrm{Y}}\right) \propto \prod_{\mathrm{i}=1}^{\mathrm{n}} \mathrm{p}(\theta)\,.\,p(y_i|\theta) \qquad (3)$$

Where θ is the parameter of a given distribution and let $\tilde{\mathrm{Y}}= \{\tilde{y}_1, \ldots, \tilde{y}_{n1}\}$ be the set of n observations. Following Bayes theorem, the probability of θ given $\tilde{\mathrm{Y}}$ (posterior) is proportional to the product of the probability of θ (prior) and the probability of $\tilde{\mathrm{Y}}$ given θ (likelihood function). The posterior distribution is then delineated using a hybrid-evolution MCMC approach proposed by Sadegh et al. (2017). The MCMC simulation searches for the region of interest with multiple chains running in parallel, which share information on the y.

Model diagnostics and selection

The goodness of fit (GOF) assessment in ProNEVA includes: quantile and probability plots for a graphical assessment, two-sample Kolmogorov-Smirnov (KS) test, Akaike Information Criterion (AIC), Bayesian Information Criterion (BIC), and Maximum Likelihood (ML). The hybrid-evolution MCMC approach (Sadegh et al., 2017) within the Bayesian framework provides an ensemble of solutions for the (non)stationary statistical model fitted to the data. ProNEVA uses

the best set of parameters which maximizes the posterior distribution. Marginal posteriors will then provide uncertainty estimates of the parameters.

Return level curves under nonstationarity

Extreme event intensity is expressed as a function of the return period (i.e., the average length of time between events of a given depth/intensity and duration). The Return Level (RL) expresses the quantile Q_i for which the probability of an annual maximum exceeding the selected quantile is q_i (Cooley, 2013). The quantile Q_i is the value of intensity such that $Pr(P \geq Q_i) = 1-F_P(Q_i)$, where F_P is the probability distribution of the annual maxima of intensities. In the stationary analysis, the probability q_i of the quantile Q_i does not change on a yearly basis. The Return Period (RP) of the quantile Q_i is defined as the inverse of its exceedance probability, $T_i = 1/q_i$ in years. The RL curves are defined by the following points under the stationary assumption:

$$(\,(\mathrm{Ti};\ \mathrm{Qi}),\quad \mathrm{Ti} > 1\quad \mathrm{yr},\quad \mathrm{i} = 1,\cdots) \tag{4}$$

In a nonstationary assumption, ProNEVA integrates two different proposed concepts to account for ambiguous terms of RP and RL (Cooley, 2013): the expected waiting time (Salas and Obeysekera, 2014), and the effective RL curves (Katz et al., 2002).

Explanatory Analysis: Mann-Kendall and White Tests

ProNEVA utilizes the Mann-Kendall (MK) monotonic trend test and the White Test (WT) for evaluating homoscedasticity in the datasets. Based on the statistical significance trend test, then the user can decide whether to incorporate a trend function in one or more of the model parameters or not.

Chapter 4 Anthropogenic Climate Change

Integrating Future Climate Information into Engineering Design Concepts

Overview

Extreme weather events have posed a major threat to engineering practices operating in the energy, transportation, and construction systems (NCA4, 2018; FEMA, 2016; Neumann et al., 2015; Aghakouchak et al., 2017; CACC, 2018; Moftakhari et al., 2017). The variability in magnitude and frequency of climatic hazards (i.e., floods, droughts, and hurricanes) has undermined the integrity of critical infrastructure such as power transmission lines, regional road networks, and levees (e.g., Das et al., 2013; 72 Milly et al., 2005; Pachauri et al., 2015; Voss et al., 2002; Wang et al., 2017 ; Friedman & Schwartz, 2017; McGrath, 2019; Mooallem, 2019; Otto et al., 2020). For example, in 2017, a series of extreme precipitation events, following a prolonged drought, in northern and central California caused a structural failure of Oroville Dam's spillway, forcing vast evacuations (National Climate Data Center, 2017; Vahedifard et al., 2017). More recently, extreme events resulted in vast flooding in the Midwest during the spring of 2019, which caused damages of approximately $20 billion. The ongoing sea level rise along with the intensified precipitation extremes have elevated the coastal and inland flooding risk. (Hallegatte et al., 2013; Neumann et al., 2015; Willis et al., 2016; Buchanan et al., 2017; Jongman et al., 2012; Vitousek et al., 2017;

IPCC 2012; Read and Vogel, 2015, Dettinger et al., 2016; Jasim et al., 2017; Mallakpour et al., 2015, Peirce das, 2013; Groisman et al., 2005). Additionally, human activities (e.g., land use changes) have magnified flooding events in many regions, increasing the impact of flood-related damage (Pielke et al., 2002; Hirsch & Ryberg, 2012; Villarini et al., 2009; Yang & Hill, 2012; Vogel et al., 2011; NCEI, 2020).

Consistent with the observed increasing trend, climate models also project increases in the intensity and/or frequency of climatic extremes, attributed in part to the co-evolution of anthropogenic emissions with land use and land cover changes (e.g., 30–90% increase in streamflow in Northern Sierra Nevada Das, Peirce, 2013; Zbigniew, 2014; Seneviratne et al. 2012; Trenberth, 1999, Milly et al., 2002, Kunkel et al., 2013). A number of studies have examined the changing patterns of extremes to predict the expected changes in the their likelihood and return intervals in the future (ASCE, 2015; Forzierli et al., 2018; Grmany, 2017; Hagenlocher, 2018; DFID, 2005; World Bank, 2006; EEA,2007; UNDP, 2007; WRI, 2007). However, infrastructure design, maintenance, operation, and regulatory standards currently do not account for the new patterns of extremes under a changing climate (CACC, 2018; Hu, 2018). Any changes in the statistics of extreme events will directly impact the overall stability and reliability of the infrastructure. This study's overarching goal is to combine climate information with structural performance to argue that infrastructure should be designed to withstand the growing risk of extreme events. As the future unfolds, decision-makers must adapt their plans and respond to new conditions (e.g., extremes that have never happened before). This direction would help evolve the infrastructure risk management conversation from understanding future hazards to discovering and acting on decision-relevant consequences and adaptive decision pathways.

We propose a theoretical framework (Figure 16) for integrating future climate information and the underlying uncertainty into the planning of flood protection infrastructure such as a levee. Specifically, the proposed study strives to achieve two main objectives: (a) Advance how engineering requirements and design constraints are determined in a rapidly changing climate. This includes identifying current and future climate hazards and estimating their likelihood of occurrence (b) Quantify engineering infrastructure vulnerability and exposure to changing hazards, accounting for future uncertainties; This includes infrastructure performance objectives (e.g., withstanding historical or future 100-yr floods).

Flood risk analysis has long relied on hazard-centric approaches (Hershfield, 1961; White, 1973), which either fail to account the structural reliability (Phoon, 2008) or at best consider empirical levee-failure functions (e.g., probable failure point (PFP) formulate based on geometry, USACE, 1999). Here, we integrate hydrologic failures (risk of flood exceeding the design height, left panel) with structural/geotechnical failures (middle panel). Levee physical modeling is simulated by a set of transient coupled finite-element seepage and limit equilibrium slope stability analyses. Variability in hydraulic and mechanical properties of soils was addressed using a Monte Carlo sampling method to evaluate the probability of failure of the levee against three individual modes of failure (under seepage, uplift, and slope stability) along with lower and upper bounds for the combined mode.

For a riverine levee, we face a challenge projecting future streamflow, for which the associated uncertainties are significant due to application of hydrological modeling with several variables

(Dankers & Feyen, 2008; Kundzewicz et al., 2010; USACE, 2009c; IPET, 2009b; Wilby, 2012; Pierce et al., 2016; Wilby & Keenan, 2012). That is the main reason some proxies such as a hypothetical increase in the distribution of current peak flood have been employed in the literature (e.g., Hui et al., 2018, Kundzewicz et al., 2014; Wobus et al., 2014). However, we take advantage of the daily streamflow projections (1950-2099) developed for the 4th California Climate Change Assessment (in 59 locations across Northern California, Scripps Institution of Oceanography, Pierce et al., 2014, 2015, 2018). For the levee's physical modeling, the streamflow loading is represented by flood water level behind the levee for different flood return periods (past (1950 – 2000, left panel) and future (2049 – 2099), right panel).

Finally, the risks of structural failure over an n-year timespan due to the projected and historical floods can then be evaluated. We present the final product that could serve as a measure of reliability, including both projected changes in flood hazards and the potential change in the structural performance of the levee system. With this methodology, we can adjust the potential add-on design variable by comparing the baseline scenario and future simulations. We discuss to see if this framework can integrate future climate projections into current design concepts.

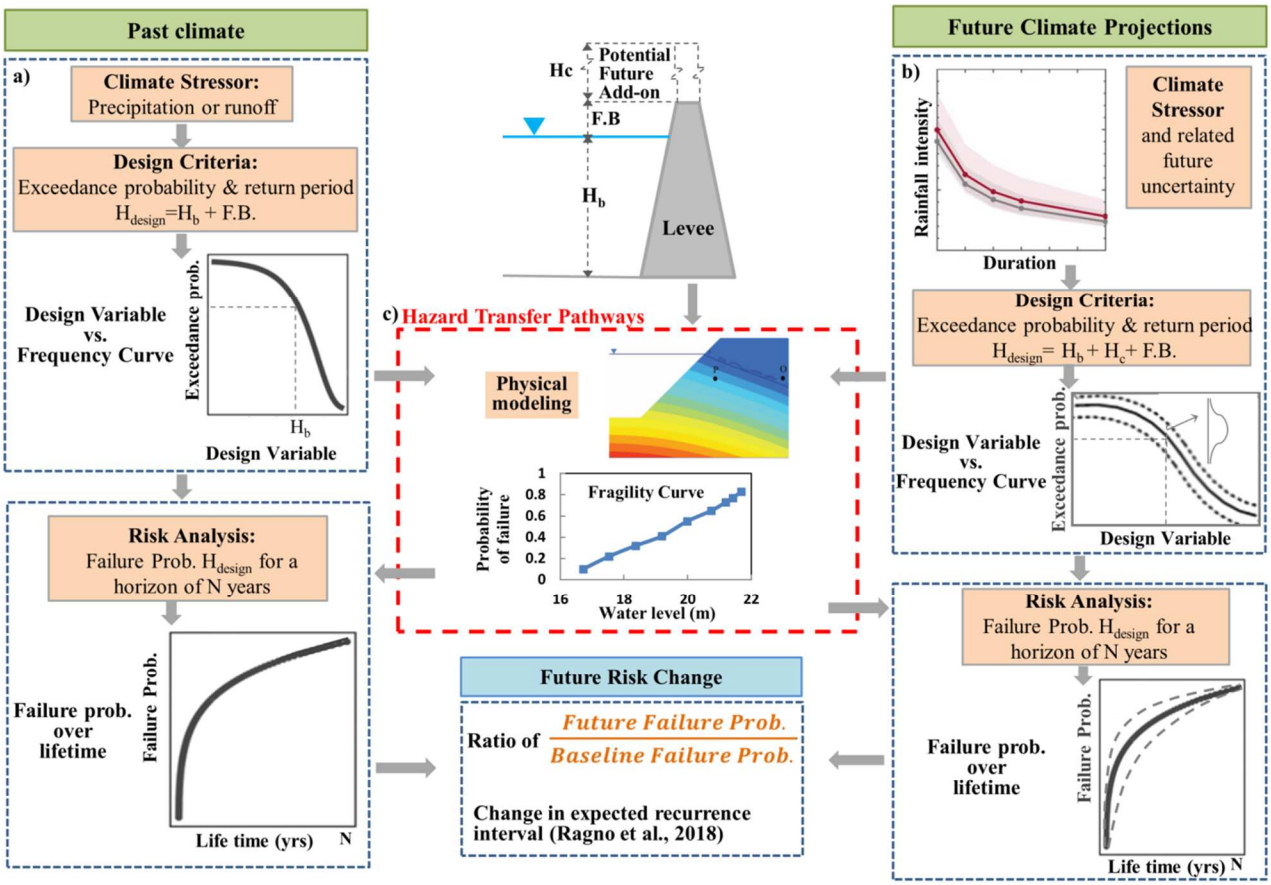

Figure 16 Conceptual pathway to integrate future climate information and the underlying uncertainty into a flood infrastructure planning such as a levee, comparing past climate (left panel: hydrologic design) to future projections (right panel). Hazard transfer pathway (middle panel) exhibits the physical modeling which provides fragility curves (levee failure analysis). H_b and H_c represent the design variable in the baseline scenario and the potential future add-on under a changing climate, respectively. F.B. represents the considered freeboard for the levee safety in the design height.

Local Levee performance implementing the proposed pathway

Levees, which play a fundamental role in the current flood protection systems (NRC, 2012, CACC, 2018), are working under marginal conditions with an average age of 56 years (e.g., NRC, 2012; ASCE, 2017; US National Levee Database (NLD), 2020). Within the USACE levee portfolio, approximately 13% of the levees work under marginal conditions: moderate to high risk with an estimated $21 billion improvements and maintenance cost (LSAC I, II or III, Army Corps, 2018,

ASCE, 2017). Expected changes in the future flood's frequency and severity would add some degree of uncertainty into breaching risk of such levees. We investigate the impacts of future flood projections on the structural integrity of current and future levee systems as an application of our proposed methodology. The framework is applied to the Elkhorn Levee, which lists as an earthen levee located within a high-risk flooding zone (Reclamation District No. 1000) in Sacramento, California. Over 21,000 kilometers of levees protect land and infrastructure from floods in California (CDWR, 2011), where any possible structural failures could lead to unprecedent impacts (CDWR 2011, Independent Review Panel, 2007, Florsheim and Dettinger, 2007).

Results

Streamflow projections

Daily streamflow projections (1950-2099) across Northern California were developed by the Scripps Institution of Oceanography for the 4th California Climate Assessment (Pierce et al., 2014, 2015, 2018). The Variable Infiltration Capacity (VIC) hydrological model (Lohmann et al., 1996, 1998) that simulates surface and subsurface processes was forced with downscaled global climate model (GCM) simulations to route streamflow at a daily temporal scale. The bias-corrected inputs to the hydrologic model (VIC) were based on ten GCMs from the Fifth Coupled Model Intercomparing Project (CMIP5) and two representative concentration pathways (RCPs): RCP4.5 and RCP8.5. For impact studies purposes, the Climate Action Team Research Working Group introduced those ten GCMs, as they covered a wide range of possible conditions in California's future climate (CDWR, 2015).

The Elkhorn Levee is adjacent to Camp Far West , one of the 59 locations across Northern California where daily streamflow projections are available (Pierce et al., 2014, 2015, 2018). For flood frequency analysis, we explore the streamflow projections from all ten climate models for this site (Figure 17a). To fit a distribution and estimate the flood return levels for different return periods (Groves et al. 2006), we use Process-Informed Nonstationary Extreme Value Analysis (ProNEVA, Ragno, et al., 2019; Cheng et al., 2014). ProNEVA employs a generalized framework for considering nonstationarity assumptions in analyzing climatic extremes, including potential changes in the frequency and variability of extreme events (e.g., based on GEV distribution, the methodology is presented in Appendix B). Figure 17a shows the variability in streamflow projections for ten climate models in RCP 8.5 at the Elkhorn Levee location (1950-2099). Comparing the future flood events (2049-2099) into past flood events (1950-2000) demonstrates that the climate models mostly predict higher streamflow in the future. However, model 1 and model 7 project lower streamflow for the future compared to the past as they consider other possible conditions in California's future climate.

For flood risk analysis in Elkhorn Levee, we employ the most extreme projected streamflow scenario, which belongs to model MICRO5, RCP8.5, one of California's four representative climate models (Pierce et al., 2014, 2018). The flood frequency analysis runs based on daily annual maxima streamflow as it is a key design variable for flood risk assessment when instantaneous observations are not available (e.g., England et al., 2019). The levee's loading is represented by flood water level behind the levee for different recurrence intervals (e.g., 10-yr, 25-yr, 50-yr flood events). Applying the rating curve concept (i.e., river stage and discharge relationship at the

gauging station), we estimate the flood water level corresponding to the streamflow from each recurrence interval.

Figure 17b illustrates the streamflow projections for the selected CanESM2 model (RCP 8.5) and the corresponding flood levels derived from the rating curve in different recurrence intervals. Our preliminary results projected higher future peak water levels (2049-2099) compared to the corresponding flood levels in the baseline (1950-2000) simulations, implying higher flood risk in the future. Specifically, the water level corresponding to the future 50-year flood event is expected to be 1.34 m higher-6.5% increase relative to the current condition (21.9 m and 20.6 m for future and past, respectively). Notably, 1.34 m higher flood level corresponds to a 34.9% increase in streamflow (1478.5 m3/s and 1095.6 m3/s for future and past, respectively). This indicates the possibility of more intense floods in the future and hence, a higher chance of failure from a hydrologic perspective consistent with the findings of Mallakpour et al. (2018). These changes in future flood levels can have a significant impact on the failure probability of the levee. In the following, we describe how the proposed framework can translate the projected change in extremes to change in physical failure probability as our key objective.

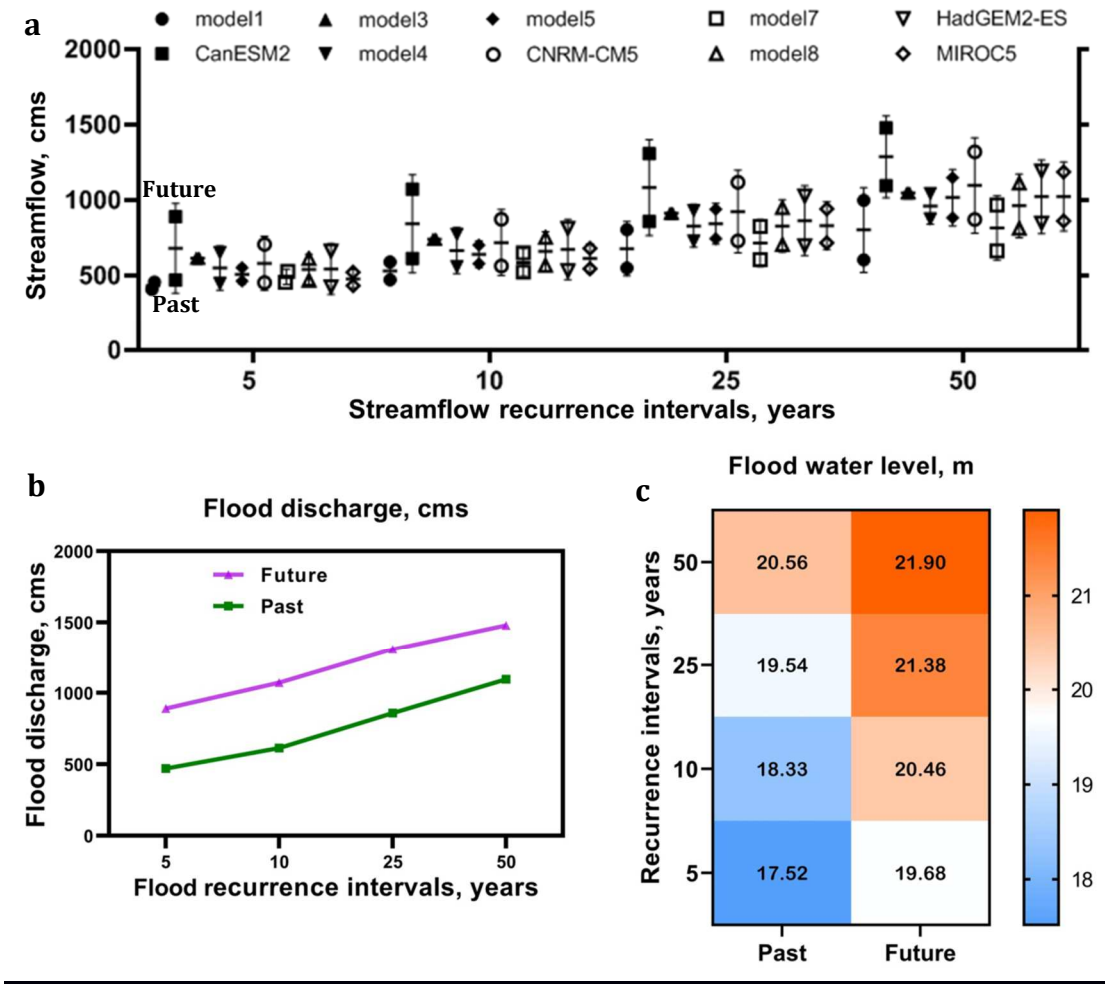

Figure 17. a) Streamflow projections at Elkhorn Levee location (1950-2099) for 10 climate models derived from the 4th California Climate Assessment, RCP 8.5; b) Streamflow and c) Corresponding flood levels for different recurrence intervals using baseline and projected future data (CanESM2 model, RCP 8.5) at Elkhorn Levee location.

Structural Failure:

A wide range of phenomena such as slope stability, uplift, piping, and internal erosion due to under seepage and/or through seepage can adversely affect the structural integrity of an earthen levee leading to failure. In most cases, the failure occurs because of more than one failure mode. The overall likelihood of a levee failure is often based on a combination of different individual modes of failure. Thus, it is prudent to perform the levee risk analysis under both individual and multiple

modes of failure. The probability of failure-load relationship, commonly referred to as the fragility curve (or system response curve), offers an effective tool for levee risk analysis (e.g., Schultz et al., 2010; USBR, 2019). Among others, an analytical approach based on quantitative models of load and resistance is shown to be a robust framework for risk analysis (e.g., Lanzafame and Sitar, 2019; USBR, 2019; Zimmaro et al., 2019). In this proposed procedure, the levee's probability of failure for each failure mode ($P_{f,i}$) is determined by considering the uncertainty in one or more variables (e.g., response threshold, loading, soil types, soil properties, levee geometry and dimensions, and water level) that affect load or resistance of the system capacity (See Appendix B). After determining the probability of failure for each mode, the combined probability of failure can be calculated. The upper and lower bounds of the combined probability of failure can be determined by assuming mutually exclusive (upper bound) or complete dependence (lower bound) between *n* modes of failure as follows (Lendering et al., 2018):

$$\mathrm{Max}\,(\mathrm{P_{f,i}}) \leq \mathrm{P_{f,t}} \leq \sum_{\mathrm{i=1}}^{\mathrm{n}} \mathrm{P_{f,i}} = 1 - \prod_{\mathrm{i=1}}^{\mathrm{n}} (1 - \mathrm{P_{f,i}}) \quad (1)$$

where $\mathrm{P_{f,t}}$ is the combined (aggregate) probability of failure. Most previous studies (e.g., Wolff, 2008; Rice & Polanco, 2012; Jongejan et al., 2013; Bogárdi & Balogh, 2014; Schultz et al., 2018; Lendering et al., 2018) determine the combined probability of failure of earthen levees by assuming independence among failure modes. However, different failure modes can somewhat dependent because they share common triggering and resisting factors. To properly represent the range of possible $\mathrm{P_{f,t}}$ values, we consider both lower and upper bounds in this study (Vahedifard et al. 2020).

Numerical simulations are performed using two codes, SEEP2D-COUPLED-HPC and SLOPE2D-HPC (Tracy et al., 2020). The former is a two-dimensional coupled transient finite-element

seepage/structural plane strain program designed to run on a high-performance computing facticity belongs to the US Army Engineer Research and Development Center (ERDC). The latter is a limit equilibrium slope stability code that uses the simplified Bishop method. The pore-water pressures obtained from the coupled finite element seepage are incorporated into the limit equilibrium slope stability analysis (Vahedifard et al. 2020). A total of 11 random variables (including sampled and derived variables) for each soil type were considered covering mechanical and hydraulic properties of the soil layers in saturated and unsaturated conditions.

Risk imposed by climatic stressors

Hydrologic failure corresponds to the probability of flood exceeding the design level (e.g., Bras, 1990; Rootzén and Katz, 2013; Serinaldi and Kilsby, 2015; Read and Vogel, 2016). Flood level may exceed the design level indicating hydrologic failure, but the structure may not necessarily fail (Phoon, 2008). Contrary to hydrologic failure, structural failure may occur in levels lower than the design height that accounts for the common breach prior to overtopping (likely in 80% of high- or very high-risk levees, U.S. Army Corps of Engineers, 2018; Phoon, 2008; Kuijper & Vrijling, 1998). A comprehensive risk assessment in leveed areas is a function of three components, hazard, exposure, and vulnerability. Herein, we specifically focus on two components of risk: hazard (i.e., hydrologic failure) and vulnerability (structural failure). Based on this definition, the annualized failure probability (AFP, Kuijper & Vrijling, 1998), or the risk of levee failure occurring in any given year can be calculated as:

Annualized failure probability = hazard prob.$\times$structural failure prob. (levee performance) (2)

where hazard prob. is the annual exceedance probability function of the flood hazard (corresponds to hydrological failure probability). We first utilize the annual block maximum sampling technique to extract the maximum daily streamflow for each year. Then, we fit the Generalized Extreme Value (GEV) distribution to annual maxima data using ProNEVA; Ragno et al., 2018. The structural failure prob. shows the probability of unsatisfactory performance (PUP) under a range of loads (e.g., Schultz et al., 2010). In the proposed framework, design criteria, including the factor of safety and probability of failure, represent the levee's structural performance (detailed methodology in Supplementary Material). We then calculate the risk of failure over the lifetime based on annualized failure probability for a given design lifetime n:

$$\text{Risk of failure over lifetime} = 1 - (1 - \text{p})^{\text{n}} \quad (3)$$

where p is annualized failure probability, which is equal to product of flood exceeding prob. and structural failure prob.

Results

Structural failure and risks: To illustrate our methodology, we present the results of applying the framework to Elkhorn Levee. Figure 18 shows the probability of failure in combined failure modes for historical and future flood events in different recurrence intervals using the Monte Carlo sampling method. The upper and lower bounds for the combined probability of failure are

determined by employing the individual probabilities of failure along with the equation (1). Considering the combined probability of failure provides an effective measure to assess the overall performance of the levee properly. The probability of failure significantly increases towards higher recurrence intervals with the high water level. For all cases, the results from the lower and upper bounds were close, leading to a narrow band. Considering the combined mode of failure, the probability of failure quickly approached 1.0 for 25- and 50-year projected future floods.

Figure 18b displays the probability of failure versus time (during 30 days) for under seepage, uplift, and slope stability modes of failure using 50-year past and future flood events. The future events, for all modes, exhibit a higher failure probability than the corresponding past scenario. In other words, a 1.34 m higher flood level in the future would result in a 26% increase in the probability of failure against slope instability. Incorporating future climate predictions (higher flood stage) rather than relying on the past dataset can undermine the levee stability.

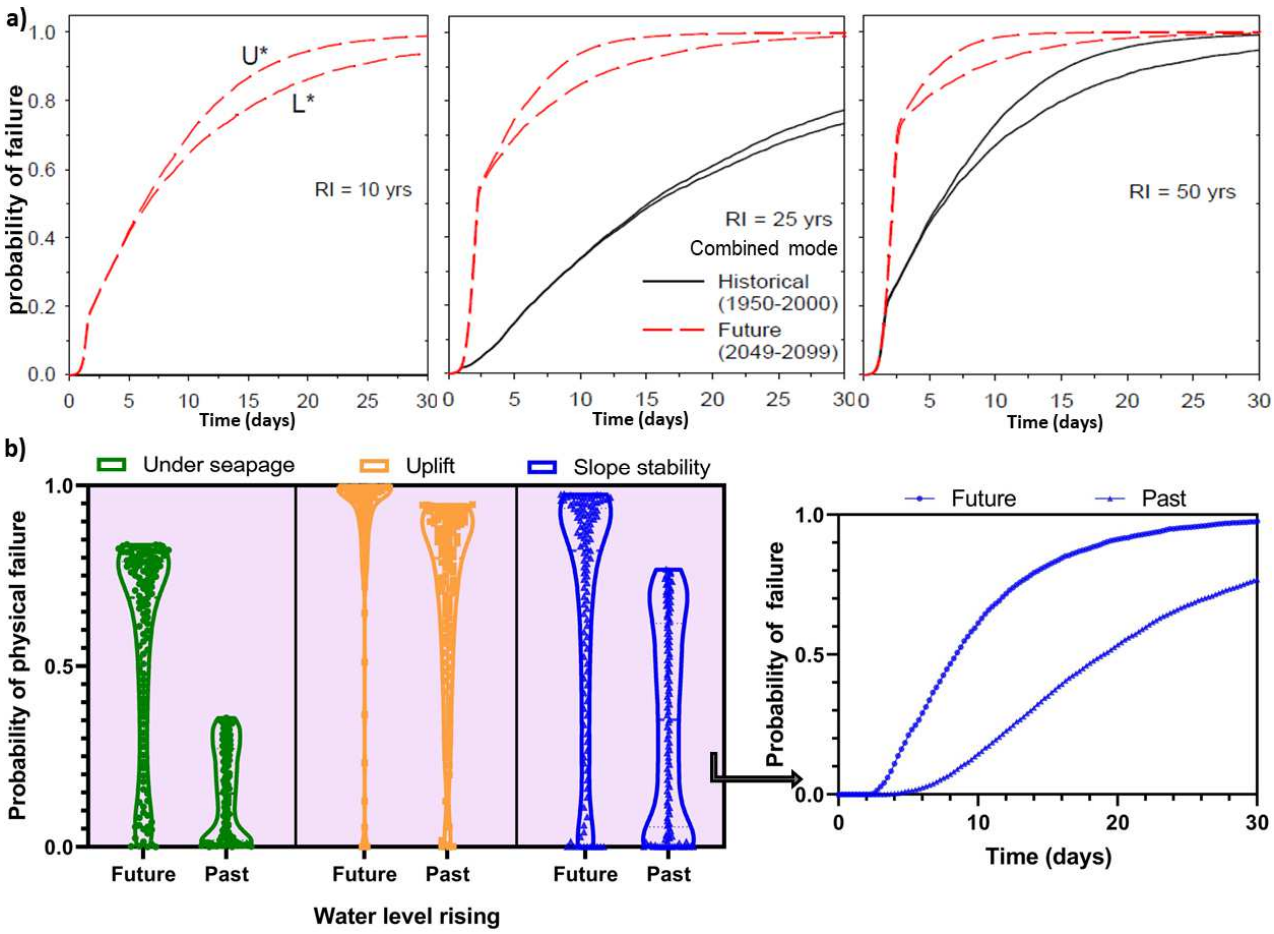

Figure 18 a) Upper and lower bounds for combined probability of failure versus time using the historical (1950-2000) and future (2049-2099) flood scenarios for different recurrence intervals: 10 years, 25 years, and 50 years in Elkhorn Levee. b) Probability of failure versus time for under seepage, uplift, and slope stability modes of failure in recurrence intervals of 50 years.

Figure 19 shows the risk of failure (hazard-performance basis, slope stability) for Elkhorn Levee due to 50-year past and future flood events for a design horizon of 50 years. The slope instability results suggest that a 1.3 m higher flood level in the future leads to a 27% increase in the probability of failure. The probability of failure of the levee would increase up to 27% when considering future streamflow projections (failure probabilities of 0.77 and 0.98 under past and future climate, respectively, RCP8.5, CanESM2 model). The predicted increase in the probability of failure

indicates the importance of considering future climate scenarios to understand better the current infrastructure in a warming climate.

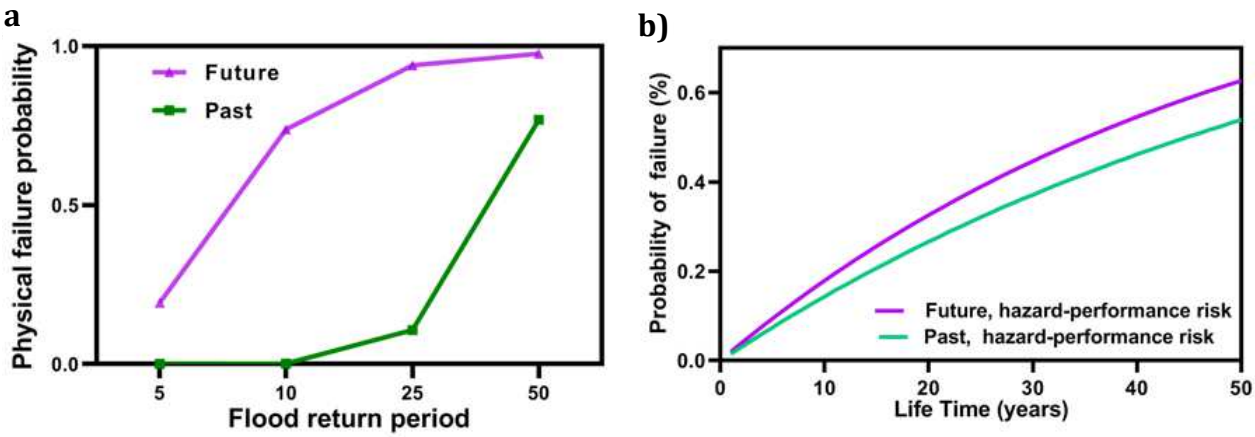

Figure 19 a) Levee's probability of physical failure for different flood return periods and their corresponding exceeding probabilities, Elkhorn Levee. b) Risk of failure due to a 50-year flood event for a temporal horizon of 50 years. The solid purple and green curves show the estimated failure probabilities for the future (RCP8.5, CanESM2) and the past hazard-performance scenarios, respectively.

Required Factor of Safety as design criteria

A factor of safety, which is the ratio of the capacity to resist a demand (i.e., load), serves as the design criteria in engineering practices. A factor of safety accounts for the uncertainties which are because of the interactions between the hydrologic loading and hydraulic resistance of the structure (Ebeling & White, 2021). When the factor of safety is less than the pre-defined performance criteria, the levee's performance is considered unsatisfactory. In this case study, for each mode and at each specified time, factors of safety corresponding to 6,000 realizations were averaged to determine the mean factor of safety. In the guidelines, the minimum required FOS is mainly used

for design purposes. However, for risk analysis, the standards mainly consider the limit state, where the levee is on the verge of failure (FOS = 1.0, USACE, 2000)

For this levee modeling, the minimum threshold for the factor of safety (or load carrying capacity of the system) is 3 for under seepage, 1.5 for uplift, and 1.1 for slope stability. As shown in Figure 20, the factor of safety for slope stability mode varies in safe and acceptable ranges for a design based on past climate, whereas the factor of safety would drop below the minimum threshold (1.1) employing projected future climate. For instance, in slope instability failure mode, employing projected future flood results in a drop in factor of safety from 1.03 to 0.89 for a 50-year event. The highest reduction in the mean factor of safety is 54.2% for under seepage for the 10-year flood scenario. This highlights that incorporating the future climate (i.e., higher flood stage) rather than relying on the historical dataset resulted in a further decrease in the factor of safety.

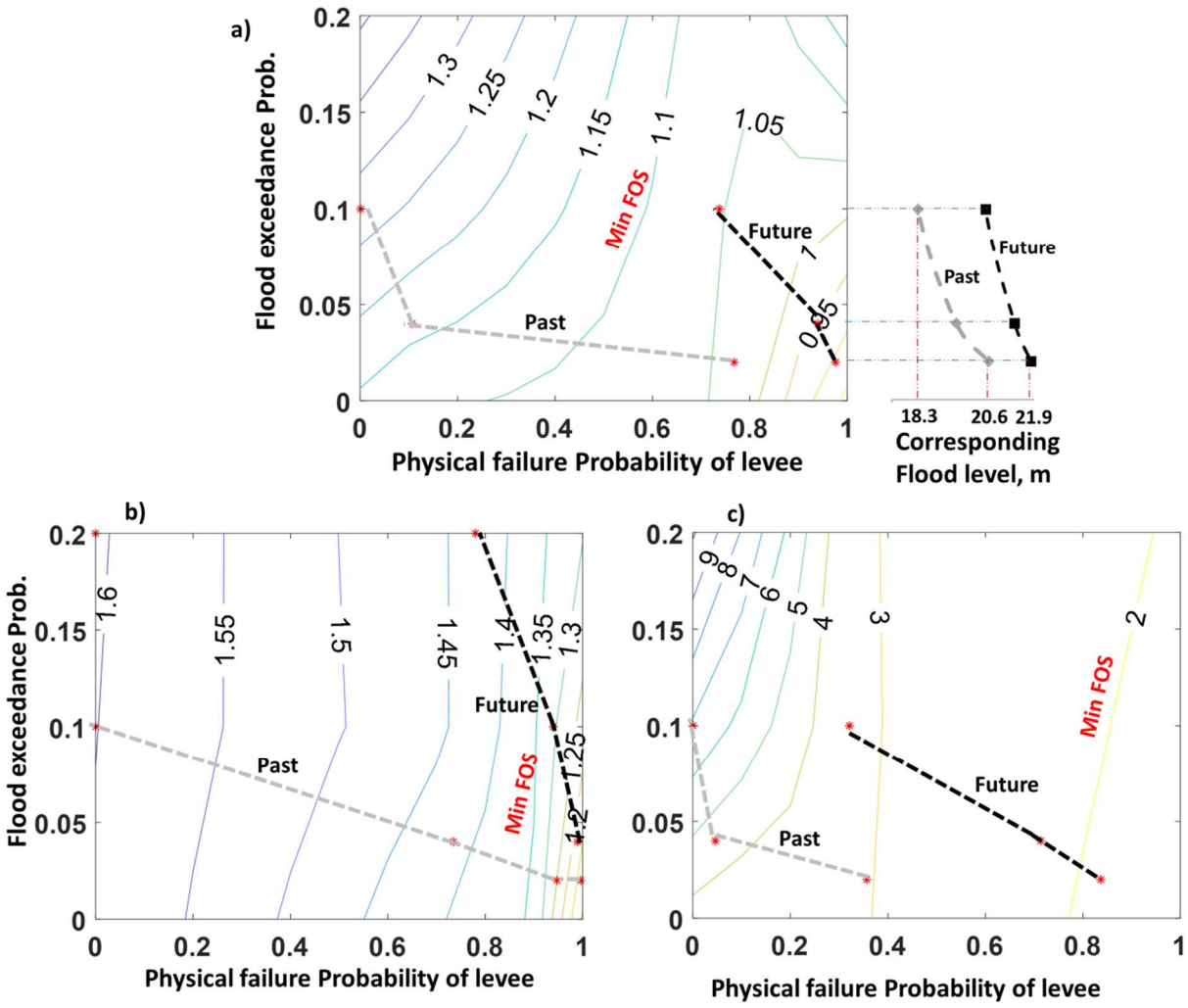

Figure 20 Contour lines of factor of safety (design criteria) for past and future in comparison with the required acceptable factor of safety. a) Slope stability mode of failure (in this levee case study minimum threshold of 1.1). b) Uplift mode of failure. c) Under seepage mode of failure.

Discussion and Conclusion

Climatic extreme events are projected to continue to change in the future, threatening critical infrastructure. Variability in the frequency and magnitude of precipitation extremes is anticipated

to result in future changes in the flood characteristics and, consequently higher risk of infrastructure failure. This study argues that current frequency analysis methods, design guidelines, and operation procedures do not consider changes in statistics of extreme events. We develop integrated and risk-based probabilistic and numerical (process-based) investigations of the underlying hazards and their impacts, including multiple modes of hydrologic and structural failures. As an example, we investigate the effects of changes in the projected flood hazard on the performance of an earthen levee, Elkhorn Levee, in Sacramento, California.

Toward achieving a climate-ready levee system, we first identify the new patterns of the natural hazard (i.e., flood) that affects the levee in the future. The daily streamflow projections (1950-2099) are used for flood frequency analysis at the Elkhorn Levee location using ProNEVA. Our results based on the most extreme climate model (CanESM2 model, RCP 8.5) projected higher future peak water levels in the future (2049-2099) compared to the corresponding flood levels in the baseline (1950-2000) period, implying higher flood risk in the future. The water level corresponding to the future 50-year flood event is expected to be a 1.34 m higher-6.5% increase relative to the current condition.

We translate the information on changing streamflow extremes to actual physical levee response (e.g., failure probability). In the levee's physical modeling, the flood level for different return periods represents the hydraulic load which is applied into a set of transient coupled finite-element seepage and limit equilibrium slope stability analyses. The failure probability of the levee would increase up to 27% when considering future streamflow projections (failure probabilities of 0.77 and 0.98 under past and future climate, respectively). These results indicate that a 1.3 m higher flood level in the future would lead to a 27% higher risk of levee failure, which is considerable in

risk assessment. Our method allows translating the change in hazard to change in performance. Currently, these evaluations are not available, and we achieve our main goal by generating this information.

Method

Levee numerical modeling

The probability of failure-load relationship is commonly referred to as a fragility curve (or system response curve), which offers an effective tool for levee risk analysis (e.g., Schultz et al., 2010; USBR, 2019). Among others, the analytical method, which is based on quantitative models of load and resistance, is shown to be best suited for robust risk analysis purposes (e.g., Schultz et al., 2018; Lanzafame & Sitar, 2019; USBR, 2019; Zimmaro et al., 2019). In this approach, the levee's probability of failure is determined by considering the uncertainty in one or more variables (e.g., soil types, soil properties, levee geometry and dimensions, and water level) that affect load or resistance. The probability of unsatisfactory performance, referred to as the probability of failure, could be calculated by treating the soils' hydro-mechanical properties as random variables. The performance function, $\mathrm{G}(\mathbf{X})$, can be defined as:

$$\mathrm{G}(\mathbf{X}) = \mathrm{G}(\mathrm{R}, \mathrm{S}) = \frac{\mathrm{G_R}(\mathbf{X})}{\mathrm{G_S}(\mathbf{X})} \tag{3}$$

where $\mathbf{X}$ is the vector of random variables, $S = G_S(\mathbf{X})$ is the load imposed on the levee, and $R = G_R(\mathbf{X})$ is the capacity of levee to resist the load. In this equation, $G(R, S)$ represents the factor of safety, which is the ratio of the capacity to resist a demand (i.e., load) placed on the levee. When $G(\mathbf{X})$ is less than the pre-defined performance criteria ($G_{design}(\mathbf{X})$), the performance of the levee is considered unsatisfactory. The probability of failure for i^{th} mode of failure ($P_{f,i}$) is determined by integrating the multivariate density function, $f_X(\mathbf{X})$, for the n-dimensional vector of random variables over the unsatisfactory performance domain (e.g., Schultz et al., 2018):

$$P_{f,i} = P[G(\boldsymbol{X}) < 1] = \int \dots \int_{G(\boldsymbol{X}) < G_{design}(X)} f_X(\boldsymbol{X}) d\boldsymbol{X} \quad (4)$$

The historical and future flood levels were applied in a set of coupled transient finite element seepage and limit equilibrium slope stability analyses to simulate the levee subjected to extreme streamflow. Monte-Carlo method with 6,000 realizations of soil properties (treated as random variables) were used to estimate the probability of failure for each mode at each water level. Input data sets needed for the Monte Carlo simulation were from sampling the probability distributions of uncertain mechanical and hydraulic properties of each soil type (based on its USCS classification) in the levee embankment and foundation. Eleven random variables (including sampled and derived variables) for each soil type were considered covering mechanical and hydraulic properties of the soil layers in saturated and unsaturated conditions. Each realization was examined to see if the levee met performance criteria defined for under seepage, uplift, and slope stability. The probability of failure at selected times during the simulation was calculated as the

fraction of 6,000 realizations that failed to satisfy the performance criteria for that failure mode. The following performance functions were used for different modes of failure:

$$G(R,S)_{un} < \frac{0.33 i_{cv}}{i_v} \tag{5}$$

$$G(R,S)_{up} < \frac{0.667\, u_t}{u_u} \tag{6}$$

$$G(R,S)_{sl} < 0.909 \left(\frac{\tau}{\tau_f}\right)_{min} \tag{7}$$

where $G(R,S)_{un}$, $G(R,S)_{up}$, and $G(R,S)_{sl}$ represent the performance functions for under seepage, uplift, and slope stability modes of failure, respectively, i_{cu} is the critical vertical exit gradient at the landside toe of the levee, i_v is the vertical exit gradient at the landside toe of the levee, u_t is the pressure applied by the weight of the saturated soil at the toe beneath the confining layer of the levee, u_u is the uplift pressure at the same location, τ is the shear stress, and τ_f is the shear strength of soil along the most critical failure surface sought in the limit equilibrium slope stability analysis of the landside levee slope. The above performance functions embody the following factors of safety: 3 for under seepage, 1.5 for uplift, and 1.1 for slope stability. These values were selected within the range of recommended values by guidelines for design and risk analysis of earthen levees (e.g., USACE, 2000; USBR, 2019).

After estimating the probability of failure for each mode, the combined probability of failure can be calculated. As discussed by Lendering et al (2018), the upper and lower bounds of

the combined probability of failure can be determined by assuming mutually exclusive (upper bound) or complete dependence (lower bound) between n modes of failure as follows:

$$\text{Max}\,(P_{f,i}) \leq P_{f,t} \leq \sum_{i=1}^{n} P_{f,i} = 1 - \prod_{i=1}^{n}(1 - P_{f,i}) \quad (8)$$

where $P_{f,t}$ is the combined (aggregate) probability of failure. Most previous studies (e.g., Wolff, 2008; Rice & Polanco, 2012; Jongejan et al., 2013; Bogárdi & Balogh, 2014; Schultz et al., 2018; Lendering et al., 2018) determine the combined probability of failure of earthen levees by assuming independence among failure modes. However, different failure modes can somewhat dependent, because they share common triggering and resisting factors. To properly represent the range of possible $P_{f,t}$ values, we considered and presented both lower and upper bounds in this study. Other possible uncertainties not considered in this study include uncertainties in the response threshold, model error, and flood scenarios. The latter itself includes uncertainties from inter-model variability when multiple models are used, and uncertainties from future RCPs.

Nonstationarity Extreme Value Analysis using ProNEVA

We fit the GEV distribution to estimate the flood frequency distribution using Process-informed Nonstationary Extreme Value Analysis (ProNEVA (Cheng et al., 2014; Ragno et al., 2019)). ProNEVA employs a generalized framework for considering nonstationarity assumption in the analysis of climatic extremes, including potential changes in the frequency and variability of extreme events. This framework allows nonstationary analyses employing user-defined covariates, which could be temporal or process-based (i.e., a physical driver such as urbanization or CO_2

emission). ProNEVA offers parameter estimation, uncertainty quantification, and a comprehensive assessment of the goodness of fit. In the study, based on statistical significance trend test, either stationary or nonstationary GEV distributions were fit to each block maxima series.

Generalized Extreme Value (GEV)

The GEV distribution is widely used to model time series of block maxima, such as deriving precipitation Intensity-Duration-Frequency (IDF) curves (The National Oceanic and Atmospheric Administration (NOAA)). The GEV cumulative distribution function is (Coles et al., 2001):

$$\Psi_{GEV}(x) = exp\{-\left(1 + \xi \cdot \left(\frac{x-\mu}{\sigma}\right)\right)^{-\frac{1}{\xi}} \quad (1)$$

The GEV distribution has the location parameter (μ), the scale parameter (σ), and the shape parameter (ξ) to specify the center of the distribution, the deviation around the center, and the tail behavior of the GEV distribution, respectively (Renard et al., 2013).

Under a nonstationary assumption, however, the parameters of the underlying distribution function are time-dependent, and the properties of the distribution would therefore vary with time. This means, we let the parameters of the distribution be a function of a general covariate x_c, i.e., μ (x_c), σ (x_c), ξ (x_c) (Coles et al., 2001). Hence, the nonstationary form of eq. 1 is:

$$\Psi_{GEV}(x|x_c) = exp\{-\left(1 + \xi(x_c) \cdot \left(\frac{x-\mu(x_c)}{\sigma(x_c)}\right)\right)^{-\frac{1}{\xi(x_c)}} \quad (2)$$

σ (x_c) functions in the log scale for the positivity of the scale parameter (Coles et al., 2001; Katz, 2013). As a result, the exponential function is not available for σ (x_c). For the shape parameter ξ (x_c), a linear function is considered (Coles et al., 2001).

Parameter estimation: Bayesian analysis and Markov chain Monte Carlo sampling

A Bayesian approach is integrated into the nonstationary GEV for uncertainty assessment (Stephenson and Tawn, 2004). This approach combines the knowledge brought by a prior distribution and the observation vector of annual maxima into the posterior distribution of parameters (Cheng et al., 2014; Luke et al., 2017; Sadegh et al., 2018, 2017; Thiemann et al., 2001). Assuming independence between observations, the Bayes theorem for estimation of GEV parameters under the nonstationary assumption can be expressed as:

$$\mathrm{p}\left(\theta\middle|\tilde{\mathrm{Y}}\right) \propto \prod_{\mathrm{i}=1}^{\mathrm{n}} \mathrm{p}(\theta)\,.\,p(y_i|\theta) \qquad (3)$$

Where θ is the parameter of a given distribution and let $\tilde{\mathrm{Y}}= \{\tilde{y}_1, \ldots, \tilde{y}_{n1}\}$ be the set of n observations. Following Bayes theorem, the probability of θ given $\tilde{\mathrm{Y}}$ (posterior) is proportional to the product of the probability of θ (prior) and the probability of $\tilde{\mathrm{Y}}$ given θ (likelihood function). The posterior distribution is then delineated using a hybrid-evolution MCMC approach proposed by Sadegh et al. (2017). The MCMC simulation searches for the region of interest with multiple chains running in parallel, which share information on the y.

Model diagnostics and selection

The goodness of fit (GOF) assessment in ProNEVA includes: quantile and probability plots for a graphical assessment, two-sample Kolmogorov-Smirnov (KS) test, Akaike Information Criterion

(AIC), Bayesian Information Criterion (BIC), and Maximum Likelihood (ML). The hybrid-evolution MCMC approach (Sadegh et al., 2017) within the Bayesian framework provides an ensemble of solutions for the (non)stationary statistical model fitted to the data. ProNEVA uses the best set of parameters which maximizes the posterior distribution. Marginal posteriors will then provide uncertainty estimates of the parameters.

Return level curves under nonstationarity

Extreme event intensity is expressed as a function of the return period (i.e., the average length of time between events of a given depth/intensity and duration). The Return Level (RL) expresses the quantile Q_i for which the probability of an annual maximum exceeding the selected quantile is q_i (Cooley, 2013). The quantile Q_i is the value of intensity such that $Pr(P \geq Q_i) = 1-F_P(Q_i)$, where F_P is the probability distribution of the annual maxima of intensities. In the stationary analysis, the probability q_i of the quantile Q_i does not change on a yearly basis. The Return Period (RP) of the quantile Q_i is defined as the inverse of its exceedance probability, $T_i = 1/q_i$ in years. The RL curves are defined by the following points under the stationary assumption:

$$((\mathrm{Ti};\ \mathrm{Qi}), \quad \mathrm{Ti} > 1 \quad \mathrm{yr}, \quad \mathrm{i} = 1, \cdots) \tag{4}$$

In a nonstationary assumption, ProNEVA integrates two different proposed concepts to account for ambiguous terms of RP and RL (Cooley, 2013): the expected waiting time (Salas and Obeysekera, 2014), and the effective RL curves (Katz et al., 2002).

Explanatory Analysis: Mann-Kendall and White Tests

ProNEVA utilizes the Mann-Kendall (MK) monotonic trend test and the White Test (WT) for evaluating homoscedasticity in the datasets. Based on the statistical significance trend test, then the user can decide whether to incorporate a trend function in one or more of the model parameters or not.

Chapter 5 Adaptive Design

Framework for Adaptive Design of Infrastructure under a Changing Climate

Overview

Current infrastructure design concepts rely on historical events assuming temporal stationarity (i.e., statistics of past extremes do not change significantly over time) (e.g., Cheng et al., 2014; Dittrich et al., 2016; Ragno et al., 2018; Sadegh et al., 2015; Salas & Obeysekera, 2014; Shortridge et al., 2017). However, global warming and land use changes have increased the risk of climatic extreme events, and the associated damage to critical infrastructure (Hallegatte et al., 2013; Neumann et al., 2015a; Willis et al., 2016; Vahedifard et al., 2017, 2020). The observed increasing trend in severity and frequency of extreme events (Lall et al., 2018; Kundzewicz et al. 2014; Wilby & Keenan, 2012; Fischer & Knutti, 2015; IPCC, 2013; Patricola & Wehner, 2018; Scoccimarro et al., 2013; Trenberth, 2001, 2008) introduces a new level of challenge and uncertainty that should be included in planning, risk assessment, design, and operation of infrastructure systems.

Consistent with the observed increasing trends, climate models project increases in intensity and frequency of climatic extreme events, attributed in part to anthropogenic climate change (IPCC

2007, 2012, 2013). Historical records show that the number of billion-dollar disasters is on the rise due to changing climate and increasing exposure to hazards. From 1980 to 2020, natural disasters and climatic extremes resulted in $1876 billion CPI-adjusted losses and 14,485 deaths in the United States (NCDC, 2021). The 1980–2020 annual average of weather/climate disaster events with losses exceeding $1 billion each is 7 events (CPI-adjusted), whereas this annual average for the most recent 5 years (2016–2020) has reached to 16.2 events (NCDC, 2021). The observed increase in the impacts of extreme events offers a direct reflection of the vulnerability of existing infrastructure systems, and a glimpse of what to expect in a warming world (IPCC, 2012; Neumann et al., 2015b; Willis et al., 2016).

To enhance safety of life, our infrastructure systems must be resilient against the growing frequency and severity of extremes (CACC, 2018; Vahedifard and AghaKouchak, 2020). Mitigating the adverse consequences of future extreme events on infrastructure will directly contribute to community resilience which asserts the need to stablish adaptive capacity (Babovic et al., 2018). Adaption warrants an "adjustment in natural or human systems in response to actual or expected climatic stimuli or their effects, which moderates harm or exploits beneficial opportunities" (IPCC, 2007). Realistic models of short and long-term loading patterns imposed by climatic extremes will be needed for design of future adaptive infrastructure systems. The uncertainty and inter-model variability in future projections is particularly pronounced for extreme events (e.g., extreme precipitation, floods), which drive the design of critical infrastructure systems such as levees and seawalls. Failure to account for changes in future climate extremes in infrastructure design elevates the risk of under-designing infrastructure systems. Thus, integration of climate data analysis in resilient design methodologies has become an active area in a number of fields (Choate et al., 2017; DFID, 2005; Vahedifard et al., 2017; CACC, 2018).

The current approaches for adaptive planning can be summarized in following main steps: accounting for a wide variety of relevant changes and uncertainties, identifying short-term and long-term actions (e.g., decisions) and targets (e.g., performance), and continuously monitoring the world and taking actions as necessary (Walker et al., 2015; Stephens et al., 2018; Kapetas & Fenner, 2020). In an anti-fragile strategy, the design of possible adaptation pathways can offer multiple alternatives for future planning to improve structural performance.

The main objective of this chapter is to present a framework for adaptive infrastructure design that can properly account for variability and uncertainties associated with projected future climatic extremes (e.g., sea level rise, extreme precipitation). We aim to provide insight into how to revisit the existing design codes with a vision toward embracing climate adaptive methods in engineering practice. Recent efforts on integrating future climate simulations have mainly focused on the so-called robust infrastructure concept. The robust infrastructure concept evaluates risk based upon current climate projections and offers a single design load (i.e., a critical threshold) based on a single acceptable risk (e.g., deterministic hazard-centric or economy perspectives (Wisner et al., 2004; Groves et al. 2015). The adaptive design concept, on the other hand, relies on a base design considering a critical threshold that can be modified in the future (Hui et al., 2018, Ayyub and Wright, 2016) provided that the adjusted costs are significantly lower than if the system is built completely anew (Rosner et al., 2014). Given the uncertainty in the current climate projections, the robust infrastructure can potentially lead to an over-designed infrastructure with a very high upfront cost. Our proposed adaptive concept allows designing for a certain acceptable load at a lower upfront cost but with the option of more investment and monitoring during the project lifetime. A risk-based adaptive platform identifies the possible hazards and their likelihood of occurrence, and what conditions might arise in the structure in future. A conceptual iterative design

example is presented to show how the proposed framework can be employed for adaptive design of a seawall. Using satisfactory performance concepts, we estimate the performance function of the seawall facing sea level rise to identify adaptation-threshold. Finally, the alternative adaption pathways, such as increasing seawall height, are presented and discussed.

Background and Concept for Adaptive Design

The adaptive design methods lead to a base design (based on current or future risk) that can be modified in the future as the climate evolves, instead of offering a fixed single design for the future. We develop and promote a new adaptive design framework by extending the existing so-called observational method for infrastructure design. The observational method was originally developed for geotechnical engineering applications (Peck, 1969; Terzaghi et al., 1996) but has been used in several fields as a strategy to address uncertainty. The goal would be to offer a flexible design, which is not based on the worst-case scenario, and involves observing a structure's behavior to adjust it in the future as needed (Hallegatte 2009; Ayyub & Wright, 2016; CACC, 2018). For infrastructure design, the method historically relies on the construction of an initial design, followed by observation of selected performance variables or site conditions. The critical design threshold may change over time, and the changing risk can be integrated into an adaptive design concept. The observational method may not be suitable for projects that cannot be modified during or after construction and for structures that can exhibit brittle or sudden failure (Špačková & Straub, 2017; CACC, 2018; Dittes et al., 2018).

Proposed Framework

Figure 21 presents a flowchart outlining the proposed framework toward a climate adaptive infrastructure design for flood protection purposes. The flowchart consists of four main phases: initial design, construction, observation, and adaptation. Prior to the design, identification of pertinent climate hazards and the consequences of exceedance is critical. The entire process may be broken into a series of steps presented below. Steps 1 to 6 correspond to the initial design phase presented in Figure 21:

1. *Selection of Design Climate Hazards.* An ensemble of most probable hazards based on climate model outputs is used to determine the distribution of future hazards (Moss et al., 2010; Kilgore et al., 2019). Defining the most probable scenario requires a case-by-case assessment and cannot be simply generalized. Alternatively, an intermediate level of emissions or the corresponding representative concentration pathway (RCP) can be considered as the most probable scenario for the initial design (e.g., RCP 4.5). The historic baseline case is then identified along with an upper bound based on the ensemble outputs (e.g., upper bound or 95th percentile of the future climate model simulations as a conservative extreme condition). This upper bound may be selected based on percentiles or maximum feasible conditions from a constructability standpoint.
2. *Selection of Non-Climatic Design Inputs*. These include various parameters and loads such as material properties, loads not influenced by climatic conditions, and project limits. The number and extent of these inputs will vary based on the type of project.

3. *Identification of Consequences and Evaluation of Risk.* This evaluation is based on the probability of failure and the consequences of that failure. The level of acceptable risk must be defined or selected depending on the type of infrastructure.
4. *Base Design.* A base design case ("risk-based initial design" in Figure 21) would then be completed. This design is based on a hazard condition that falls between the historic and upper bound cases, and should be based on the acceptable risk level for the project.

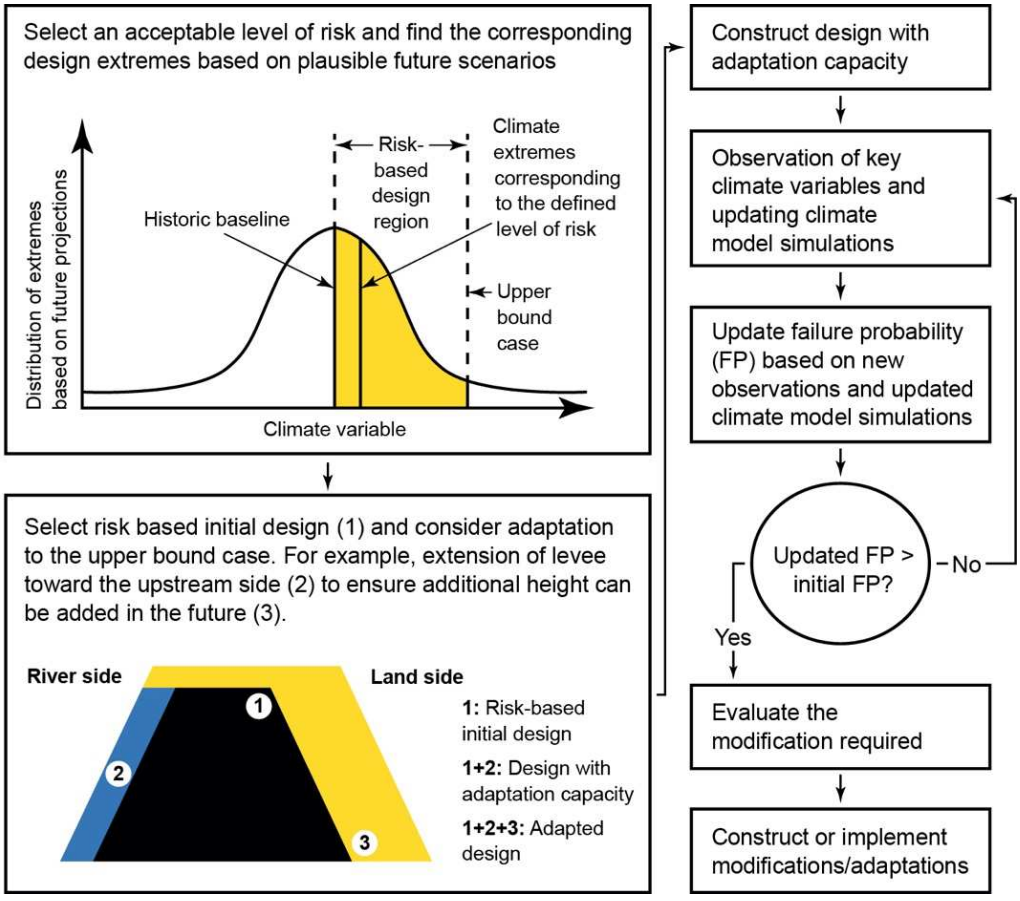

Figure 21 Adaptive design concept.

5. *Evaluation of Adaptation Capacity.* Before the design is finalized, the designer needs

to evaluate the need to implement a portion of the upper bound design into the base design for ease of adaptation. This approach ensures that the proposed design has the built-in capabilities for future modifications as necessary. Specific examples of these considerations as they pertain to some common problems are provided in the following subsection (e.g., ensuring sufficient space is available for future expansions, preemptively placing material in areas that may be difficult to access after construction due to inundation or site use, or overdesigning foundations for a more severe future case).

6. *Adaptive Design.* The adaptive design is should then be what is potentially possible based on future climate information (referred to as "design with adaptation capacity" in Figure 21). This design is based on future climate information used for the baseline design, but has the capacity to be adapted should a preidentified tipping point be observed. Such tipping points should be identified as part of the design and may be based on observed information or directly tied to changes in the computed risk of exceedance based on updated climate projections (e.g., water reaching above a certain threshold, freeboard below a certain threshold).
7. *Observation and adaptation thresholds.* Following the completion of construction, evaluating changes in hazards and the corresponding adaption pathways and/or adaption tipping point would then rely on continuous monitoring and reevaluation of extremes in a changing climate (Haasnoot et al., 2019; Walker et al., 2013). *We introduce two thresholds for recognizing the tipping point. Here,* adaptation-thresholds are associated with both changes in extreme events and the performance of the system of concern. Once the most probable emission scenario is exceeded (or relevant

hazards changed significantly), the hazard occurrence probabilities will need to be updated (e.g., deriving hazards based on a higher emissions scenario relative to that of the initial design (e.g., RCP 8.5 relative to RCP 4.5 or RCP 8.5 relative to an older version of the same RCP). The updated information on statistics of hazards defines the acceptable risk and the corresponding design variables influencing the probability of unsatisfactory performance of the structure. Once the performance function is less than the pre-defined performance criteria, the structural performance is considered unsatisfactory; thus, adaptation modification is needed.

8. *Adaptation.* Once a predetermined tipping point has been exceeded, a modification must be made to the structure. The extent of the modification may be predetermined during the adaptive design or may be selected based on the anticipated change in risk for the proposed structure. Once the extent of modification is determined and evaluated, implementation/construction of the modification may be carried out.

Adaptation Considerations

Proper implementation of an adaptive design requires evaluation of a structures capacity to be adapted should a tipping point be reached. For different infrastructure systems, the relevant considerations and potential areas of concern vary significantly. Three common types of considerations for geotechnical structures are provided as examples:

1. Capacity of Permanent Embedded Features. Retrofitting foundation systems, and other similar structure, may be cost prohibitive. Therefore, it may be more effective

to overdesign the foundation of the base design to the upper design level. For example, a T-Wall foundation could be sized to provide adequate factors of safety for the upper design level, but the protection level of the initial wall built to the based design level. A similar consideration should also be taken for geosynthetic reinforcement for earthen structures.

2. Future Inundation. For some flood protection structures, climate change may inundate one side of the structure making adaptation difficult (e.g., coastal levees). In this case the adaptive design may preemptively install any necessary components where future inundation may occur. An example of this is the construction of a flood side berm similar to the example shown in Figure 21.
3. Project Extent. Future structures may require a larger footprint than the base design (such as a future levee adaptation requiring larger stability berms, or a wider channel excavation for future precipitation levels). It should be confirmed that future modification fit within the project right of way and will not require additional land acquisition to simplify the modification.

This list is not comprehensive, and a variety of project specific considerations may be required depending on the infrastructure type and location.

Sea level rise projections

In this section, we present an illustrative design example for a seawall to showcase how the proposed framework can be employed for adaptive design purposes. Sea level rise (SLR) affects flood risk in coastal regions (Nicholls et al., 1999; Penland & Ramsey, 1990). Recent studies have

provided updated SLR projections by developing probabilistic SLR projections for California based on the most current methods, which incorporate new dynamics to an ice sheet model (Cayan et al., 2016). The probabilistic SLR projections were developed based on a time□dependent probability distribution of the different components and used a sampling method to sample the different components times 10,000 to calculate the SLR probabilities (Kopp et al., 2014). Figure 22 provides the probabilistic SLR projections to be used for adaptive seawall design to mitigate coastal flood risk. The SLR projections are in cm above 2000 levels for San Francisco for the two different RCP scenarios from 2010 to 2100 at decadal time steps.

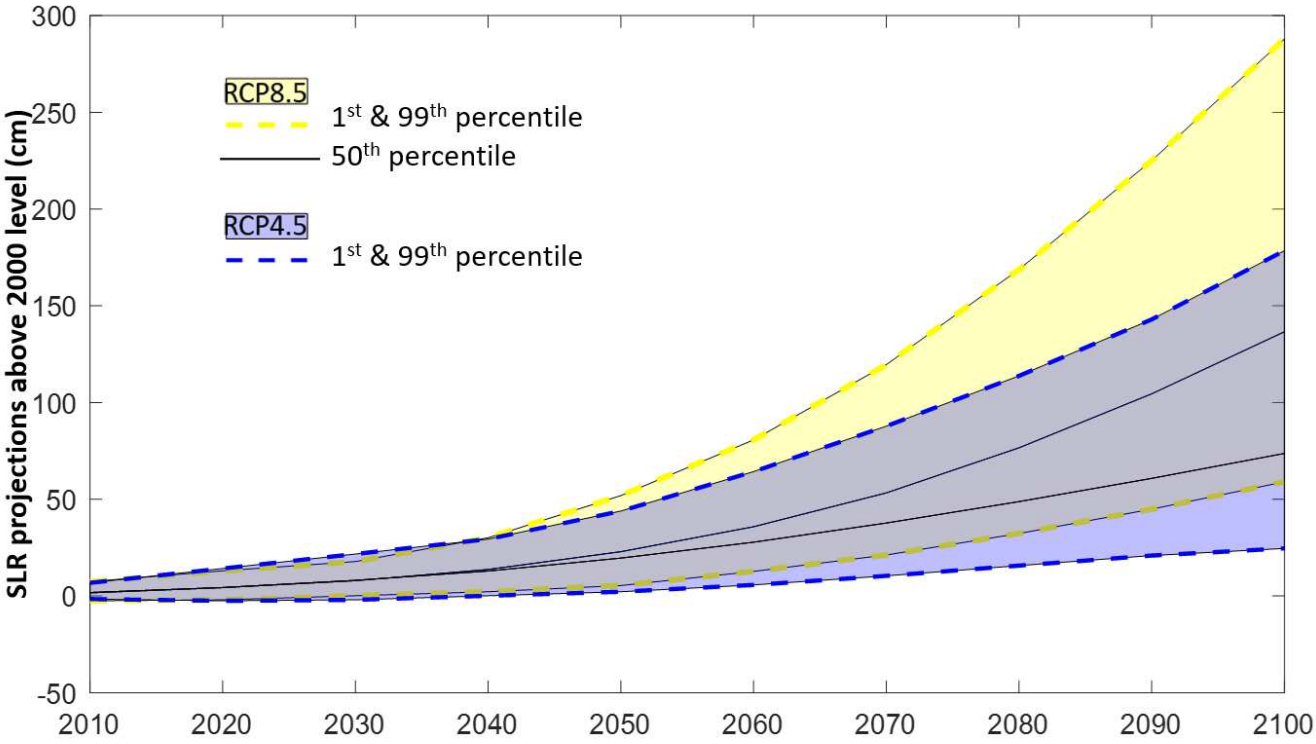

Figure 22 The probabilistic SLR projections for seawall design in San Francisco, CA using two different RCPs from 2010 to 2100. The solid lines show the 50th percentile values and the dash lines represent the 1st and 99th percentiles.

The local SLR projections are provided under CMIP phase 5 simulations (RCP 4.5 and RCP 8.5). These values suggest that by 2100 under the high emission scenario (RCP 8.5), the maximum SLR of what is physically possible is 288 cm which corresponds to the 99.9^{th} percentile. As a first step toward implementing an adaptive seawall design, the contributing future climatic hazards need to be identified over time. Here, SLR projections represent the climatic load and random variable (sea water level) behind the seawall. Our hypothetical example design is based on sea level in the year 2100 in which, the corresponding SLR projections are 75.6 cm and 288 cm for moderate (RCP 4.5) and upper bound of the high (RCP 8.5) emission scenarios, respectively.

Design freeboard: Here, we assess the integrity of a seawall in terms of change in freeboard and the associated performance under a changing climate. Code of Federal Regulations (CFR) for the National Flood Insurance Program defines the freeboard as a factor of safety above a flood level (FEMA, 2000). Freeboard aims to account for the many unknown factors that could contribute to flood heights. The Federal Emergency Management Agency (FEMA) requires seawall systems to have a required "Freeboard" of at least two feet above the base flood (FEMA, 2000).

Unsatisfactory Performance function

To determine the capacity of a structural system, the loads and resistances of the system need to be examined to find where the system will exceed the limitations (Ebeling & White, 2021). Performance function or a factor of safety, which is the ratio of the capacity to resist a demand (i.e., load), serves as the design criteria in engineering practices. When the performance function is less than the pre-defined performance criteria, the structural performance is considered

unsatisfactory (e.g., Schultz et al., 2018). The probability for the exceedance of limitations is called the Probability of Unsatisfactory Performance (PUP). In fact, the structural failure probability shows the probability of unsatisfactory performance (PUP) under a range of loads (e.g., Schultz et al., 2010). This terminology recognizes that a structure may not fail, but the integrity may be threatened, thus needing repair or adaptation. For the seawall example, we characterize the performance function without conducting physical modeling:

$$PF = \frac{FB_i - \Delta_{slr}}{FB_{min}} \quad (1)$$

where PF represents the performance function of the seawall, Δ_{slr}represents the SLR projection above 2000 level, FB_{min} is the minimum required freeboard for safe operation (to be decided by the designer), and FB_i stands for the freeboard in base design (Figure 23). We consider three common initial freeboards of 66 cm, 100 cm, and 150 cm and three different min F.B. of 20 cm, 30 cm, and 40 cm to demonstrate performance of the seawall. The performance function larger than 1 represents a satisfactory performance, and a performance function less than 1 indicates an unsatisfactory performance. Here we estimate the probability of performance empirically by investigating each individual climate model relative to the total possible outcomes. For simplicity, we use 8 percentiles of SLR projections provided by the 4th California Climate Change Assessment Report. Then, the probability of unsatisfactory performance (PUP) for each RCPs with its uncertainty bounds is defined as follows:

$$PUP = \frac{N_{UPprc}}{TN_{Prc}} \quad (2)$$

where PUP is the probability of unsatisfactory performance, N_{UPprc} shows the number of SLR percentiles for which the performance function is less than 1, and TN_{Prc} represents the total number of SLR percentiles (here, 8 for RCP 8.5 and RCP 4.5 and 16 for combined RCPs scenario).

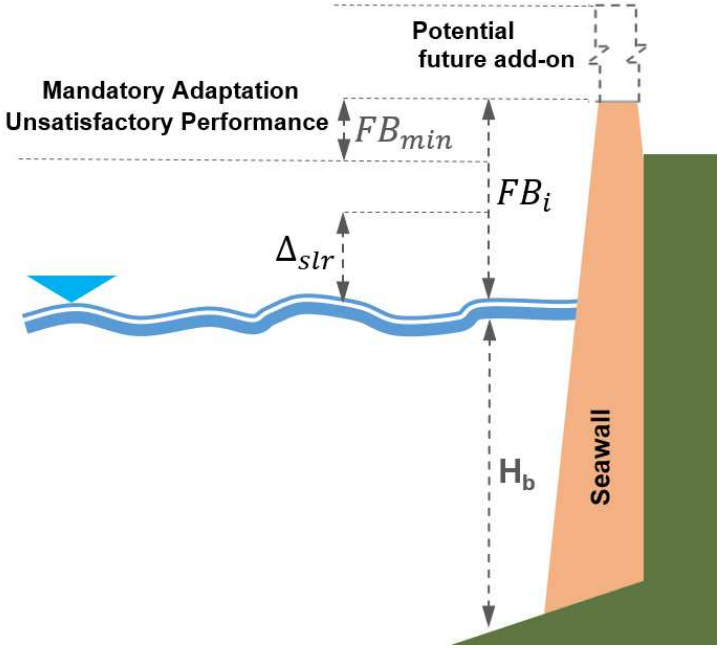

Figure 23. Seawall schematic presenting initial freeboard (FB_i), SLR projections (Δ_{slr}), and minimum freeboard (FB_{min}).

For each SLR percentile, we estimate the seawall's performance function over time at the decadal scale. Figure 24 presents the performance function for a seawall in San Francisco. Over time, the performance of the seawall tends to decrease due to the projected SLR. The seawall's performance is shown for the 50th percentile of the RCP 8.5 SLR projections (dots) and the 99th percentile and

1st percentile uncertainty bounds (dashed lines). The differences in performances between the high-end and 1st percentile scenarios become evident after the mid-century. If future projections follow the upper bound (RCP 8.5, 99th percentile), the seawall's performance will drop below 1 (performance threshold) in the year 2052, indicating unsatisfactory performance and thus, adaption is needed. Under RCP 8.5, 50th percentile scenario, the seawall would perform desirably based on the selected minimum freeboard until 2070, before falling into unsatisfactory performance.

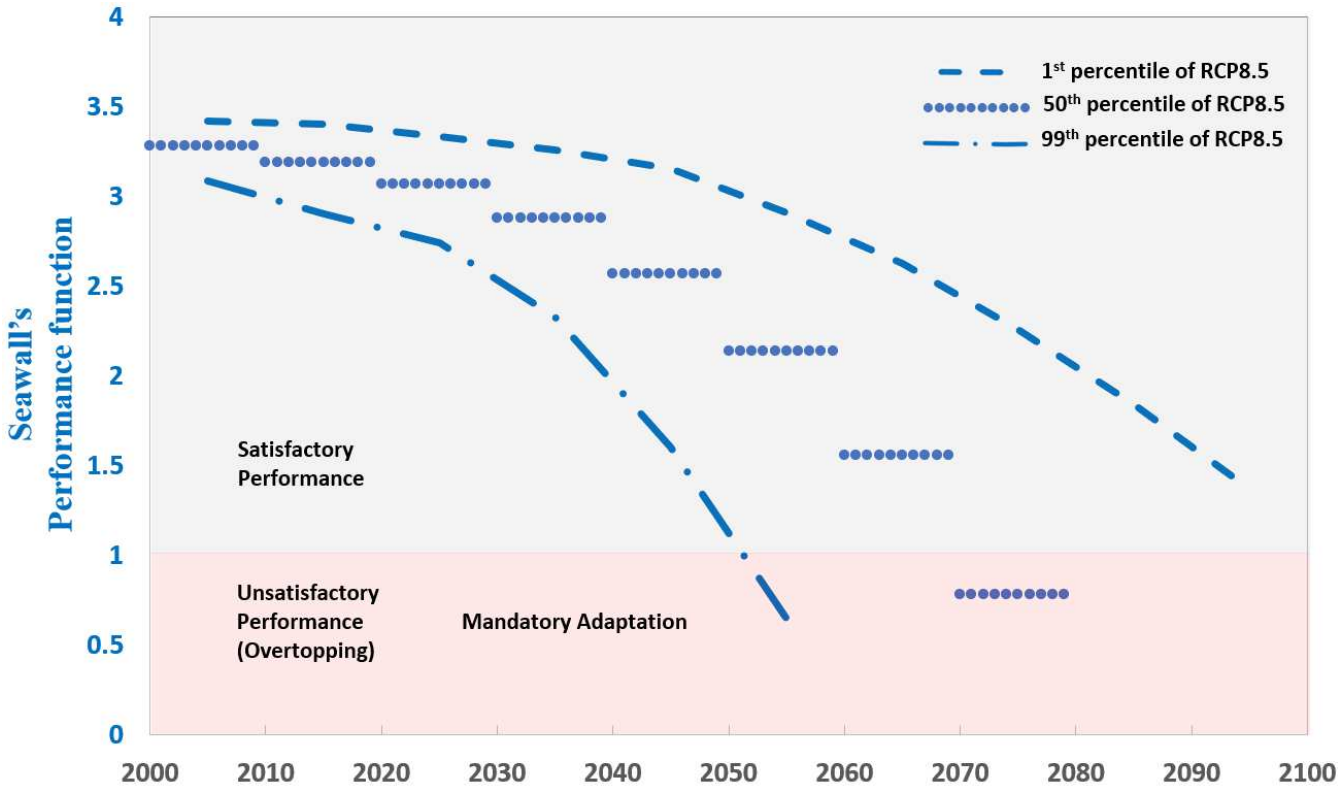

Figure 24. Performance function for a seawall facing sea level rise in San Francisco at the decadal time steps. The dots show the seawall's performance based on the 50th percentile of the RCP 8.5 SLR projections. Dashed lines represent the uncertainty bounds for RCP 8.5 based on 99th percentile and 1st percentile. Initial and minimum freeboard are assumed to be 100 cm and 30 cm, respectively.

In the following, we show how considering different initial freeboards and minimum freeboards would affect the performance function and adaptation threshold. Figure 25 illustrates the performance function for a seawall in San Francisco under 50th percentile of RCP8.5 SLR projections with three different minimum freeboard values. In all three cases, initial freeboard is assumed 100 cm. The blue, yellow, and gray dots show the seawall's performance based on minimum freeboard of 20 cm, 30 cm, and 40 cm, respectively. For both minimum freeboard of 40 cm and 30 cm, the seawall's performance drops below 1 (performance threshold) in the 2070s. If we assume a minimum freeboard of 20 cm, the seawall will perform satisfactorily until the 2080s (i.e., almost the entire lifetime). However, the risk of overtopping would be more significant assuming a minimum freeboard of 40 cm or 30 cm. The proposed adaptation indicator informs seawall's unsatisfactory performance in advance, enabling implementing timely modifications (e.g., increasing seawall's height) in the future.

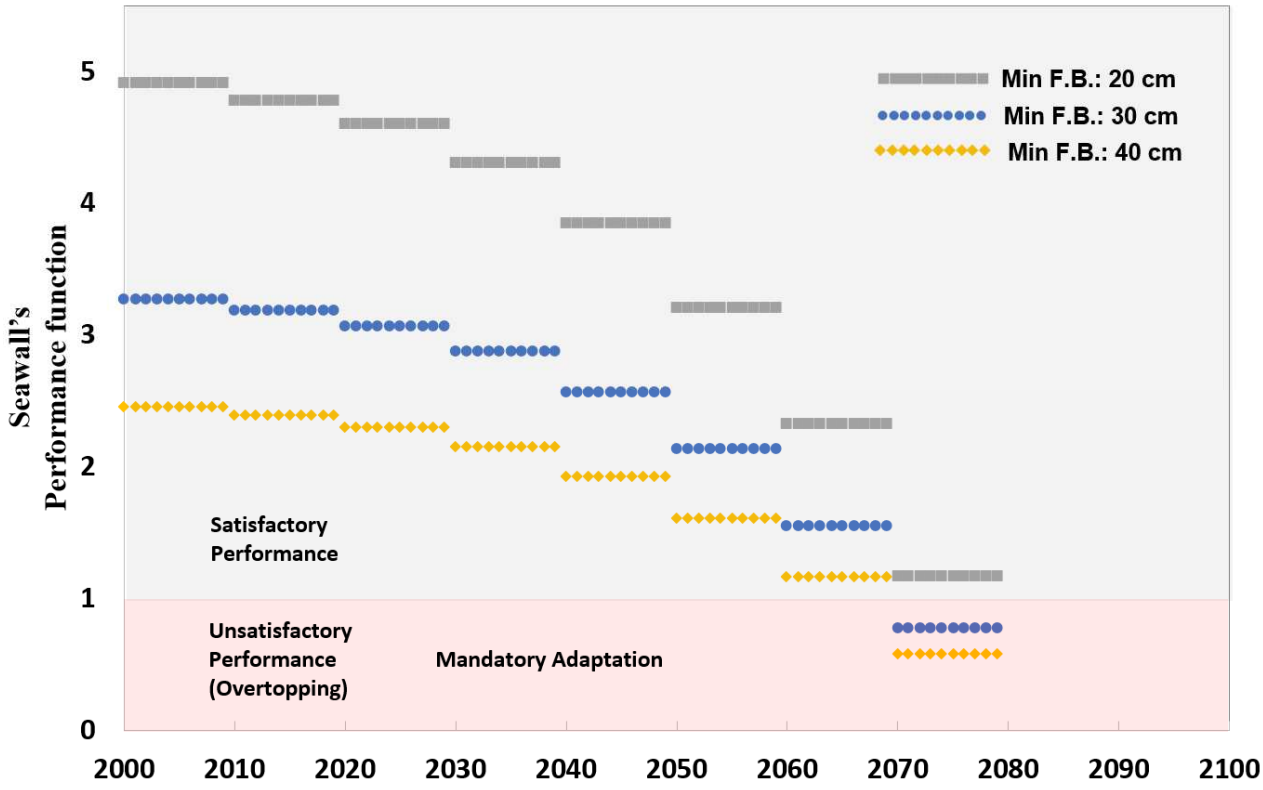

Figure 25. Performance function for a seawall facing sea level rise in San Francisco under 50th percentile of RCP8.5 SLR projections with 3 different Min F.B. values. The gray, blue, and yellow dots show the seawall's performance for min F.B. of 20 cm, 30 cm, and 40 cm, respectively. In all three cases the initial freeboard is assumed 100 cm.

Figure 26 shows the performance function for a seawall facing sea level rise in San Francisco under 50th percentile of RCP8.5 SLR projections assuming 3 different initial freeboards at the design stage. The gray, blue, and yellow dots show the seawall's performance for three initial freeboards of 66 cm, 100 cm, and 150 cm, respectively. In all three cases, the minimum freeboard is assumed to be 20 cm. For the commonly used freeboard of 66 cm, the seawall's performance will drop below 1 (performance threshold) in the year 2060, indicating adaption is needed before then. However, if we design for a larger freeboard (e.g., 150 cm) at the design stage, the seawall will perform desirably in the gray area until almost the end of its lifetime (i.e., 2090s).

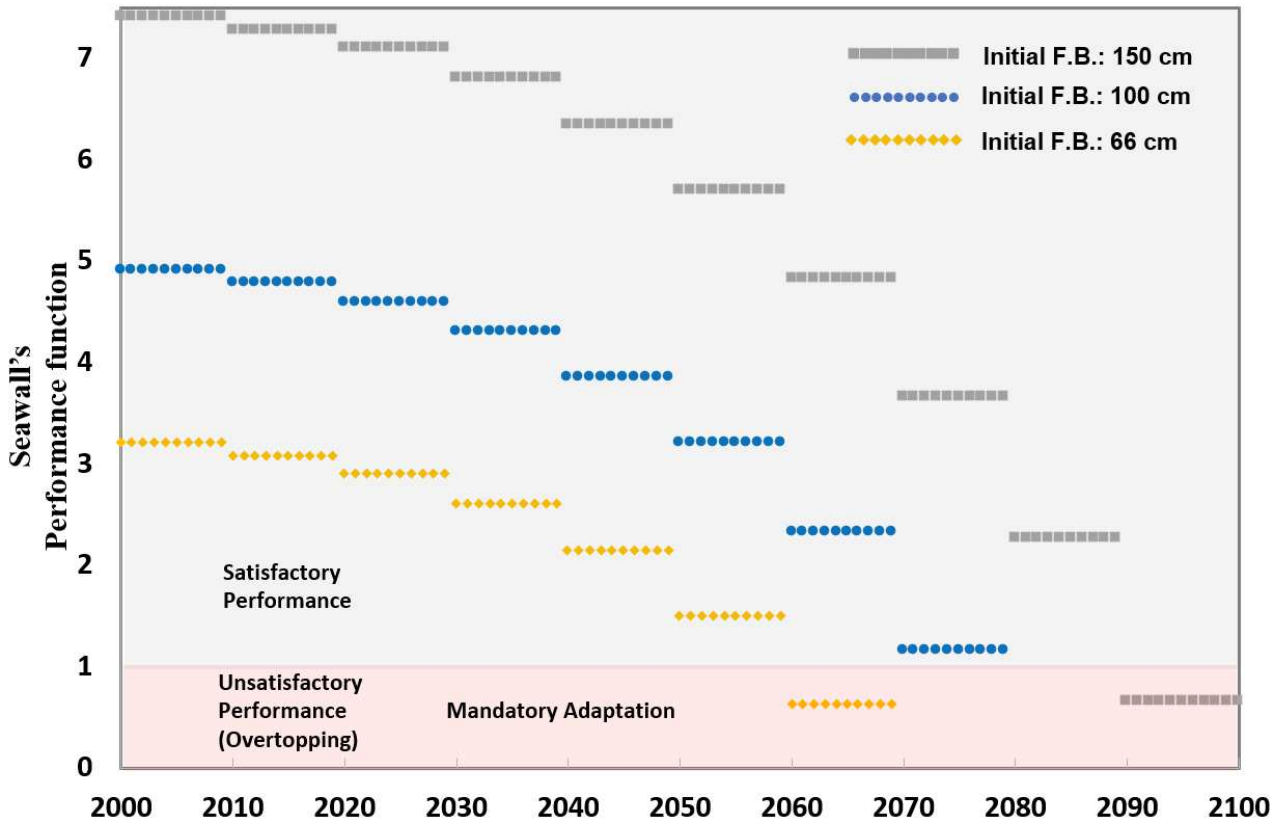

Figure 26. Performance function for a seawall facing sea level rise in San Francisco under 50th percentile of RCP8.5 SLR projections with 3 different initial F.B.. The gray, blue, and yellow dots show the seawall's performance for three initial freeboards of 66 cm, 100 cm, and 150 cm, respectively. Minimum freeboard is assumed 20 cm.

Figure 27 illustrates the probability of unsatisfactory performance for a seawall facing sea level rise in San Francisco. The seawall's PUP values are presented for RCP 4.5, RCP 8.5, and combined RCPs. In this case, initial and minimum freeboards are assumed to be 100 cm and 30 cm, respectively. In our methodology, SLR is the random variable; thus, PUP values represent the probability of unsatisfactory performance under the projected SLR distribution (e.g., RCP 8.5 with its uncertainty bounds) in each year. These PUP values are proportional to the number of events (here, SLR percentiles) that their performance functions are not satisfactory (performance less than

1). In the year 2100, if we consider the RCP 8.5 scenario, including its uncertainty bounds (e.g., 1st to 99th percentiles), the PUP of the seawall will increase up to 0.9, which is considerable for design and planning. Under a moderate future climate scenario (RCP 4.5), the PUP of the seawall could elevate up to 0.63 in the year 2100.

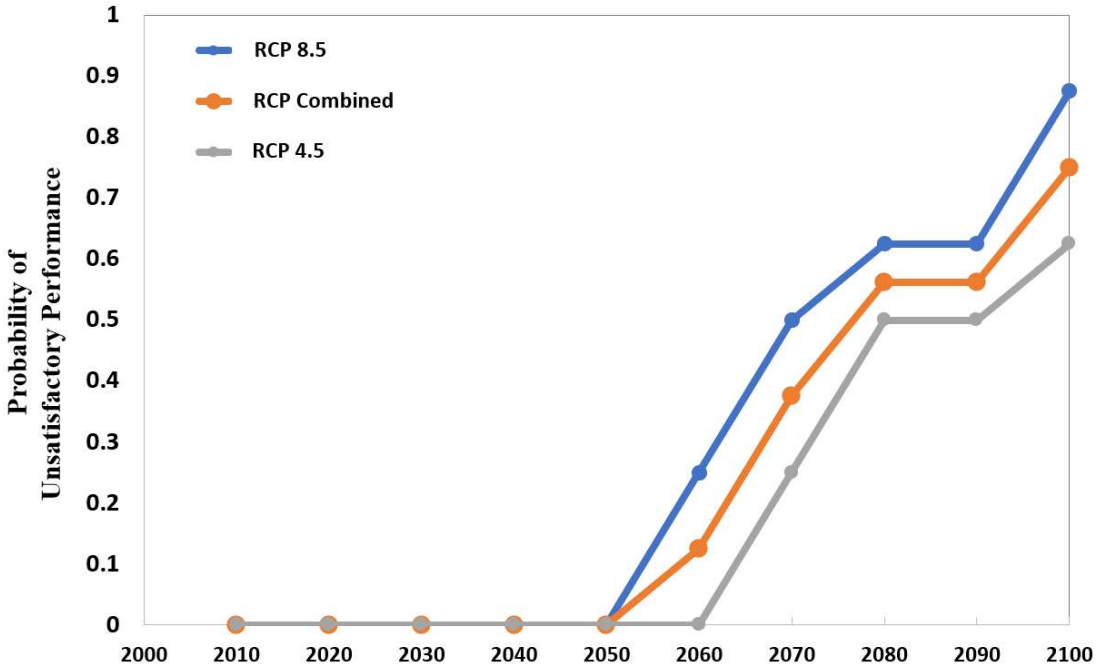

Figure 27. Probability of unsatisfactory performance for a seawall facing sea level rise in San Francisco. Gray, orange, and blue lines show the seawall's PUP values under RCP 4.5, RCP 8.5, and combined RCPs SLR scenarios. Initial and minimum freeboard are assumed to be 100 cm and 30 cm, respectively.

In the following, we show how the seawall adaptive design can be used in practice considering different sea level rise projections and RCPs. Figure 28 depicts the proposed adaptive and flexible design over lifetime. Let's assume that the initial design is based on the moderate SLR scenario (50th percentile of RCP 4.5 projections) in 2100 (i.e., 74 cm). This initial design is case specific

and depends on the sensitivity of the project and acceptable risk. Following the completion of the initial construction, the design will be adjusted if new observed information indicates changes in projected extremes toward a more extreme RCP scenario (e.g., RCP 8.5). By continuously evaluating future changes, risk managers need to compare the observed sea level rise (yellow asteroids, Figure 28) with the projected sea level rise used in the initial design. Upon observing a shift toward RCP8.5 (e.g., in the 2040s as shown in Figure 28), a new design height should be determined based on the most updated ensemble and the accepted risk (e.g., 83rd percentile of RCP 8.5 – 216 cm). Without any adaptive measure, the probability of unsatisfactory performance of the structure increases over time and may exceed the acceptable threshold (i.e., 1) before the end of its lifetime (see the yellow line reaching the red zone in Figure 28). In this example, after observing a shift from what was initially considered for the initial design (RCP 4.5), the seawall will be adopted (see the gray dots and line if Figure 28). In the revised version (gray line), the performance remains well above 1 during the life of the project.

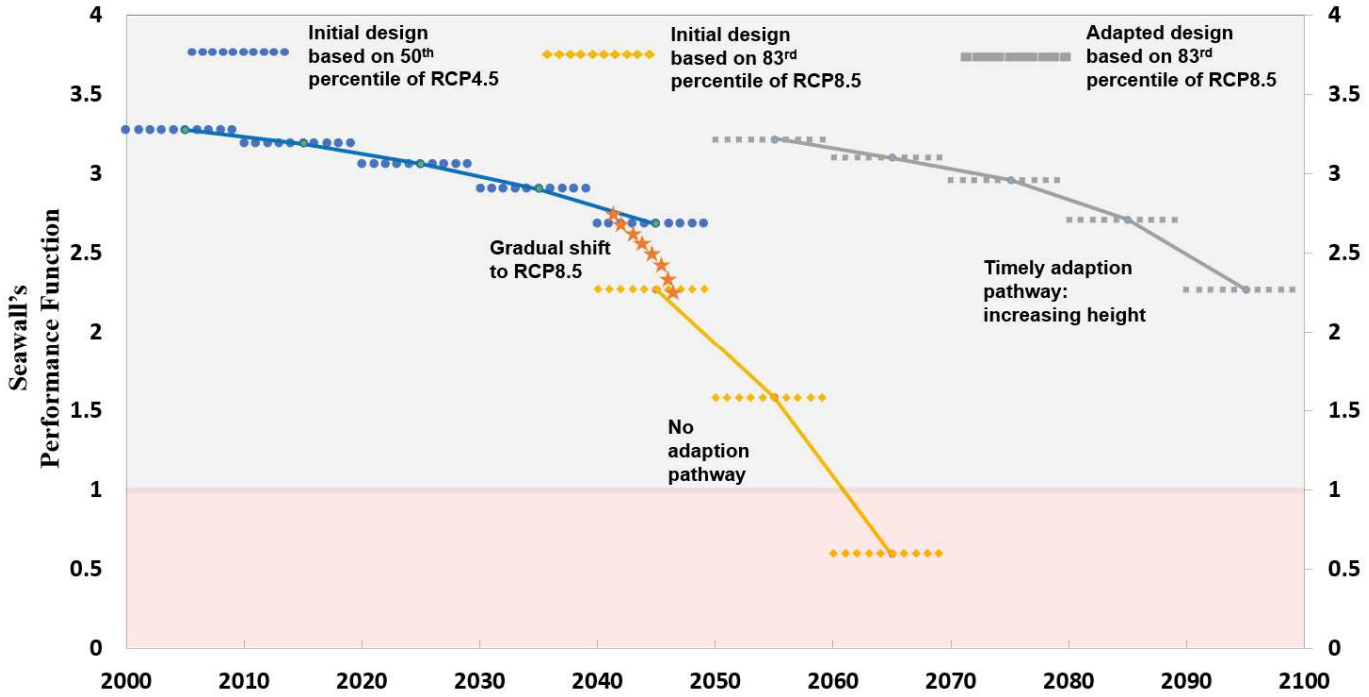

Figure 28. An example adaptive seawall design concept in San Francisco. Initial design is based on a moderate SLR scenario (here, 50th percentile of RCP 4.5) in 2100 (74 cm) – blue line. Observations over the life of the project shows that sea levels follow the RCP8.5 and without adaptation, performance function will go below 1 before the end of the project (yellow line reaching the red zone). By updating the design based on the 83rd percentile of the RCP 8.5 in 2100 (216 cm), for example, one can ensure the performance will remain well above one over the life of the project (gray line). The y axis shows the performance function at the decadal time steps. The Initial and minimum freeboards are assumed 100 cm and 30 cm, respectively.

Summary

Climatic extremes pose disruption to infrastructure systems. To ensure the safety and durability of infrastructure systems in the future, we propose a framework for infrastructure desing in a changing climate. This framework aims to quantify the impacts of natural hazards and climatic extremes (e.g., floods) on the structural integrity of current and future infrastructure systems at component and system levels. The proposed adaptive iteration includes selection of a most probable, but not inherently most conservative base design case with the ability to adjust if new observed information (or climate projections) indicates increases in future extremes. The choice

of most probable condition for design cannot be generalized and depends on the specifics of the project and acceptable risk in the study area.

Offering an applicable approach, we implement the proposed adaptive design on a conceptual seawall system for the planning horizon of year 2100, under different sea level rise (SLR) scenarios. In this example, after observing a shift from the most probable SLR to high SLR scenario in the year 2070, the design height would be adjusted based on the most credible SLR scenario at the time of re-design (here, 2 m: 0.4 m higher than the initial design). After implementing the adaptive design modification (increasing seawall height), the risk of failure decreases over the lifetime. Adaptive design methodology will require further refinements for region-specific and structure-specific applications before it can be fully implemented in the practice. However, this approach provides a broad definition and general steps leading toward climate-ready infrastructure designs. Such a method has the potential to prevent overinvestment that would be incurred if extremely robust designs are implemented, while providing a way forward to deal with uncertainty in climate projections and changing extremes.

Chapter 6 Summary and Conclusion

Human activities have altered the natural hydrologic cycle, leading to changes to the quantity, quality, and distribution of water. Over the past decades, human□induced climate change has caused additional variability in the frequency and/or intensity of climatic hazards such as drought and flood. The compounding effects of human□induced climate change with water and land use practices have elevated the complexity of water resources management and infrastructure systems planning. In this dissertation, we develop frameworks for modeling and assessing human activities in the natural and built environment. The objectives include:

(OB) 1- Evaluate compounding effects of meteorological drought and unsustainable water resource management contributing to catastrophic environmental degradation.

(OB) 2- Investigate the notion of anthropogenic flood events where human disruptions have caused or intensified flood risk to unprecedented levels.

(OB) 3- Evaluate performance (i.e., factor of safety) of water infrastructure under anthropogenic climate change, and propose adaptive strategies toward climate-ready infrastructure systems.

This Chapter summarized our conclusions for the objectives listed above.

(OB) 1: We explored frameworks for quantifying human influence on the observed changes in Lake Urmia. Located in northwestern Iran, Lake Urmia is an exemplar of how unsustainable water management to meet growing water demand can worsen meteorologic drought and create massive socio-ecological challenges. We developed a detailed water resources systems model of the basin and lake interactions, including datasets of infrastructure (i.e., reservoir capacity and operating policies), observed streamflow, and agricultural and urban water demand. Results demonstrate that a growing anthropogenic drought combined with meteorological drought drove the lake toward a state of hydrological overshoot and collapse. The rapid water level decline after the drought of record (1998-2002) when annual runoff decreased by 48% is synchronous with an approximately 25% increase in surface water withdrawals, especially in the agricultural sector. The lake level remained significantly below the designated ecological threshold (1274 m above sea level) even in a relatively normal period immediately after the drought.

We develop a dynamic and climate-informed environmental inflow plan, which is critical for reviving the lake. We estimate that the lake's environmental inflow requirements range from 2900 mcm/yr (during dry conditions) to 5400 mcm/yr (during wet conditions), with the average being 4100 mcm/yr. Depending on the climatic condition, water withdrawal reduction plan, and environmental releases, Lake Urmia's recovery time can range from 3 to 16 years.

(OB) 2: To explore the notion of anthropogenic floods, we investigate a series of severe flood events over two weeks (late March and early April 2019) that devastated several areas across Iran following a multi-year dry period. Our analysis reveals several takeaways pertinent to the interlinked hydro-climatic drivers and anthropogenic catalyzers of flooding. The risk of flooding for loss of life and assets has been remarkably raised by man-made changes to river basins to the point that some urban areas are particularly vulnerable to anthropogenic floods (e.g., Darvazeh Quran Catchment in Shiraz, Fars Province, Iran). We illustrate how spring 2019 flood impacts in Iran were exacerbated by various human-induced changes, including construction along rivers, deforestation, aggradation, natural channel constriction, and poorly sized water conveyance structures. It is necessary to rethink urban planning and floodplain management in light of increased flood risks due to changing extreme events and cascading hydro-climatological effects compounded with growing exposure and severity of flood incidents in urbanizing areas.

(OB) 3: To evaluate the impacts of climatic extremes on infrastructure, we study a levee that is subjected to past and future streamflow projections. Toward achieving a climate-ready levee system, we first identify the new patterns of the natural hazard (i.e., flood) that affects the levee in the future. The daily streamflow projections (1950-2099) are used for flood frequency analysis at the Elkhorn Levee location (Sacramento, California) using ProNEVA. Our results based on the most extreme climate model (CanESM2 model, RCP 8.5) projected higher future peak water levels in the future (2049-2099) compared to the corresponding flood levels in the baseline (1950-2000) period, implying higher flood risk in the future. The water level corresponding to the future 50-year flood event is expected to be a 1.34 m higher-6.5% increase relative to the current condition.

We translate the information on changing streamflow extremes to actual physical levee response (e.g., failure probability). In the levee's physical modeling, the flood level for different return periods represents the hydraulic load which is applied into a set of transient coupled finite-element seepage and limit equilibrium slope stability analyses. The failure probability of the levee would increase up to 27% when considering future streamflow projections (failure probabilities of 0.77 and 0.98 under past and future climate, respectively). These results indicate that a 1.3 m higher flood level in the future would lead to a 27% higher risk of levee failure, which is considerable in risk assessment. Our method allows translating the change in hazard to change in performance. Currently, these evaluations are not available, and we achieve our main goal by generating this information.

Finally, to ensure the safety and durability of infrastructure systems in the future, we define a framework for adapting to climatic changes. The proposed adaptive iteration includes the selection of a moderate climate scenario but not inherently conservative base design case with the ability to adjust if new observed information (or even climate projections) admits exceeding the initial acceptable risk. We implement the proposed adaptive design on a conceptual seawall system for the planning horizon of the year 2100 under different sea level rise (SLR) scenarios. In this hypothetical example, after observing a shift from the moderate SLR (RCP 4.5) to the high SLR scenario in 2040, the adjusted design height after the modification stage would be based on the most credible SLR scenario (RCP 8.5). Adaptive design methodology will require further refinements for region-specific and structure-specific applications before it can be fully implemented in practice. However, this approach provides a broad definition and general steps leading toward climate-ready infrastructure design. Such a method has the potential to minimize overinvestment that would be incurred if extremely robust designs are implemented while

providing a means to deal with uncertainty in climate projections. However, this approach would require careful consideration and planning to provide resources for observation and potential modification of the structure during the life of the project.

References

Abbaspour, M., and Nazaridoust, A. (2007). Determination of environmental water requirements of Lake Urmia, Iran: an ecological approach. International Journal of Environmental Studies, 64(2), 161–169. https://doi.org/10.1080/00207230701238416

Adams, L.E., Lund, J.R., Moyle, P.B., Quiñones, R.M., Herman, J.D., and O'Rear, T.A. (2017). Environmental hedging: Theory and method for reconciling reservoir operations for downstream ecology and water supply. Water Resources Research, 53(9), 7816–7831, doi:10.1002/2016WR020128.

AghaKouchak, A., Norouzi, H., Madani, K., Mirchi, A., Azarderakhsh, M., Nazemi, A., …, and Hasanzadeh, E. (2015). Aral Sea syndrome desiccates Lake Urmia: Call for action. Journal of Great Lakes Research, 41(1), 307–311. https://doi.org/10.1016/j.jglr.2014.12.007

Ahmadi, R., Mohebbi, F., Hagigi, P., Esmailly, L., and Salmanzadeh, R. (2011). Macro-invertebrates in the wetlands of the Zarrineh estuary at the south of Urmia Lake (Iran), International Journal of Environmental Studies, 5 (4), 1047-1052.

Ahmadzadeh Kokya, T., Pejman, A., Mahin Abdollahzadeh, E., Ahmadzadeh Kokya, B., and Nazariha, M. (2011). Evaluation of salt effects on some thermodynamic properties of Urmia Lake water Int. J. Environ. Res., 5 (2), 343-348.

Ahn, S. R., Jeong, J. H., and Kim, S. J. (2016). Assessing drought threats to agricultural water supplies under climate change by combining the SWAT and MODSIM models for the

Geum River basin, South Korea. Hydrological Sciences Journal, 61(15), 2740–2753. https://doi.org/10.1080/02626667.2015.1112905.

Alfieri, L., Burek, P., Feyen, L., Forzieri, G., 2015. Global warming increases the frequency of river floods in Europe. Hydrol. Earth Syst. Sci. 19, 2247.

Alfredsen, K., 2017. An assessment of ice effects on indices for hydrological alteration in flow regimes. Water 9, 914.

Allan, J.A., (1998). Virtual water: A strategic resource global solutions to regional deficits. Groundwater, 36(4), 545-546.

Ardalan, A., Holakouie Naieni, K., Kabir, M.-J., Zanganeh, A.-M., Keshtkar, A.-A., Honarvar, M.-R., Khodaie, H., Osooli, M., 2009. Evaluation of Golestan Province's Early Warning System for flash floods, Iran, 2006–7. Int. J. Biometeorol. 53, 247–254. https://doi.org/10.1007/s00484-009-0210-y

Argyroudis, S. A., Mitoulis, S. A., Hofer, L., Zanini, M. A., Tubaldi, E., & Frangopol, D. M. (2020). Resilience assessment framework for critical infrastructure in a multi-hazard environment: Case study on transport assets. Science of The Total Environment, 714, 136854.

Arkian, F., Nicholson, S. E., and Ziaie, B. (2018). Meteorological factors affecting the sudden decline in Lake Urmia's water level. Theoretical and Applied Climatology, 131(1–2), 641–651. https://doi.org/10.1007/s00704-016-1992-6

ASCE. (2017). Report Card on America's Infrastructure: Dams. The American Society of Civil Engineers (ASCE). Retrieved from https://www.infrastructurereportcard.org/wp-content/uploads/2017/01/Dams-Final.pdf

Ashraf Vaghefi, S., Abbaspour, K. C., Faramarzi, M., Srinivasan, R., and Arnold, J. G. (2017). Modeling Crop Water Productivity Using a Coupled SWAT–MODSIM Model. Water, 9(3), 157. https://doi.org/10.3390/w9030157

Ashraf, B., AghaKouchak, A., Alizadeh, A., Baygi, M. M., Moftakhari, H. R., Mirchi, A., …, and Madani, K. (2017). Quantifying Anthropogenic Stress on Groundwater Resources. Scientific Reports, 7(1), 12910. https://doi.org/10.1038/s41598-017-12877-4

Aven, T. & Guikema, S. Risk assessment under deep uncertainty: A methodological comparison. Reliab. Eng. Syst. Saf. 159, 12–23 (2017).

Averyt, K., Meldrum J., Caldwell, P., Sun, G., McNulty, S., Huber-Lee, A., and Madden, N. (2013). Sectoral contributions to surface water stress in the coterminous United States. Environmental Research Letters, 8(3), 35046.

Ayyub, B. M., & Wright, R. N. (2016). Adaptive Climate Risk Control of Sustainability and Resilience for Infrastructure Systems. Journal of Geography & Natural Disasters, 6(2). https://doi.org/10.4172/2167-0587.1000e118

Babovic, F., Mijic, A., & Madani, K. (2018). Decision making under deep uncertainty for adapting urban drainage systems to change. Urban Water Journal, 15(6), 552-560.

Barigozzi, C., Varotto, V., Baratelli, L., and Giarrizzo, R. (1987). The Artemia of Urmia Lake (Iran): mode of reproduction and chromosome numbers, Atti della Accademia Nazionale dei Lincei. Classe di Scienze Fisiche, Matematiche e Naturali. Rendiconti, Serie 8, 81(1), 87-90.

Barnum, D. A., Bradley, T., Cohen, M., Wilcox, B., and Yanega, G. (2017). State of the Salton Sea—A science and monitoring meeting of scientists for the Salton Sea (USGS Numbered Series No. 2017–1005). Reston, VA: U.S. Geological Survey. Retrieved from http://pubs.er.usgs.gov/publication/ofr20171005

Beitollahi, A., basiri, M., Mahdavi, M., Soleimani, M., Dehghan, F., Abedi, A., 2019a. Darvazeh Quran Shiraz Flood- Risk Working Group Report. Ministry of Roads and Urban Development, Iran.

Beitollahi, A., Soodmand, N., Mahdavi, M., Soleimani, M., Dehghan, F., 2019b. Golestan Flood-Risk Working Group Report. Ministry of Roads and Urban Development.

Belward, A.S., Estes, J.E., Kline, K.D., 1999. The IGBP-DIS global 1-km land-cover data set DISCover: A project overview. Photogramm. Eng. Remote Sens. 65, 1013–1020.

Berhe, F. T., Melesse, A. M., Hailu, D., and Sileshi, Y. (2013). MODSIM-based water allocation modeling of Awash River Basin, Ethiopia. CATENA, 109, 118–128. https://doi.org/10.1016/j.catena.2013.04.007

Blöschl, G., Hall, J., Parajka, J., Perdigão, R.A.P., Merz, B., Arheimer, B., Aronica, G.T., Bilibashi, A., Bonacci, O., Borga, M., Čanjevac, I., Castellarin, A., Chirico, G.B., Claps, P., Fiala, K., Frolova, N., Gorbachova, L., Gül, A., Hannaford, J., Harrigan, S., Kireeva,

M., Kiss, A., Kjeldsen, T.R., Kohnová, S., Koskela, J.J., Ledvinka, O., Macdonald, N., Mavrova-Guirguinova, M., Mediero, L., Merz, R., Molnar, P., Montanari, A., Murphy, C., Osuch, M., Ovcharuk, V., Radevski, I., Rogger, M., Salinas, J.L., Sauquet, E., Šraj, M., Szolgay, J., Viglione, A., Volpi, E., Wilson, D., Zaimi, K., Živković, N., 2017. Changing climate shifts timing of European floods. Science 357, 588–590. https://doi.org/10.1126/science.aan2506

Bolten, J.D., Crow, W.T., Zhan, X., Jackson, T.J., Reynolds, C.A., 2009. Evaluating the utility of remotely sensed soil moisture retrievals for operational agricultural drought monitoring. IEEE J. Sel. Top. Appl. Earth Obs. Remote Sens. 3, 57–66.

Bras, R. L. (1990). Hydrology: an introduction to hydrologic science. Addison Wesley Publishing Company.

Bronstert, A., 2003. Floods and climate change: interactions and impacts. Risk Anal. Int. J. 23, 545–557.

Brown, M.E., Escobar, V., Moran, S., Entekhabi, D., O'Neill, P.E., Njoku, E.G., Doorn, B., Entin, J.K., 2013. NASA's Soil Moisture Active Passive (SMAP) Mission and Opportunities for Applications Users. Bull. Am. Meteorol. Soc. 94, 1125–1128. https://doi.org/10.1175/BAMS-D-11-00049.1

Buchanan, M. K., Oppenheimer, M., & Kopp, R. E. (2017). Amplification of flood frequencies with local sea level rise and emerging flood regimes. Environmental Research Letters, 12(6), 064009. https://doi.org/10.1088/1748-9326/aa6cb3

CACC (Committee on Adaptation to a Changing Climate). (2018). Climate Resilient Infrastructure: A Manual of Practice on Adaptive Design and Risk Management, B. M. Ayyub, et al., ASCE, Reston, VA.

CDWR (2011). "Flood control system status report." California Department of Water Resources. Sacramento, CA.

Chang, H., Franczyk, J., Kim, C., 2009. What is responsible for increasing flood risks? The case of Gangwon Province, Korea. Nat. Hazards 48, 339.

Change, I.P. on C., 2012. Managing the Risks of Extreme Events and Disasters to Advance Climate Change Adaptation: Special Report of the Intergovernmental Panel on Climate Change. Cambridge University Press.

Cheng, L., AghaKouchak, A., Gilleland, E., & Katz, R. W. (2014). Non-stationary extreme value analysis in a changing climate. Climatic Change, 127(2), 353–369. https://doi.org/10.1007/s10584-014-1254-5

Cheng, L., AghaKouchak, A., Gilleland, E., Katz, R.W., 2014. Non-stationary extreme value analysis in a changing climate. Clim. Change 127, 353–369.

Choate, A., Dix, B., Rodehorst, B., Wong, A., Jaglom, W., Keller, J., Lennon, J., Dorney, C., Kuchibhotla, R., Mallela, J. and Sadasivam, S., 2017. Synthesis of Approaches for Addressing Resilience in Project Development (No. FHWA-HEP-17-082).

Christidis, N., Stott, P. A., & Brown, S. J. (2011). The Role of Human Activity in the Recent Warming of Extremely Warm Daytime Temperatures. Journal of Climate, 24(7), 1922–1930. https://doi.org/10.1175/2011JCLI4150.1

Coe, M. T., and Foley, J. A. (2001). Human and natural impacts on the water resources of the Lake Chad basin. Journal of Geophysical Research: Atmospheres, 106(D4), 3349–3356. https://doi.org/10.1029/2000JD900587

Coles, S., Bawa, J., Trenner, L., Dorazio, P., 2001. An introduction to statistical modeling of extreme values. Springer.

Cooley, D., 2013. Return periods and return levels under climate change, in: Extremes in a Changing Climate. Springer, pp. 97–114.

Corbane, C., Martino, P., Panagiotis, P., Aneta, F.J., Michele, M., Sergio, F., Marcello, S., Daniele, E., Gustavo, N., Thomas, K., 2020. The grey-green divide: multi-temporal analysis of greenness across 10,000 urban centres derived from the Global Human Settlement Layer (GHSL). Int. J. Digit. Earth 13, 101–118.

Das, T., Dettinger, M. D., Cayan, D. R., & Hidalgo, H. G. (2011). Potential increase in floods in California's Sierra Nevada under future climate projections. Climatic Change, 109(1), 71–94. https://doi.org/10.1007/s10584-011-0298-z

Das, T., Maurer, E.P., Pierce, D.W., Dettinger, M.D., Cayan, D.R., 2013. Increases in flood magnitudes in California under warming climates. J. Hydrol. 501, 101–110. https://doi.org/10.1016/j.jhydrol.2013.07.042

Delju, A., Ceylan, A., Piguet, E., and Rebetez, M., (2013). Observed climate variability and change in Urmia Lake Basin, Iran. Theor. Appl. Climatol. 111 (1–2), 285–296.

Dettinger, M., Anderson, J., Anderson, M., Brown, L.R., Cayan, D., Maurer, E., 2016. Climate Change and the Delta. San Franc. Estuary Watershed Sci. 14. https://doi.org/10.15447/sfews.2016v14iss3art5

Devastating flood in Shiraz claims lives of 11, injured 45 others [WWW Document], 2019. . Mehr News Agency. URL https://en.mehrnews.com/news/143627/Devastating-flood-in-Shiraz-claims-lives-of-11-injured-45-others (accessed 9.25.20).

Dezfuli, A., 2020. Rare atmospheric river caused record floods across the Middle East. Bull. Am. Meteorol. Soc. 101, E394–E400.

DFID, U. (2005). Climate Change and Development: South Asia Report.

Dittes, B., Kaiser, M., Špačková, O., Rieger, W., Disse, M., & Straub, D. (2018). Risk-based flood protection planning under climate change and modeling uncertainty: a pre-alpine case study. Natural Hazards and Earth System Sciences, 18(5), 1327–1347.

Dittrich, R., Wreford, A., & Moran, D. (2016). A survey of decision-making approaches for climate change adaptation: Are robust methods the way forward? Ecological Economics, 122, 79–89.

Dittrich, R., Wreford, A., & Moran, D. (2016). A survey of decision-making approaches for climate change adaptation: Are robust methods the way forward? Ecological Economics, 122, 79–89. https://doi.org/10.1016/j.ecolecon.2015.12.006

Ebeling, R. M., & White, B. C. (2021). Load and Resistance Factors for Earth Retaining, Reinforced Concrete Hydraulic Structures Based on a Reliability Index () Derived from the Probability of Unsatisfactory Performance (PUP): Phase 2 Study. ENGINEER RESEARCH AND DEVELOPMENT CENTER VICKSBURG MS.

England Jr, J. F., Cohn, T. A., Faber, B. A., Stedinger, J. R., Thomas Jr, W. O., Veilleux, A. G., ... & Mason Jr, R. R. (2019). Guidelines for determining flood flow frequency—Bulletin 17C (No. 4-B5). US Geological Survey.

Englhardt, J., de Moel, H., Huyck, C.K., de Ruiter, M.C., Aerts, J.C.J.H., Ward, P.J., 2019. Enhancement of large-scale flood risk assessments using building-material-based vulnerability curves for an object-based approach in urban and rural areas. Nat. Hazards Earth Syst. Sci. 19, 1703–1722. https://doi.org/10.5194/nhess-19-1703-2019

Enhanced resolution modelling study on anthropogenic climate change: changes in extremes of the hydrological cycle - Voss - 2002 - International Journal of Climatology - Wiley Online Library [WWW Document], n.d. URL https://rmets.onlinelibrary.wiley.com/doi/abs/10.1002/joc.757 (accessed 9.24.20).

Entekhabi, D., Njoku, E.G., O'Neill, P.E., Kellogg, K.H., Crow, W.T., Edelstein, W.N., Entin, J.K., Goodman, S.D., Jackson, T.J., Johnson, J., Kimball, J., Piepmeier, J.R., Koster, R.D., Martin, N., McDonald, K.C., Moghaddam, M., Moran, S., Reichle, R., Shi, J.C., Spencer, M.W., Thurman, S.W., Tsang, L., Van Zyl, J., 2010. The Soil Moisture Active Passive (SMAP) Mission. Proc. IEEE 98, 704–716. https://doi.org/10.1109/JPROC.2010.2043918

Falkenmark, M. and Rockström, J., (2004). Balancing water for humans and nature: the new approach in ecohydrology. London: Earthscan, p. 247.

Farokhnia, A. and Morid, S. (2014). Assessment of the effects of temperature and precipitation variations on the trend of river flows in Urmia Lake watershed. J.Water Wastewater 25 (91), 86–97.

Farzin, S., Ifaei, P., Farzin, N., Hassanzadeh, Y., and Aalami, M. (2012). An investigation on changes and prediction of Urmia Lake water surface evaporation by chaos theory, Int. J. Environ. Res. Public, 6 (3), 815-824.

Fathian, F., Morid, S., and Kahya, E. (2015). Identification of trends in hydrological and climatic variables in Lake Urmia basin, Iran. Theoretical and Applied Climatology, 119(3–4), 443–464. https://doi.org/10.1007/s00704-014-1120-4

FEMA. (2000). Federal Emergency Management Agency. Code of Federal Regulations (CFR) for the National Flood Insurance Program: 44 CFR § 59.1, § 65.10.

FEMA. (2015). Guidance for Flood Risk Analysis and Mapping; Combined Coastal and Riverine Floodplain. Federal Emergency Management Agency (FEMA). Retrieved from https://www.fema.gov/media-library-data/1436989628107-db27783b8a61ebb105ee32064ef16d39/Coastal_Riverine_Guidance_May_2015.pdf

FEMA. (2016). FEMA National Dam Safety Program Fact Sheet. Federal Emergency Management Agency (FEMA). Retrieved from https://www.fema.gov/media-library-data/1486735320675-8b0597aca8b23c7e2df293310e248bee/NDSPFlashFactSheet2015.pdf

Feng, Z., Leung, L.R., Hagos, S., Houze, R.A., Burleyson, C.D., Balaguru, K., 2016. More frequent intense and long-lived storms dominate the springtime trend in central US rainfall. Nat. Commun. 7, 13429. https://doi.org/10.1038/ncomms13429

Ficchì, A., Stephens, L., 2019. Climate Variability Alters Flood Timing Across Africa. Geophys. Res. Lett. 46, 8809–8819. https://doi.org/10.1029/2019GL081988

Fischer, E. M., & Knutti, R. (2015). Anthropogenic contribution to global occurrence of heavy-precipitation and high-temperature extremes. Nature Climate Change, 5(6), 560–564. https://doi.org/10.1038/nclimate2617

Fischer, E. M., & Knutti, R. (2016). Observed heavy precipitation increase confirms theory and early models. Nature Climate Change, 6(11), 986–991. https://doi.org/10.1038/nclimate3110

Floods Ravage Iran and Iraq [WWW Document], 2019. URL https://earthobservatory.nasa.gov/images/144785/floods-ravage-iran-and-iraq (accessed 9.24.20).

France-Presse, A., 2019. Iran Hit With 3rd Major Flood in 2 Weeks. N. Y. Times.

Fredericks Jeffrey W., Labadie John W., and Altenhofen Jon M. (1998). Decision Support System for Conjunctive Stream-Aquifer Management. Journal of Water Resources Planning and Management, 124(2), 69–78. https://doi.org/10.1061/(ASCE)0733-9496(1998)124:2(69)

Friedl, M.A., Sulla-Menashe, D., Tan, B., Schneider, A., Ramankutty, N., Sibley, A., Huang, X., 2010. MODIS Collection 5 global land cover: Algorithm refinements and characterization of new datasets. Remote Sens. Environ. 114, 168–182.

Gao, H., Bohn, T.J., Podest, E., McDonald, K.C., and Lettenmaier, D.P. (2011). On the causes of the shrinking of Lake Chad. Environmental Research Letters, 6(3), 034021.

Gariano, S. L., & Guzzetti, F. (2016). Landslides in a changing climate. Earth-Science Reviews, 162, 227–252. https://doi.org/10.1016/j.earscirev.2016.08.011

Garner, G., Van Loon, A.F., Prudhomme, C., Hannah, D.M., 2015. Hydroclimatology of extreme river flows. Freshw. Biol. 60, 2461–2476.

Gaybullaev, B., Chen, S.-C., and Kuo, Y.-M., (2012). Large-scale desiccation of the Aral Sea due to over-exploitation after 1960. J. Mt. Sci. 9 (4), 538–546.

Ghaheri, M., Baghal-Vayjooee, M., and Naziri, J., (1999). Lake Urmia, Iran: a summary review, Int. J. Salt Lake Res., 8 (1), 19-22.

Ghale, Y. A. G., Altunkaynak, A., and Unal, A. (2018). Investigation Anthropogenic Impacts and Climate Factors on Drying up of Urmia Lake using Water Budget and Drought Analysis. Water Resources Management, 32(1), 325–337. https://doi.org/10.1007/s11269-017-1812-5

Gholampour, A., Nabizadeh, R., Hassanvand, M. S., Taghipour, H., Nazmara, S., and Mahvi, A. H. (2015). Characterization of saline dust emission resulted from Urmia Lake drying.

Journal of Environmental Health Science and Engineering, 13, 82. https://doi.org/10.1186/s40201-015-0238-3

Gleeson, T., Wada, Y., Bierkens, M.F. and van Beek, L.P. (2012). Water balance of global aquifers revealed by groundwater footprint. Nature, 488(7410), 197-200.

Gohari, A., Eslamian, S., Mirchi, A., Abedi-Koupaei, J., Massah Bavani, A., and Madani, K. (2013). Water transfer as a solution to water shortage: A fix that can Backfire. Journal of Hydrology, 491, 23–39. https://doi.org/10.1016/j.jhydrol.2013.03.021

Gohari, A., Mirchi, A., and Madani, K. (2017). System Dynamics Evaluation of Climate Change Adaptation Strategies for Water Resources Management in Central Iran. Water Resources Management, 31(5), 1413–1434. https://doi.org/10.1007/s11269-017-1575-z

Gorelick, N., Hancher, M., Dixon, M., Ilyushchenko, S., Thau, D., Moore, R., 2017. Google Earth Engine: Planetary-scale geospatial analysis for everyone. Remote Sens. Environ. 202, 18–27.

Graham, L. P., Labadie, J. W., Hutchison, I. P. G., and Ferguson, K. A. (1986). Allocation of Augmented Water Supply Under a Priority Water Rights System. Water Resources Research, 22(7), 1083–1094. https://doi.org/10.1029/WR022i007p01083

Griffin, D.W. and Kellogg, C.A. (2004). Dust storms and their impact on ocean and human health: dust in Earth's atmosphere. EcoHealth, 1(3), 284-295.

Groves, D., Mao, Z., Liden, R., Strzepek, K. M., Lempert, R., Brown, C., ... & Bloom, E. (2015), Adaptation to Climate Change in Project Design, 131-154.

Ha, S., Kim, H., Kim, K., Lee, H., & Kim, H. (2017). Algorithm for Economic Assessment of Infrastructure Adaptation to Climate Change. Natural Hazards Review, 18(4), 04017007.

Haasnoot, M., Warren, A., & Kwakkel, J. H. (2019). Dynamic adaptive policy pathways (DAPP). In Decision Making under Deep Uncertainty (pp. 71-92). Springer, Cham.

Hall, D.K., Salomonson, V.V., Riggs, G.A., 2006. MODIS/Terra snow cover daily L3 global 500m grid. Boulder Colo. USA Natl. Snow Ice Data Cent. Version 5Tile H09v04.

Hallegatte, S. (2009). Strategies to adapt to an uncertain climate change. Global Environmental Change, 19(2), 240–247.

Hallegatte, S., Green, C., Nicholls, R. J., & Corfee-Morlot, J. (2013). Future flood losses in major coastal cities. Nature Climate Change, 3(9), 802–806.

Hallegatte, Stephane, Green, C., Nicholls, R. J., & Corfee-Morlot, J. (2013). Future flood losses in major coastal cities. Nature Climate Change, 3(9), 802–806. https://doi.org/10.1038/nclimate1979

Hallegatte, Stéphane. (2009). Strategies to adapt to an uncertain climate change. Global Environmental Change, 19(2), 240–247. https://doi.org/10.1016/j.gloenvcha.2008.12.003

Harvey, L. D. (2018). Global warming. Routledge.

Hassanzadeh, E., Elshorbagy, A., Wheater, H., Gober, P., and Nazemi, A. (2015). Integrating supply uncertainties from stochastic modeling into integrated water resource management: a case study of the Saskatchewan River Basin. ASCE Journal of Water

Resource Planning and Management, 10.1061/(ASCE)WR.1943-5452.0000581, 05015006.

Hassanzadeh, E., Zarghami, M., and Hassanzadeh, Y. (2012). Determining the Main Factors in Declining the Lake Urmia Level by Using System Dynamics Modeling. Water Resources Management, 26(1), 129–145. https://doi.org/10.1007/s11269-011-9909-8

Hatchett, B. J., Boyle, D. P., Putnam, A. E., and Bassett, S. D. (2015). Placing the 2012–2015 California-Nevada drought into a paleoclimatic context: Insights from Walker Lake, California-Nevada, USA. Geophysical Research Letters, 42(20), 2015GL065841. https://doi.org/10.1002/2015GL065841

Heidari, A., 2009. Structural master plan of flood mitigation measures. Nat. Hazards Earth Syst. Sci. 9.

Hershfield, D. M. (1961). Rainfall frequency atlas of the United States. Technical paper, 40.

Ho, M., Lall, U., Allaire, M., Devineni, N., Kwon, H. H., Pal, I., et al. (2017). The future role of dams in the United States of America. Water Resources Research, 53(2), 982–998. https://doi.org/10.1002/2016WR019905

Hoekstra A.Y., Chapagain A.K. (2006) Water footprints of nations: Water use by people as a function of their consumption pattern. In: Craswell E., Bonnell M., Bossio D., Demuth S., Van De Giesen N. (eds) Integrated Assessment of Water Resources and Global Change. Springer, Dordrecht, p. 35-48.

Hoekstra, A.Y. and Hung, P.Q. (2002). Virtual water trade. A quantification of virtual water flows between nations in relation to international crop trade. Value of water research report series, 11, p.166.

Hoekstra, A.Y., Mekonnen, M.M., Chapagain, A.K., Mathews, R.E., and Richter, B.D. (2012). Global monthly water scarcity: blue water footprints versus blue water availability. PLoS One, 7(2), e32688.

Hui, R., Herman, J., Lund, J., & Madani, K. (2018). Adaptive water infrastructure planning for nonstationary hydrology. Advances in water resources, 118, 83-94.

Hummel, M. A., Berry, M. S. & Stacey, M. T. Sea Level Rise Impacts on Wastewater Treatment Systems Along the U.S. Coasts. Earths Future 6, 622–633 (2018).

Introduction to Google Earth Engine [WWW Document], n.d. URL https://www.google.com/earth/outreach/learn/introduction-to-google-earth-engine/ (accessed 9.26.20).

IPCC (2007) Working Group II: Impacts, Adaptation and Vulnerability, Fourth Assessment Report: Climate Change.

IPCC (Ed.). (2012). Managing the risks of extreme events and disasters to advance climate change adaptation. A Special Report of Working Groups I and II of the Intergovernmental Panel on Climate Change [Field, C.B., V. Barros, T.F. Stocker, D. Qin, D.J. Dokken, K.L. Ebi, M.D. Mastrandrea, K.J. Mach, G.-K. Plattner, S.K. Allen, M. Tignor, and P.M. Midgley (eds.)]. (1. publ). Cambridge: Cambridge Univ. Press.

IPCC (Ed.). (2013). Climate change 2013: the physical science basis: Working Group I contribution to the Fifth assessment report of the Intergovernmental Panel on Climate Change. New York: Cambridge University Press.

Iran's Ministry of Energy (IME), Deputy of Water and Wastewater, Macro Planning Bureau, (2013). The National Water Master Plan Study in the Aras, Sefidrood, between Sefidrood and Haraz, Atrac and Urmia: Water allocation for the development projects in Urmia Lake basin. Report Number: 2385070-2050-24142. 2385070-2050-24142.

Iran's Ministry of Energy (IME), Deputy of Water and Wastewater, Macro Planning Bureau, (2014). The National Water Master Plan Study in the Aras, Sefidrood, between Sefidrood and Haraz, Atrac and Urmia: agricultural water use study in Urmia Lake Basin. Report Number: 2385070-4420-19464. 2385070-4420-19464.

Jaafari, A., Najafi, A., Pourghasemi, H.R., Rezaeian, J., Sattarian, A., 2014. GIS-based frequency ratio and index of entropy models for landslide susceptibility assessment in the Caspian forest, northern Iran. Int. J. Environ. Sci. Technol. 11, 909–926. https://doi.org/10.1007/s13762-013-0464-0

Jaafari, S., 2019. Iran Wasn't Ready for These Huge Floods: But They Should Get Ready for More in the Future. PRI April 29.

Jalili, M., Fekri, M., 2020. Consequences of Golestan flood management initiatives (No. 98–116), 313. Center for Strategic Studies, Iran.

Jongman, B., 2018. Effective adaptation to rising flood risk. Nat. Commun. 9, 1–3.

Jongman, B., Ward, P. J., & Aerts, J. C. J. H. (2012). Global exposure to river and coastal flooding: Long term trends and changes. Global Environmental Change, 22(4), 823–835. https://doi.org/10.1016/j.gloenvcha.2012.07.004

Jongman, B., Ward, P.J., Aerts, J.C., 2012. Global exposure to river and coastal flooding: Long term trends and changes. Glob. Environ. Change 22, 823–835.

Kapetas, L., & Fenner, R. (2020). Integrating blue-green and grey infrastructure through an adaptation pathways approach to surface water flooding. Philosophical Transactions of the Royal Society A, 378(2168), 20190204.

Karbassi, A., Bidhendi, G. N., Pejman, A., and Bidhendi, M. E. (2010). Environmental Impacts of Desalination on the Ecology of Lake Urmia. Journal of Great Lakes Research, 36(3), 419–424. https://doi.org/10.1016/j.jglr.2010.06.004

Kasperson, R.E., Kasperson, J.X., Turner, B.L., Dow, K., Meyer, W.B., 1995. Critical environmental regions: concepts, distinctions, and issues. Reg. Risk Comp. Threat. Environ. 1–41.

Katz, R.W., 2013. Statistical methods for nonstationary extremes, in: Extremes in a Changing Climate. Springer, pp. 15–37.

Katz, R.W., Parlange, M.B., Naveau, P., 2002. Statistics of extremes in hydrology. Adv. Water Resour. 25, 1287–1304.

Khosravi, K., Nohani, E., Maroufinia, E., Pourghasemi, H.R., 2016. A GIS-based flood susceptibility assessment and its mapping in Iran: a comparison between frequency ratio

and weights-of-evidence bivariate statistical models with multi-criteria decision-making technique. Nat. Hazards 83, 947–987.

Kiani, F., Jalalian, A., Pashaee, A. and Khademi, H., 2004, September. Effect of deforestation on selected soil quality attributes in loess-derived landforms of Golestan province, northern Iran. In Proceedings of the Fourth International Iran and Russia Conference (pp. 546-550).

Kilgore, R., Thomas Jr, W. O., Douglass, S., Webb, B., Hayhoe, K., Stoner, A., ... & Anderson, C. (2019). Applying Climate Change Information to Hydrologic and Coastal Design of Transportation Infrastructure (No. NCHRP Project 15□61).

Kjeldsen, T.R., 2010. Modelling the impact of urbanization on flood frequency relationships in the UK. Hydrol. Res. 41, 391–405.

Kopp, R. E., R. M. Horton, C. M. Little, J. X. Mitrovica, M. Oppenheimer, D. J. Rasmussen, B. H. Strauss, and C. Tebaldi. (2014). Probabilistic 21st and 22nd century sea-level projections at a global network of tide-gauge sites, Earth ’s Future, 2, 383–406.

Kundzewicz, Z.W., Kanae, S., Seneviratne, S.I., Handmer, J., Nicholls, N., Peduzzi, P., Mechler, R., Bouwer, L.M., Arnell, N., Mach, K. and Muir-Wood, R., (2014). Flood risk and climate change: global and regional perspectives. Hydrological Sciences Journal, 59(1), pp.1-28.

Kunkel, K.E., Karl, T.R., Brooks, H., Kossin, J., Lawrimore, J.H., Arndt, D., Bosart, L., Changnon, D., Cutter, S.L., Doesken, N., Emanuel, K., Groisman, P.Y., Katz, R.W., Knutson, T., O’Brien, J., Paciorek, C.J., Peterson, T.C., Redmond, K., Robinson, D.,

Trapp, J., Vose, R., Weaver, S., Wehner, M., Wolter, K., Wuebbles, D., 2013. Monitoring and Understanding Trends in Extreme Storms: State of Knowledge. Bull. Am. Meteorol. Soc. 94, 499–514. https://doi.org/10.1175/BAMS-D-11-00262.1

Labadie, J.W. and Larson, R. (2007). MODSIM 8.1: River basin management decision support system: User manual and documentation, (last accessed 06.10.2014). ftp://dwrftp.state.co.us/cdss/projects/MODSIM/MODSIMv8.1UserManual.pdf

Lall, U., Johnson, T., Colohan, P., Aghakouchak, A., Arumugam, S., Brown, C., et al. (2018). Chapter 3 : Water. Impacts, Risks, and Adaptation in the United States: The Fourth National Climate Assessment, Volume II. U.S. Global Change Research Program. https://doi.org/10.7930/NCA4.2018.CH3

Lohmann, D., NOLTE□HOLUBE, R. A. L. P. H., & Raschke, E. (1996). A large□scale horizontal routing model to be coupled to land surface parametrization schemes. Tellus A, 48(5), 708-721.

Loveland, T.R., Belward, A.S., 1997. The international geosphere biosphere programme data and information system global land cover data set (DISCover). Acta Astronaut. 41, 681–689.

Luke, A., Vrugt, J.A., AghaKouchak, A., Matthew, R., Sanders, B.F., 2017. Predicting nonstationary flood frequencies: Evidence supports an updated stationarity thesis in the U nited S tates. Water Resour. Res. 53, 5469–5494.

Ma, R., Duan, H., Hu, C., Feng, X., Li, A., Ju, W., …, and Yang, G. (2010). A half-century of changes in China's lakes: Global warming or human influence? Geophysical Research Letters, 37(24), L24106. https://doi.org/10.1029/2010GL045514

Madani, K. (2014). Water management in Iran: what is causing the looming crisis? J. Environ. Stud. Sci., 1-14, 10.1007/s13412-014-0182-z.

Madani, K., AghaKouchak, A., and Mirchi, A. (2016). Iran's Socio-economic Drought: Challenges of a Water-Bankrupt Nation. Iranian Studies, 49(6), 997–1016. https://doi.org/10.1080/00210862.2016.1259286

Mahtab, F. uddin, Karim, Z., 1992. Population and Agricultural Land Use: Towards a Sustainable Food Production System in Bangladesh. Ambio 21, 50–55.

Maleki, R., Nooripoor, M., Azadi, H. and Lebailly, P., (2018). Vulnerability Assessment of Rural Households to Urmia Lake Drying (the Case of Shabestar Region). Sustainability, 10(6).

Mallakpour, I., Sadegh, M., AghaKouchak, A., 2018. A new normal for streamflow in California in a warming climate: Wetter wet seasons and drier dry seasons. J. Hydrol. 567, 203–211. https://doi.org/10.1016/j.jhydrol.2018.10.023

Marengo, J.A., Espinoza, J.C., 2016. Extreme seasonal droughts and floods in Amazonia: causes, trends and impacts. Int. J. Climatol. 36, 1033–1050. https://doi.org/10.1002/joc.4420

Marvel, K., Bonfils, C., 2013. Identifying external influences on global precipitation. Proc. Natl. Acad. Sci. 110, 19301–19306. https://doi.org/10.1073/pnas.1314382110

Massari, C., Camici, S., Ciabatta, L., Brocca, L., 2018. Exploiting Satellite-Based Surface Soil Moisture for Flood Forecasting in the Mediterranean Area: State Update Versus Rainfall Correction. Remote Sens. 10, 292. https://doi.org/10.3390/rs10020292

McKee, T., Doesken, N., and Kleist, J. (1993). The relationship of drought frequency and duration to time scales Proceedings of the 8th Conference of Applied Climatology, 17–22 January 1993, American Meteorological Society, Anaheim, CA, 179-184.

Mehran, A., AghaKouchak, A., Nakhjiri, N., Stewardson, M. J., Peel, M. C., Phillips, T. J., …, and Ravalico, J. K. (2017). Compounding Impacts of Human-Induced Water Stress and Climate Change on Water Availability. Scientific Reports, 7(1). https://doi.org/10.1038/s41598-017-06765-0

Mei, X., Dai, Z., Du, J., and Chen, J. (2015). Linkage between Three Gorges Dam impacts and the dramatic recessions in China's largest freshwater lake, Poyang Lake. Scientific reports, 5, 18197.

Mekonnen, M.M. and Hoekstra, A.Y., (2011). The green, blue and grey water footprint of crops and derived crop products. Hydrology and Earth System Sciences, 15(5), p.1577.

Melchiorri, M., Florczyk, A.J., Freire, S., Schiavina, M., Pesaresi, M., Kemper, T., 2018. Unveiling 25 Years of Planetary Urbanization with Remote Sensing: Perspectives from the Global Human Settlement Layer. Remote Sens. 10, 768. https://doi.org/10.3390/rs10050768

Mell, W., Maranghides, A., McDermott, R. & Manzello, S. L. Numerical simulation and experiments of burning douglas fir trees. Combust. Flame 156, 2023–2041 (2009).Shortridge, J.,

Melville, C., 1984. Meteorological hazards and disasters in Iran: a preliminary survey to 1950. Iran, 22(1), pp.113-150.

Merz, R., Blöschl, G., 2003. A process typology of regional floods. Water Resour. Res. 39. https://doi.org/10.1029/2002WR001952

Micklin, P. (2007). The Aral Sea Disaster. Annual Review of Earth and Planetary Sciences, 35(1), 47–72. https://doi.org/10.1146/annurev.earth.35.031306.140120

Micklin, P.P. (1988). Desiccation of the Aral Sea: a water management disaster in the Soviet Union. Science, 241(4870), 1170.

Milly, P.C.D., Dunne, K.A., Vecchia, A.V., 2005. Global pattern of trends in streamflow and water availability in a changing climate. Nature 438, 347–350. https://doi.org/10.1038/nature04312

Min, S.-K., Zhang, X., Zwiers, F.W., Hegerl, G.C., 2011. Human contribution to more-intense precipitation extremes. Nature 470, 378–381. https://doi.org/10.1038/nature09763

Mirchi, A., Watkins, D.W., Huckins, C.J., Madani, K., and Hjorth, P. (2014). Water resources management in a homogenizing world: Averting the Growth and Underinvestment trajectory. Water Resources Research, 50(9), 7515-7526.

Moftakhari, H. R., AghaKouchak, A., Sanders, B. F., Feldman, D. L., Sweet, W., Matthew, R. A., & Luke, A. (2015). Increased nuisance flooding along the coasts of the United States due to sea level rise: Past and future: INCREASED NUISANCE FLOODING DUE TO SLR. Geophysical Research Letters, 42(22), 9846–9852. https://doi.org/10.1002/2015GL066072

Moftakhari, H. R., Salvadori, G., AghaKouchak, A., Sanders, B. F., & Matthew, R. A. (2017). Compounding effects of sea level rise and fluvial flooding. Proceedings of the National Academy of Sciences, 114(37), 9785–9790. https://doi.org/10.1073/pnas.1620325114

Moftakhari, H., AghaKouchak, A., Sanders, B. F., Matthew, R. A., & Mazdiyasni, O. (2017). Translating Uncertain Sea Level Projections Into Infrastructure Impacts Using a Bayesian Framework: Impact Assessment of SLR Projections. Geophysical Research Letters, 44(23), 11,914-11,921. https://doi.org/10.1002/2017GL076116

Mohammed, I.N. and Tarboton, D.G., (2012). An examination of the sensitivity of the Great Salt Lake to changes in inputs. Water Resources Research, 48 (11).

MohebZade Fattahi, A., 2019. Lorestan Flood-Risk Working Group Report. Ministry of Roads and Urban Development, Iran.

Moss, R.H., J.A. Edmonds, K.A. et al. (2010). The Next Generation of Scenarios for Climate Change Research and Assessment. Nature, 463, 747–756,

Nazemi, A. and Wheater, H. S. (2014). Assessing the vulnerability of water supply to changing streamflow conditions. Eos, Transactions American Geophysical Union, 95(32), 288-288.

Nazemi, A. and Wheater, H. S. (2015a). On inclusion of water resource management in Earth system models–Part 1: Problem definition and representation of water demand. Hydrology and Earth System Sciences, 19(1), 33-61.

Nazemi, A. and Wheater, H. S. (2015b). On inclusion of water resource management in Earth system models-Part 2: Representation of water supply and allocation and opportunities for improved modeling. Hydrology and Earth System Sciences, 19(1), 63.

NCDC. (2019). Billion-Dollar Weather and Climate Disasters. Retrieved from http://www.ncdc.noaa.gov/billions/events.

NCDC. (2021). Billion-Dollar Weather and Climate Disasters. Retrieved from http://www.ncdc.noaa.gov/billions/events.

Neumann, B., Vafeidis, A. T., Zimmermann, J., & Nicholls, R. J. (2015a). Future Coastal Population Growth and Exposure to Sea-Level Rise and Coastal Flooding - A Global Assessment. PLOS ONE, 10(3), e0118571. https://doi.org/10.1371/journal.pone.0118571

Neumann, J. E., Price, J., Chinowsky, P., Wright, L., Ludwig, L., Streeter, R., et al. (2015b). Climate change risks to US infrastructure: impacts on roads, bridges, coastal development, and urban drainage. Climatic Change, 131(1), 97–109. https://doi.org/10.1007/s10584-013-1037-4

Nicholls, R. J., Hoozemans, F. M., & Marchand, M. (1999). Increasing flood risk and wetland losses due to global sea-level rise: regional and global analyses. Global Environmental Change, 9, S69-S87.

Nikbakht, J., Tabari, H., and Talaee, P.H. (2013). Streamflow drought severity analysis by percent of normal index (PNI) in northwest Iran Theor. Appl. Climatol., 112 (3–4), 565-573.

Norouzi, G., Taslimi, M., 2012. The impact of flood damages on production of Iran's Agricultural Sector. Middle East J Sci Res 12, 921–926.

NRC. (2009). Informing Decisions in a Changing ClimateRep. Washington, D.C.: The National Academies Press,.

NRC. (2012). Sea-Level Rise for the Coasts of California, Oregon, and Washington: Past, Present, and Future. Washington, D.C.: National Academies Press. https://doi.org/10.17226/13389

O'Neill, P.E., Chan, S., Njoku, E.G., Jackson, T., Bindlish, R., 2016. Smap l3 radiometer global daily 36 km ease-grid soil moisture. Version 4, R14010.

Otto, C., Piontek, F., Kalkuhl, M., & Frieler, K. (2020). Event-based models to understand the scale of the impact of extremes. Nature Energy, 5(2), 111-114.

Pachauri, R.K., Allen, M.R., Barros, V.R., Broome, J., Cramer, W., Christ, R., Church, J.A., Clarke, L., Dahe, Q., Dasgupta, P., Dubash, N.K., Edenhofer, O., Elgizouli, I., Field, C.B., Forster, P., Friedlingstein, P., Fuglestvedt, J., Gomez-Echeverri, L., Hallegatte, S., Hegerl, G., Howden, M., Jiang, K., Jimenez Cisneroz, B., Kattsov, V., Lee, H., Mach, K.J., Marotzke, J., Mastrandrea, M.D., Meyer, L., Minx, J., Mulugetta, Y., O'Brien, K., Oppenheimer, M., Pereira, J.J., Pichs-Madruga, R., Plattner, G.-K., Pörtner, H.-O., Power, S.B., Preston, B., Ravindranath, N.H., Reisinger, A., Riahi, K., Rusticucci, M., Scholes, R., Seyboth, K., Sokona, Y., Stavins, R., Stocker, T.F., Tschakert, P., van Vuuren, D., van Ypserle, J.-P., 2014. Climate Change 2014: Synthesis Report.

Contribution of Working Groups I, II and III to the Fifth Assessment Report of the Intergovernmental Panel on Climate Change. IPCC, Geneva, Switzerland.

Panteli, M. & Mancarella, P. Modeling and Evaluating the Resilience of Critical Electrical Power Infrastructure to Extreme Weather Events. IEEE Syst. J. 11, 1733–1742 (2017).

Paprotny, D., Sebastian, A., Morales-Nápoles, O., Jonkman, S.N., 2018. Trends in flood losses in Europe over the past 150 years, Nat. Commun., 9, 1985.

Parajka, J., Kohnová, S., Bálint, G., Barbuc, M., Borga, M., Claps, P., Cheval, S., Dumitrescu, A., Gaume, E., Hlavčová, K., Merz, R., Pfaundler, M., Stancalie, G., Szolgay, J., Blöschl, G., 2010. Seasonal characteristics of flood regimes across the Alpine–Carpathian range. J. Hydrol., Flash Floods: Observations and Analysis of Hydrometeorological Controls 394, 78–89. https://doi.org/10.1016/j.jhydrol.2010.05.015

Parker, D.C., Manson, S.M., Janssen, M.A., Hoffmann, M.J., Deadman, P., 2003. Multi-Agent Systems for the Simulation of Land-Use and Land-Cover Change: A Review. Ann. Assoc. Am. Geogr. 93, 314–337. https://doi.org/10.1111/1467-8306.9302004

Pastor, A V., Ludwig, F., Biemans, H., Hoff, H., and Kabat, P. (2014). Accounting for environmental flow requirements in global water assessments Hydrol. Earth Syst. Sci. 18 5041–59.

Patricola, C. M., & Wehner, M. F. (2018). Anthropogenic influences on major tropical cyclone events. Nature, 563(7731), 339–346. https://doi.org/10.1038/s41586-018-0673-2

Peck, R. B. (1969). Advantages and Limitations of the Observational Method in Applied Soil Mechanics. Géotechnique, 19(2), 171–187. https://doi.org/10.1680/geot.1969.19.2.171

Pengra B. (2012). The drying of Iran's Lake Urmia and its environmental consequences. UNEP-GRID, Sioux Falls, UNEP Global Environmental Alert Service (GEAS).

Penland, S., & Ramsey, K. E. (1990). Relative sea-level rise in Louisiana and the Gulf of Mexico: 1908-1988. Journal of Coastal Research, 323-342.

Penland, S., & Ramsey, K. E. (1990). Relative sea-level rise in Louisiana and the Gulf of Mexico: 1908-1988. Journal of Coastal Research, 323-342.

Phoon, K. K. (Ed.). (2008). Reliability-based design in geotechnical engineering: computations and applications. CRC Press.

Pierce, D. W., Cayan, D. R., & Dehann, L. (2016). Creating climate projections to support the 4th California climate assessment. University of California at San Diego, Scripps Institution of Oceanography: La Jolla, CA, USA.

Pierce, D. W., Cayan, D. R., Maurer, E. P., Abatzoglou, J. T., & Hegewisch, K. C. (2015). Improved bias correction techniques for hydrological simulations of climate change. Journal of Hydrometeorology, 16(6), 2421-2442.

Pierce, D., Kalansky, J., Cayan, D.R., 2018. CLIMATE, DROUGHT, AND SEA LEVEL RISE SCENARIOS FOR CALIFORNIA'S FOURTH CLIMATE CHANGE ASSESSMENT [WWW Document]. URL /paper/CLIMATE%2C-DROUGHT%2C-AND-SEA-LEVEL-

RISE-SCENARIOS-FOR-Pierce-Kalansky/a14d7f2f76e7d72cfd3023c86e02c567db0ee66c (accessed 9.25.20).

Pierce, D.W., Cayan, D.R., Das, T., Maurer, E.P., Miller, N.L., Bao, Y., Kanamitsu, M., Yoshimura, K., Snyder, M.A., Sloan, L.C., Franco, G., Tyree, M., 2013. The Key Role of Heavy Precipitation Events in Climate Model Disagreements of Future Annual Precipitation Changes in California. J. Clim. 26, 5879–5896. https://doi.org/10.1175/JCLI-D-12-00766.1

Poff , N.L., Allan, J.D., Bain, M.B., Karr, J.R., Prestegaard, K.L., Richter, B.D., Sparks, R.E., and Stromberg, J.C. (1997). The natural flow regime: a paradigm for river conservation and restoration. Bioscience, 47, 769–784.

Ragno, E., AghaKouchak, A., Cheng, L., Sadegh, M., 2019. A generalized framework for process-informed nonstationary extreme value analysis. Adv. Water Resour. 130, 270–282.

Ragno, E., AghaKouchak, A., Love, C. A., Cheng, L., Vahedifard, F., Lima, C. H. R., (2018). Quantifying Changes in Future Intensity-Duration-Frequency Curves Using Multi-Model Ensemble Simulations. Water Resources Research, 54(3), 1751-1764.

Raskin, P., Gleick, P., Kirshen, P., Pontius, G., and Strzepek, K. (1997). Water futures: Assessment of long-range patterns and problems. Comprehensive assessment of the freshwater resources of the world, SEI. Stockholm.

Razavi, S., Gober, P., Maier, H.R., Brouwer, R., Wheater, H., 2020. Anthropocene flooding: Challenges for science and society. Hydrol. Process. 34, 1996–2000.

Read, L. K., & Vogel, R. M. (2015). Reliability, return periods, and risk under nonstationarity. Water Resources Research, 51(8), 6381-6398.

Reidmiller, D. R., Avery, C. W., Easterling, D. R., Kunkel, K. E., Lewis, K. L. M., Maycock, T. K., & Stewart, B. C. (2018). Impacts, Risks, and Adaptation in the United States: The Fourth National Climate Assessment, Volume II. U.S. Global Change Research Program. https://doi.org/10.7930/NCA4.2018

Renard, B., Sun, X., Lang, M., 2013. Bayesian methods for non-stationary extreme value analysis, in: Extremes in a Changing Climate. Springer, pp. 39–95.

Rosner, A., Vogel, R. M., & Kirshen, P. H. (2014). A risk□based approach to flood management decisions in a nonstationary world. Water Resources Research, 50(3), 1928-1942.

Sadegh Mojtaba, Vrugt Jasper A., Xu Chonggang, & Volpi Elena. (2015). The stationarity paradigm revisited: Hypothesis testing using diagnostics, summary metrics, and DREAM(ABC). Water Resources Research, 51(11), 9207–9231. https://doi.org/10.1002/2014WR016805

Sadegh, M., Moftakhari, H., Gupta, H.V., Ragno, E., Mazdiyasni, O., Sanders, B., Matthew, R., AghaKouchak, A., 2018. Multihazard scenarios for analysis of compound extreme events. Geophys. Res. Lett. 45, 5470–5480.

Sadegh, M., Ragno, E., AghaKouchak, A., 2017. Multivariate C opula A nalysis T oolbox (MvCAT): describing dependence and underlying uncertainty using a B ayesian framework. Water Resour. Res. 53, 5166–5183.

Salas, J. D., & Obeysekera, J. (2014). Revisiting the Concepts of Return Period and Risk for Nonstationary Hydrologic Extreme Events. Journal of Hydrologic Engineering, 19(3), 554–568.

Sarauskiene, D., Kriauciuniene, J., Reihan, A., Klavins, M., 2015. Flood pattern changes in the rivers of the Baltic countries. J. Environ. Eng. Landsc. Manag. 23, 28–38. https://doi.org/10.3846/16486897.2014.937438

Schwartz, R. C., Deadman, P. J., Scott, D. J., and Mortsch, L. D. (2004). Modeling the impacts of water level changes on a Great Lakes community. Journal of the American Water Resources Association, 40(3), 647-662.

Scoccimarro, E., Gualdi, S., Bellucci, A., Zampieri, M., & Navarra, A. (2013). Heavy Precipitation Events in a Warmer Climate: Results from CMIP5 Models. Journal of Climate, 26(20), 7902–7911. https://doi.org/10.1175/JCLI-D-12-00850.1

Seyedin, H., HabibiSaravi, R., Djenab, V.H., Hamedani, F.G., 2017. Psychological sequels of flood on residents of southeast Caspian region. Nat. Hazards 88, 965–975.

Shabanikiya, H., Seyedin, H., Haghani, H., Ebrahimian, A., 2014. Behavior of crossing flood on foot, associated risk factors and estimating a predictive model. Nat. Hazards 73, 1119–1126.

Shadkam, S., Ludwig, F., van Oel, P., Kirmit, Ç., and Rezaei Kabat, P. (2016). Impacts of climate change and water resources development on the declining inflow into Iran's Lake Urmia. Journal of Great Lakes Research, 42(5), 942-952.

Shahabi, H., Shirzadi, A., Ghaderi, K., Omidvar, E., Al-Ansari, N., Clague, J.J., Geertsema, M., Khosravi, K., Amini, A., Bahrami, S., 2020. Flood detection and susceptibility mapping using sentinel-1 remote sensing data and a machine learning approach: Hybrid intelligence of bagging ensemble based on k-nearest neighbor classifier. Remote Sens. 12, 266.

Sharifi, F., Samadi, S.Z., Wilson, C.A., 2012. Causes and consequences of recent floods in the Golestan catchments and Caspian Sea regions of Iran. Nat. Hazards 61, 533–550.

Shokri, A., Sabzevari, S., Hashemi, S.A., 2020. Impacts of flood on health of Iranian population: Infectious diseases with an emphasis on parasitic infections. Parasite Epidemiol. Control e00144.

Shortridge, J., Aven, T., & Guikema, S. (2017). Risk assessment under deep uncertainty: A methodological comparison. Reliability Engineering & System Safety, 159, 12–23.

Sima, S. and Tajrishy, M. (2013). Using satellite data to extract volume–area–elevation relationships for Lake Urmia, Iran. Journal of Great Lakes Research, 39(1), 90-99.

Smakhtin, V., Revenga, C., and Döll, P. (2005). Taking into Account Environmental Water Requirements in Global-scale Water Resources Assessments International Water Management Institute. https://core.ac.uk/download/pdf/6405183.pdf

Smith, E., 2001. Pollutant concentrations of stormwater and captured sediment in flood control sumps draining an urban watershed. Water Res. 35, 3117–3126.

Smith, M., Schwartz, J., 2019. In Flood-Hit Midwest, Mayors See Climate Change as a Subject Best Avoided. N. Y. Times.

Solomon, S., Manning, M., Marquis, M., Qin, D., 2007. Climate change 2007-the physical science basis: Working group I contribution to the fourth assessment report of the IPCC. Cambridge university press.

Špačková, O., & Straub, D. (2017). Long-term adaption decisions via fully and partially observable Markov decision processes. Sustainable and Resilient Infrastructure, 2(1), 37–58.

Sprague Jr., R. H., and Carlson, E. D. (1982). Building Effective Decision Support Systems. Prentice Hall Professional Technical Reference.

Stephens, S. A., Bell, R. G., & Lawrence, J. (2018). Developing signals to trigger adaptation to sea-level rise. Environmental Research Letters, 13(10), 104004.

Stephenson, A., Tawn, J., 2004. Bayesian inference for extremes: accounting for the three extremal types. Extremes 7, 291–307.

Sternberg, H.O., 1987. Aggravation of Floods in the Amazon River as a Consequence of Deforestation? Geogr. Ann. Ser. Phys. Geogr. 69, 201–219. https://doi.org/10.1080/04353676.1987.11880208

Swain, D.L., Langenbrunner, B., Neelin, J.D., Hall, A., 2018. Increasing precipitation volatility in twenty-first-century California. Nat. Clim. Change 8, 427–433.

Tabari, H., Nikbakht, J., Talaee, P.H., 2013. Hydrological drought assessment in Northwestern Iran based on streamflow drought index (SDI). Water Resour. Manag. 27, 137–151.

Tan-Soo, J.-S., Adnan, N., Ahmad, I., Pattanayak, S.K., Vincent, J.R., 2016. Econometric Evidence on Forest Ecosystem Services: Deforestation and Flooding in Malaysia. Environ. Resour. Econ. 63, 25–44. https://doi.org/10.1007/s10640-014-9834-4

Tehrany, M.S., Pradhan, B., Mansor, S., Ahmad, N., 2015. Flood susceptibility assessment using GIS-based support vector machine model with different kernel types. Catena 125, 91–101.

Terzaghi, K., Peck, R. B., & Mesri, G. (1996). Soil mechanics in engineering practice. John Wiley & Sons.

Thiemann, M., Trosset, M., Gupta, H., Sorooshian, S., 2001. Bayesian recursive parameter estimation for hydrologic models. Water Resour. Res. 37, 2521–2535.

Trenberth, K. E. (2001a). Climate Variability and Global Warming. Science, 293(5527), 48. https://doi.org/10.1126/science.293.5527.48

Trenberth, K. E. (2001b). Stronger Evidence of Human Influences on Climate: The 2001 IPCC Assessment. Environment: Science and Policy for Sustainable Development, 43(4), 8–19. https://doi.org/10.1080/00139150109605136

Trenberth, K. E. (2008). The Impact of Climate Change and Variability on Heavy Precipitation, Floods, and Droughts. In M. G. Anderson & J. J. McDonnell (Eds.), Encyclopedia of

Hydrological Sciences. Chichester, UK: John Wiley & Sons, Ltd. https://doi.org/10.1002/0470848944.hsa211

Trenberth, K. E., Jones, P. D., Ambenje, P., Bojariu, R., Easterling, D., Klein Tank, A., ... & Zhai, P. (2007). Observations. Surface and atmospheric climate change. Chapter 3.

United Nations Environment Program (UNEP), (2012). The Drying of Iran's Lake Urmia and its Environmental Consequences. http://na.unep.net/geas/getUNEPPageWithArticleIDScript.php?article_id=79.

Urmia Lake Restoration Program (ULRP), (2016). Approved Solutions, the Executive Status and progress of projects (2).

USGS. (1982). Guidelines for determining flood flow frequency, Bulletin No. 17B (revised and corrected). Department of the Interior Geological Survey, Office of Water Data Coordination.

Vahed, S.Z., Forouhandeh, H., Hassanzadeh, S., Klenk, H. P., Hejazi, M.A., and Hejazi, M.S. (2011). Isolation and characterization of Halophilic bacteria from Urmia Lake in Iran, Microbiology, 80 (6), 834-841.

Vaheddoost, B. and Aksoy, H. (2017). Structural characteristics of annual precipitation in Lake Urmia basin. Theoretical and Applied Climatology, 128(3–4), 919–932. https://doi.org/10.1007/s00704-016-1748-3

Vahedifard, F., & AghaKouchak, A. (2020). Adaptive Infrastructure to Mitigate Future Climate Risk: Building Upon Our Geotechnical Engineering Heritage. Geo-Strata—Geo Institute of ASCE, 24(5), 28-35.

Vahedifard, F., AghaKouchak, A., Ragno, E., Shahrokhabadi, S., Mallakpour, I., 2017. Lessons from the Oroville dam. Science 355, 1139–1140. https://doi.org/10.1126/science.aan0171

Vahedifard, F., Jasim, F. H., Tracy, F. T., Abdollahi, M., Alborzi, A., & AghaKouchak, A. (2020). Levee Fragility Behavior under Projected Future Flooding in a Warming Climate. Journal of Geotechnical and Geoenvironmental Engineering, 146(12), 04020139.

Vahedifard, F., Tehrani, F. S., Galavi, V., Ragno, E., & AghaKouchak, A. (2017). Resilience of MSE walls with marginal backfill under a changing climate: Quantitative assessment for extreme precipitation events. Journal of Geotechnical and Geoenvironmental Engineering, 143(9), 04017056.

Vahedifard, Farshid, Sehat, S., & Aanstoos, J. V. (2017). Effects of rainfall, geomorphological and geometrical variables on vulnerability of the lower Mississippi River levee system to slump slides. Georisk: Assessment and Management of Risk for Engineered Systems and Geohazards, 11(3), 257–271. https://doi.org/10.1080/17499518.2017.1293272

Vitousek, S., Barnard, P. L., Fletcher, C. H., Frazer, N., Erikson, L., & Storlazzi, C. D. (2017). Doubling of coastal flooding frequency within decades due to sea-level rise. Scientific Reports, 7(1). https://doi.org/10.1038/s41598-017-01362-7

Vörösmarty, C. J., Douglas, E. M., Green, P. A., and Revenga, C. (2005). Geospatial indicators of emerging water stress: an application to Africa. AMBIO: A journal of the Human Environment, 34(3), 230-236.

Vörösmarty, C.J., Green, P., Salisbury, J., and Lammers, R.B. (2000). Global water resources: vulnerability from climate change and population growth. science, 289(5477), 284-288.

Vörösmarty, C.J., McIntyre, P.B., Gessner, M.O., Dudgeon, D., Prusevich, A., Green, P., Glidden, S., Bunn, S.E., Sullivan, C.A., Liermann, C.R., and Davies, P.M. (2010). Global threats to human water security and river biodiversity. Nature, 467(7315), 555-561.

Wada, Y., van Beek, L.P., van Kempen, C.M., Reckman, J.W., Vasak, S., and Bierkens, M.F. (2010). Global depletion of groundwater resources. Geophysical research letters, 37(20).

Walker, W. E., Haasnoot, M., & Kwakkel, J. H. (2013). Adapt or perish: A review of planning approaches for adaptation under deep uncertainty. Sustainability, 5(3), 955-979.

Wang, G., Zhang, J., He, R., Liu, C., Ma, T., Bao, Z., Liu, Y., 2017. Runoff sensitivity to climate change for hydro-climatically different catchments in China. Stoch. Environ. Res. Risk Assess. 31, 1011–1021. https://doi.org/10.1007/s00477-016-1218-6

Wheater, H., Evans, E., 2009. Land use, water management and future flood risk. Land Use Policy 26, S251–S264.

White, G. F. (1973). Natural hazards research. Directions in geography, 193.

Wilby, R.L. and Keenan, R., (2012). Adapting to flood risk under climate change. Progress in physical geography, 36(3), 348-378.

Willis, H. H., Narayanan, A., Fischbach, J. R., Molina-Perez, E., Stelzner, C., Loa, K., & Kendrick, L. (2016). Current and Future Exposure of Infrastructure in the United States to Natural Hazards. Santa Monica, Calif: Rand Corporation.

Winsemius, H.C., Jongman, B., Veldkamp, T.I., Hallegatte, S., Bangalore, M., Ward, P.J., 2015. Disaster risk, climate change, and poverty: assessing the global exposure of poor people to floods and droughts. The World Bank.

Wisner, B., Blaikie, P. M., Blaikie, P., Cannon, T., & Davis, I. (2004). At risk: natural hazards, people's vulnerability and disasters. Psychology Press.

Wobus, C., Lawson, M., Jones, R., Smith, J., & Martinich, J. (2014). Estimating monetary damages from flooding in the U nited S tates under a changing climate. Journal of Flood Risk Management, 7(3), 217-229.

Wright, D. B., Bosma, C. D., & Lopez□Cantu, T. (2019). US hydrologic design standards insufficient due to large increases in frequency of rainfall extremes. Geophysical Research Letters, 46(14), 8144-8153.

Wurtsbaugh, W. A., Miller, C., Null, S. E., DeRose, R. J., Wilcock, P., Hahnenberger, M., …, and Moore, J. (2017). Decline of the world's saline lakes. Nature Geoscience, 10(11), 816. https://doi.org/10.1038/ngeo3052

Yadollahie, M., 2019. The flood in Iran: a consequence of the global warming? Int. J. Occup. Environ. Med. 10, 54.

Yamaguchi, N., Sakotani, A., Ichijo, T., Kenzaka, T., Tani, K., Baba, T., and Nasu, M. (2012). Break down of asian dust particle on wet surface and their possibilities of cause of respiratory health effects, Biol. Pharm. Bull., 35 (7), 1187-1190.

Yari, A., Ardalan, A., Ostadtaghizadeh, A., Zarezadeh, Y., Boubakran, M.S., Bidarpoor, F., Rahimiforoushani, A., 2019. Underlying factors affecting death due to flood in Iran: A qualitative content analysis. Int. J. Disaster Risk Reduct. 40, 101258.

Youssef, A.M., Pradhan, B., Hassan, A.M., 2011. Flash flood risk estimation along the St. Katherine road, southern Sinai, Egypt using GIS based morphometry and satellite imagery. Environ. Earth Sci. 62, 611–623.

Zare, N., Talebbeydokhti, N., 2018. Policies and governance impact maps of floods on metropolitan Shiraz (the first step toward resilience modeling of the city). Int. J. Disaster Risk Reduct. 28, 298–317. https://doi.org/10.1016/j.ijdrr.2018.03.003

Zarghami M. and AmirRahmani M. (2017). A System Dynamics Approach to Simulate the Restoration Plans for Urmia Lake, Iran. In: Matsumoto A. (eds) Optimization and Dynamics with Their Applications. Springer, Singapore: http://link.springer.com/chapter/10.1007/978-981-10-4214-0_15

Zhang, X., Zwiers, F.W., Hegerl, G.C., Lambert, F.H., Gillett, N.P., Solomon, S., Stott, P.A., Nozawa, T., 2007. Detection of human influence on twentieth-century precipitation trends. Nature 448, 461–465. https://doi.org/10.1038/nature06025

Appendix A

MODSIM modeling

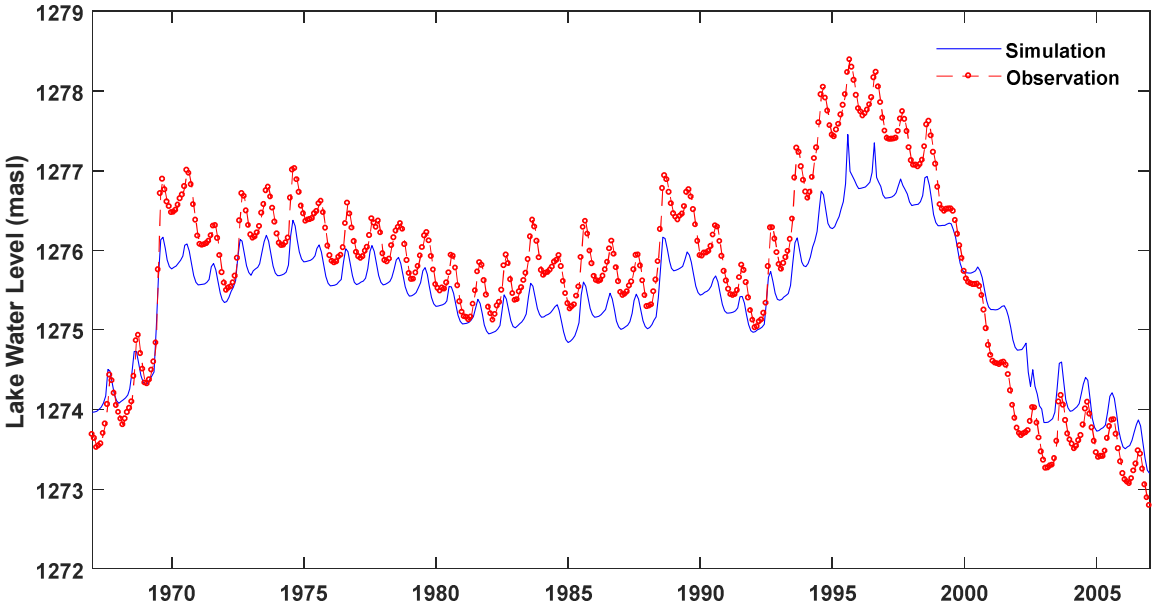

Figure S1. Monthly observed and simulated lake levels during the evaluation period (1967-2007).

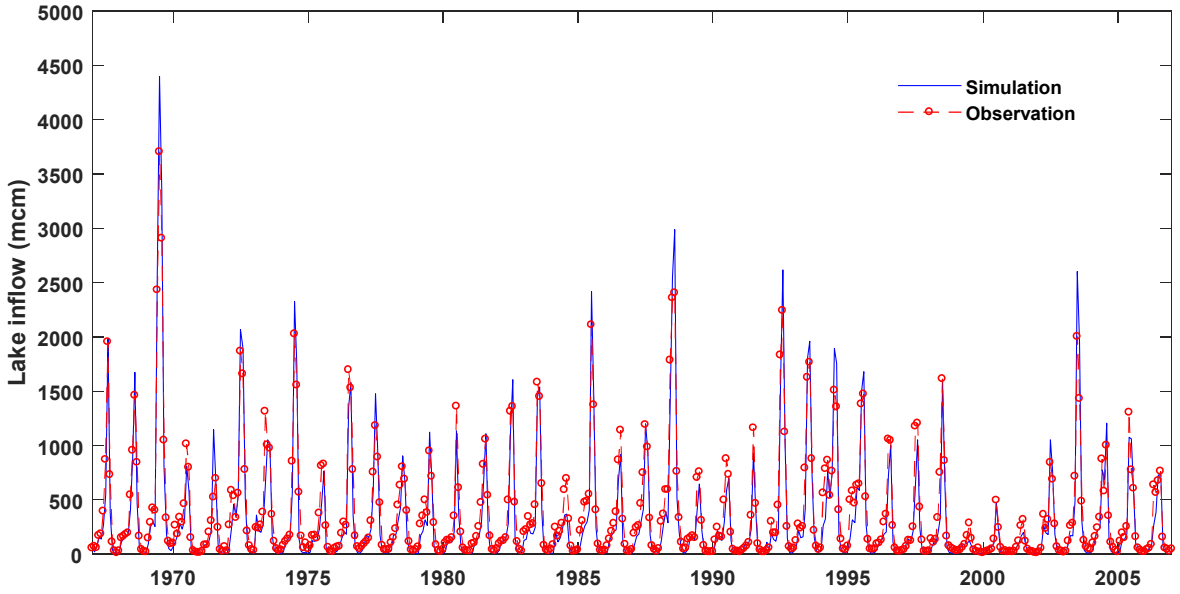

Figure S2. Monthly observed and simulated lake inflows during the evaluation period (1967-2007).

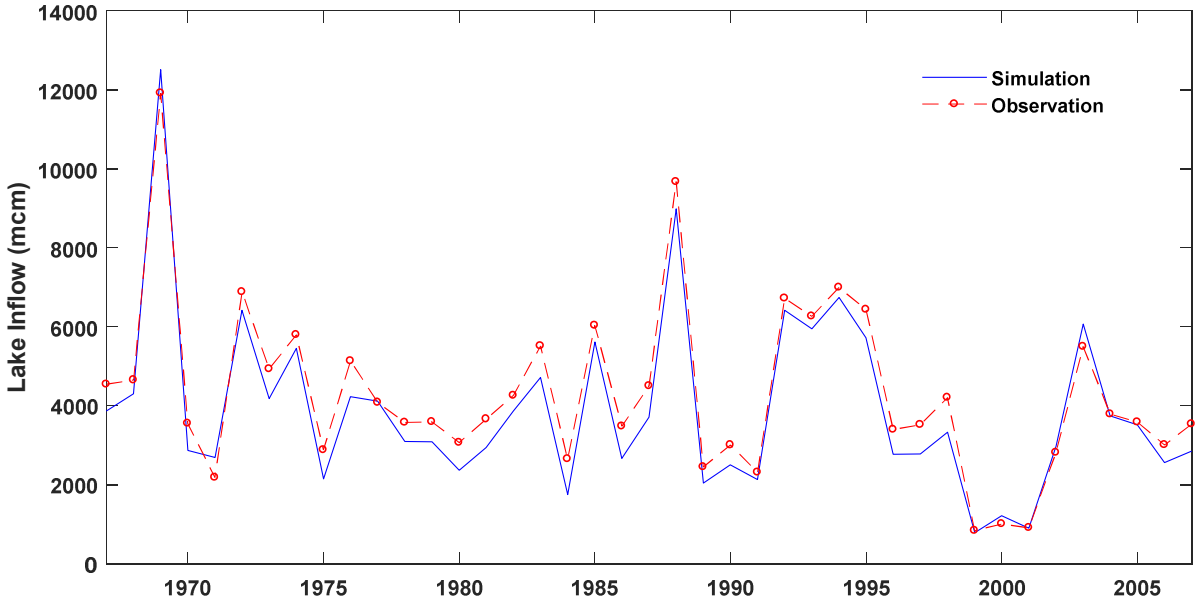

Figure S3. Annual observed and simulated lake inflows during the evaluation period (1967-2007).

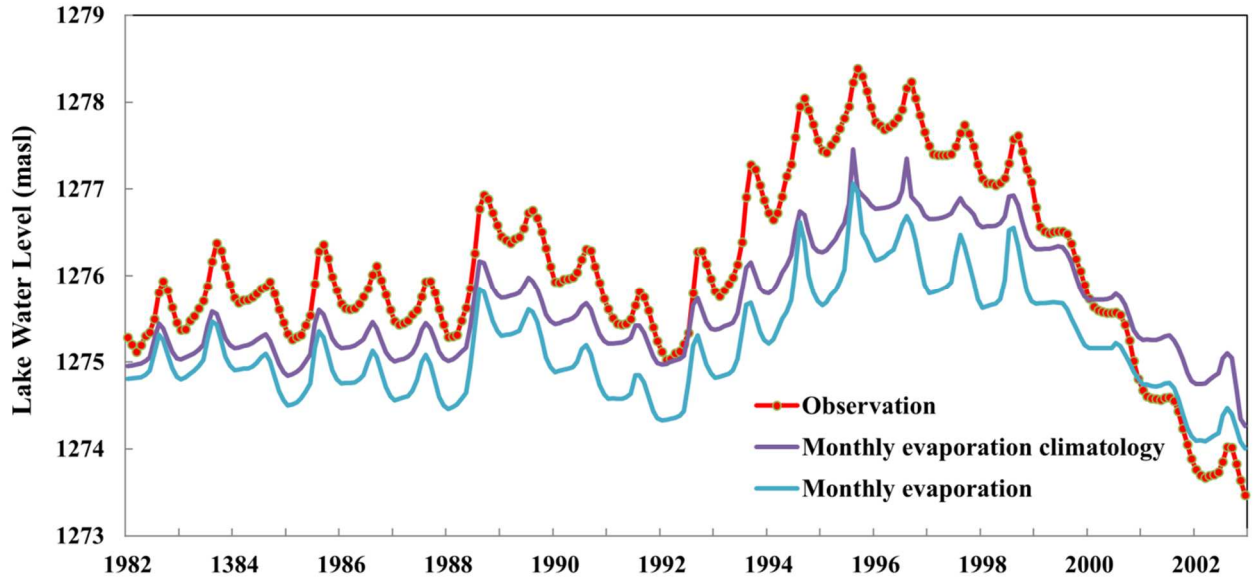

Figure S4. Comparison of model performance using monthly evaporation climatology with the total evaporation of 1100 mcm/yr and available observed monthly evaporation time series for the period of 1982-2002.

Appendix B

Flooding events

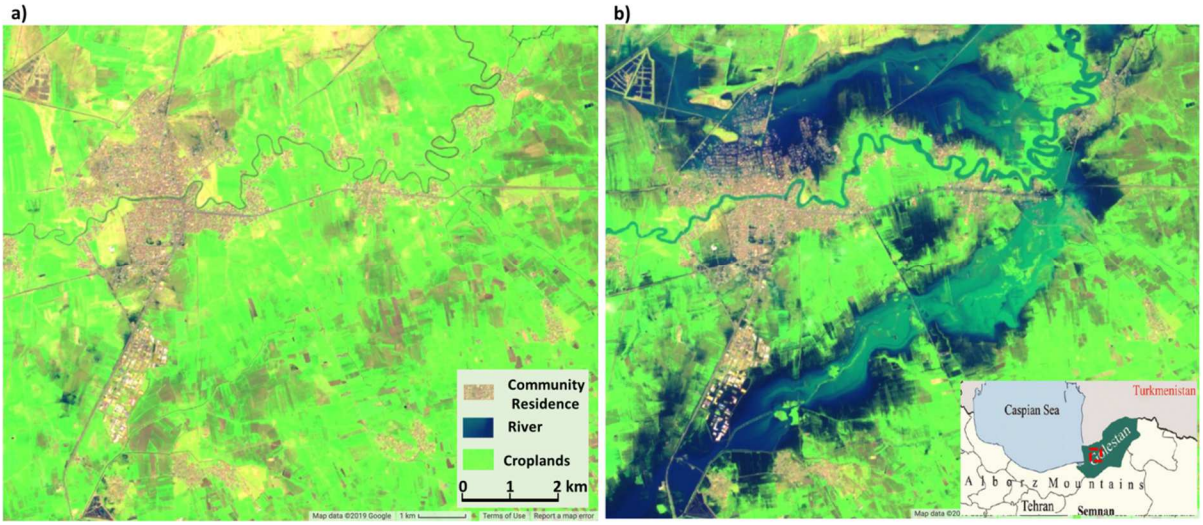

Figure S1. Combined Sentinel's satellite shortwave and infrared, near infared and blue band images show flood inundation a) before and b) after the event in AqQala, the most affected city.

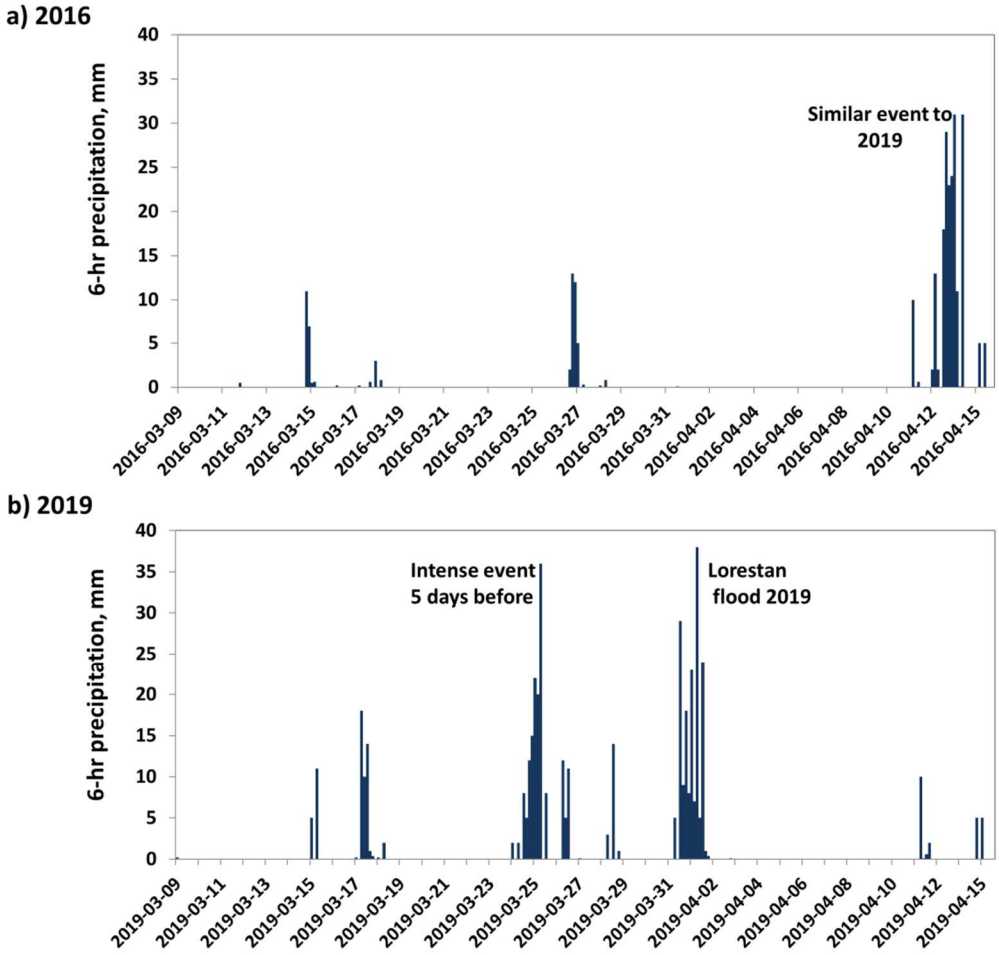

Figure S2. Comparing a similar large precipitation event in 2016 to 2019 flood event, a) 2016 6-hr precipitation, b) 2019 6-hr precipitation. It is noticeable that 5 days before the main flood. We only have one large precipitation event in 2016 although the intensity of 24-hr precipitation is the same as 2019 (100 mm). It provides further evidence that 2 following cascading high precipitation events resulted in an extreme flood.

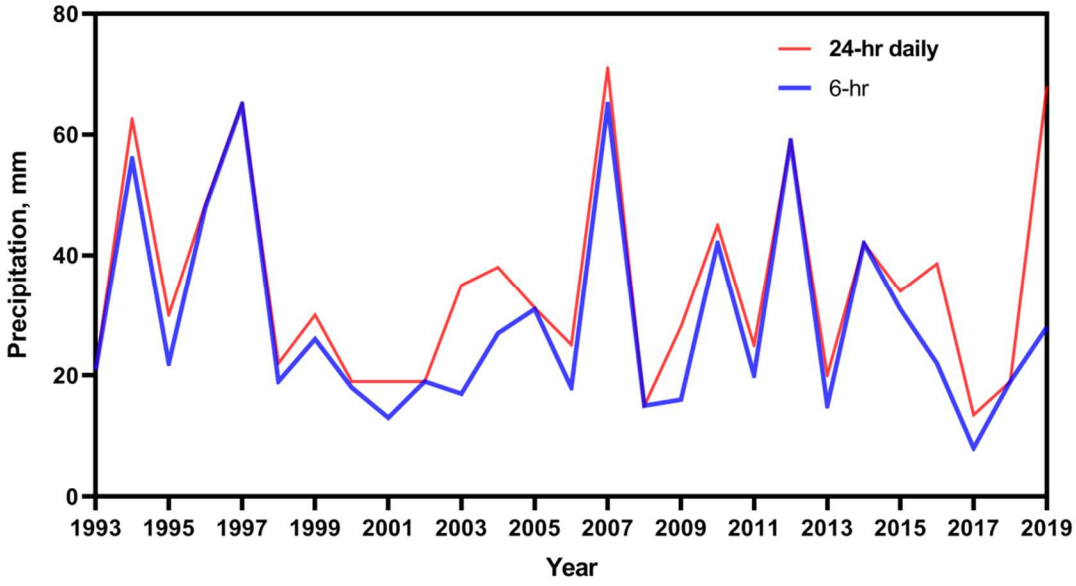

Figure S3. Annual maxima precipitation in MaraveTappe Gage Station.